EUROPEAN COMMISSION
DIRECTORATE-GENERAL
Joint Research Centre

Representing Aerosol Optical Properties with Theoretical Modelling and Global Observations

MARCO CLERICI and FREDERIC MELIN

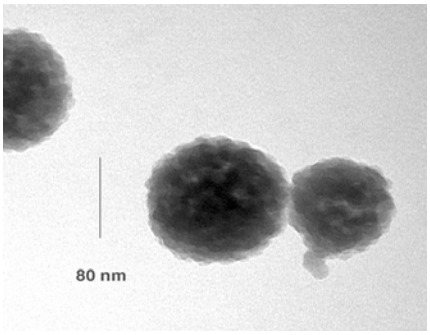

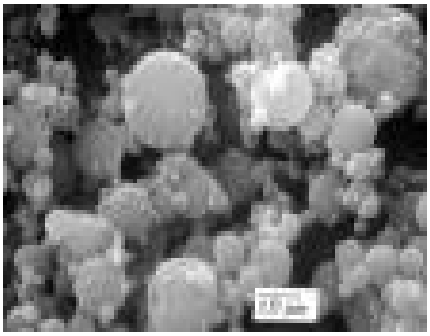

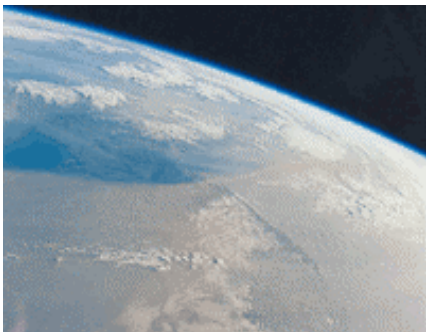

2005 **EUR 21747 EN**

EUROPEAN COMMISSION
DIRECTORATE-GENERAL
Joint Research Centre

Institute for Environment and Sustainability

Representing Aerosol Optical Properties with Theoretical Modelling and Global Observations

FREDERIC MELIN and MARCO CLERICI

European Commission – Joint Research Centre
Institute for Environment and Sustainability
Inland & Marine Waters Unit
TP 272, I-21020 Ispra (VA) – Italy

2005 **EUR 21747 EN**

EUR 21747 EN

Printed in Italy

Abstract

Aerosols are an important factor in biogeochemical cycles, climate variability and air quality. In the context of monitoring the marine ecosystems, a proper definition of the inherent optical properties of the aerosols is needed to perform radiative transfer simulations. These are useful to build inversion schemes, that will quantify the aerosol load and type and define the spectral signature of the ocean surface, and to quantify the aerosol direct radiative effect. This report describes tools that link size distribution of aerosol particles, assumed homogeneous spheres, and refractive index to optical properties through Mie theory. Then, it provides a brief survey of generic aerosol models, that is completed by a broad review of the measurements that are relevant for the definition of aerosol optical properties.

Contents

Introduction

Aerosols plays an important role in climate variability and change, mainly through their direct and indirect effects on the radiative budget and hydrological cycles of the Earth's system (IPCC 2001, Ramanathan et al., 2001b), but also as agents of atmospheric deposition at the ocean surface of chemical species of various origins, natural (e.g., Duce et al. 1991, Guerzoni et al. 1999, Jickells et al. 2005) or anthropogenic (Paerl 1997). The atmospheric content of aerosols also plays a major role on visibility and air quality, with potentially negative effects on human health (Lippmann et al. 2003).

The nature of aerosols is as multi-faceted as a single aerosol particle can be. First of all, they are produced from a variety of sources and processes. Marine aerosols for instance originates from sea salt (O'Dowd et al. 1997), non sea salt sulphate from biological activity (Charlson et al. 1987) or organic materials (e.g., Pósfai et al. 2003, O'Dowd et al. 2004). Terrestrial vegetation is also a medium of aerosol production (e.g., Artaxo et al. 1990, Mäkelä et al. 1997, O'Dowd et al. 2002), and becomes a particularly noticeable source in seasons of biomass burning (e.g., Hao and Liu 1994). Desert and arid regions represent one of the major sources of aerosols, with diversity in geographic location (Prospero et al. 2002) and mineralogy (Sokolik and Toon 1999). These desert dust aerosols can be transported to intercontinental distances (Betzer et al. 1988, Prospero 1999, Tratt et al. 2001). Densely populated regions, with their associated rural, urban and industrial areas, produce aerosols with obviously a large diversity of physicochemical properties (e.g., Putaud et al. 2004). Finally, volcanoes are an irregular point source of aerosols (e.g., Chuan et al. 1981, Russel et al. 1993). Subsequently, aerosols present in different air masses may mix and be transformed by physical and chemical processes, depending on relative humidity, light, etc... This diversity in sources and processes, along with the geographic scales of transport, makes it extremely difficult to synthesize aerosols into a few generic types that might be valid for instance in a given region and season, even though it is possible to delineate a general repartition (see for example Kahn et al. 2001 or Omar et al. 2005).

The study of this highly variable atmospheric component can greatly benefit from monitoring by remote sensing and the synoptic view it offers (Kaufman et al. 2002). For that purpose, various sets of spectral ranges and inversion techniques have been used to characterize the quantity and the type of aerosols in the field of view of a remote sensor (King et al. 1999). Moreover, in recent times, satellite remote sensing has been completed by networks of optical instruments that look at the aerosols from the bottom up (Holben et al. 1998), provide further insights into the nature of the columnar aerosols and can serve for validating the remote sensing products.

Our aim is to define the optical properties of aerosols of relevance for radiative transfer calculations (single scattering albedo, scattering phase function). In the context of our studies of the marine ecosystems, radiative transfer simulations might serve to:

- develop algorithms that determine at least the spectrum of the aerosol optical thickness over marine surfaces and possibly indicators of their type,
- quantify the atmospheric path radiance in order to derive the optical signature of the ocean surface (atmospheric correction),
- and compute the direct aerosol radiative effect.

It is clear that these optical properties are linked to the chemical composition of the different particles, their size and morphology.

To lay the basis for these potential activities, it was considered appropriate to

- have the modelling tools linking aerosol size distributions and refractive index to optical properties,
- and review the available information describing these characteristics of aerosols in order to have an insight into their diversity as well as to find general features.

Section 1 describes several tools that link size distribution of aerosol particles, assumed homogeneous spheres, and refractive index to optical properties through Mie theory. These calculations enable the setups required to use a radiative transfer model designed for the ocean-atmosphere system (Bulgarelli et al. 1999). Admittedly, the assumption of (equivalent) homogeneous spheres is a strong simplification of the actual nature of aerosol particles. At the same time, this theoretical framework has proved useful to realistically represent the optical properties of aerosols in many instances, and coping with diverse morphologies is an active and complex field of work (see for instance Mishchenko et al. 2000, Kalashnikova and Sokolik 2002). In practice, these assumptions will also be compounded by other uncertainties, like those related to the vertical distribution of the aerosols. In the context of the inversion of remote sensing signals, it is not possible to accommodate all degrees of variability; conversely, it will be necessary to assess the impact that the assumptions made may have on the inversion process.

One way of addressing this includes a survey of generic representations of the aerosol size and optical properties (called aerosol models) to understand the range of natural variability they cover (Section 2). These aerosol models are derived from syntheses of in situ data (particle size, chemical analysis, airborne optical measurements) or from optical ground measurements, and have been in some cases adopted for remote sensing operational algorithms. The description of these general models is completed by Section 3, that makes a broad review of relevant measurements. Eventually, this report serves as a working document and as a reference for our modelling activities.

Section 1

Mie Scattering

Different routines have been retrieved, mainly from internet, to compute optical properties from Mie theory, both for a single particle and for a particle size distribution. A short description of the tools, their integration in the IDL environment, examples of their use and comparison of results are the subject of the current Section.

1.1 Overview

The light scattering of monocromatic radiation by an homogenous spherical particle is described by Mie theory [1908] and can be found, e.g., in Van de Hulst (1957). The computation of the electromagnetic field involves the use of Bessel functions and Legendre polynomials and is time-consuming; therefore different approaches have been implemented to reduce the machine computational time.

Wiscombe proposed in 1979 new algorithms that resulted in considerable improvements in speed by employing more efficient formulations and vector structure, as described in Section 1.2.

LibRadtran library includes a mie computation algorithm, which calls Wiscombe or Bohren and Hoffmann code, providing at the same time the capability to handle a particle size distribution (see Section 1.3).

Furthermore, the department of Physics of Oxford University makes available at the site http://www-atm.physics.ox.ac.uk/code/mie/index_nocol.html IDL routines to compute Mie scattering for both single particle and lognormal particle distribution, that can be easily extended to whatever size distribution, as described in Section 1.4.

1.2 Wiscombe MIEV code

Detailed description of the code can be found in Wiscombe (1980) and in a technical note from National Center for Atmospheric Research (Wiscombe 1979). The code has been downloaded from ftp site climate.gsfc.nasa.gov, subdirectory /pub/wiscombe, as a list of FORTRAN source file, and interfaced to IDL through a set of simple routines to drive the compiled executable.

The list of the input variables is presented in Table 1.1: parameters XX, CREFIN define the physical problem, while the other variables set computational conditions and format of the output file. The size parameter XX is the sphere circumference divided by the wavelength; PERFCT flag can be set to force the use of special formulas for the

infinite refractive index case, also said 'totally reflecting' or 'perfectly conducting' case; MIMCUT defines the value below which the imaginary refractive index is regarded as zero; IPOLZN is set to zero to compute Legendre moments PMOM for the unpolarised unnormalised phase function.

MIEV Code Inputs		
Parameter	Type	Description
XX	float	Particle size parameter
CREFIN	complex	Complex Refractive Index
PERFCT	boolean	Perfectly Conducting case
MIMCUT	float	Imaginary Refractive Index Threshold
ANYANG	boolean	If true, any angle can be entered as mu
NUMANG	positive integer	Number of output scattering angles
XMU	float array	Cosines of output scattering angles
NMOM	positive integer	Highest Legendre Moment order
IPOLZN	integer	Polarisation Flag
MOMDIM	positive integer	Dimension of internal array PMOM
PRT(L)	boolean array	Print flags

Table 1.1: Inputs for MIEV code

In the current implementation MOMDIM and XMU are not part of the input variables, as MOMDIM is set to the value 10000 and the scattering angles are computed from NUMANG, equi-spaced in the interval [0.,180.] degree. Furthermore PRT is set to [1 1], and the resulting output variables are listed in Table 1.2.

The code computes directly the Legendre coefficients associated with the scattering phase function, while the phase function itself can be derived from I1, I2 and XX according to the following formula:

$$phf(\phi) = \frac{2 \cdot (I_1 + I_2)}{XX^2 \cdot Q_{sca}} \tag{1.1}$$

Furthermore, the single scattering albedo coefficient can be computed dividing Q_{SCA} by Q_{EXT} and asymmetry factor from G_{SCA} and Q_{SCA}. The normalized scattering phase function computed with MIEV code for the reference case described in 1.5 is displayed in Figure 1.1.

MIEV Code Outputs		
Parameter	Type	Description
Q_{EXT}	float	Extinction Efficiency Factor
Q_{SCA}	float	Scattering Efficiency Factor
G_{QSC}	float	Asymmetry factor * Scattering Efficiency
S1,S2	complex arrays	Mie Scattering amplitudes at the angles specified by XMU
S1C2	complex array	Mie Scattering amplitude S1*conjug(S2)
I1	float array	S1*conjug(S1)
I2	float array	S2*conjug(S2)
I12M	float array	(I1+I2)/2.
DEGPOL	float array	Polarisation degree
PMOM	float array	Legendre Moments of the Scattering Phase Function

Table 1.2: Outputs of MIEV code

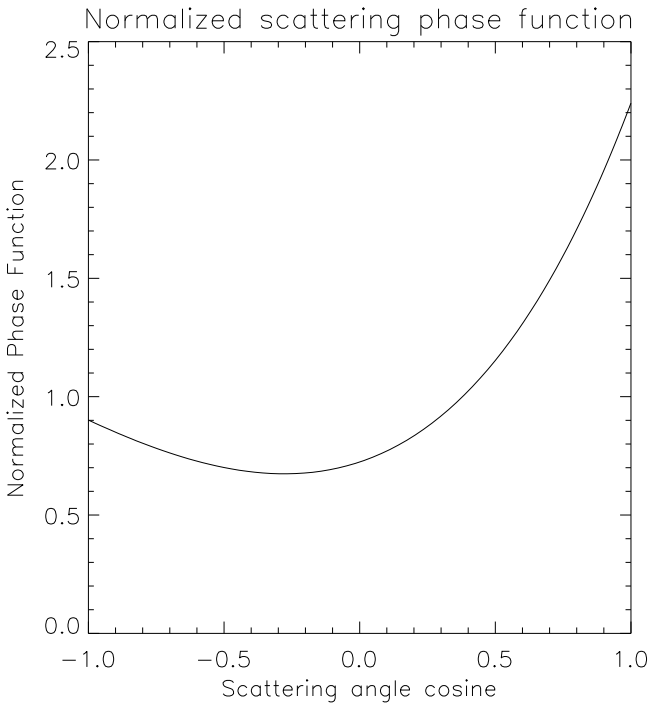

Figure 1.1: Reference case scattering phase function - MIEV code

1.3 LibRadtran Mie routine

LibRadtran is a comprehensive set of routines for radiative transfer computations, evolved from the uvspec radiative transfer model, and available at the site http://www.libradtran.org/ together with the manual (Kylling and Mayer 2003). It includes a 'mie' stand-alone application, which calls Bohren and Hoffmann (BH) or Wiscombe (MIEV0) Mie solver, and allows at the same time the computation of scattering coefficients for a particle size distribution.

Input parameters of the code, which in the following is referred to simply as 'mie', are listed in Table 1.3: most of them can be easily recognised in table 1.1.

mie Code Inputs		
Parameter	Type	Description
mie_program	string	Mie solver (BH or MIEV0)
mimcut	float	Imaginary Refractive Index Threshold
nmom	positive integer	Highest Legendre Moment order
r_mean	float	Radius of the particle [μm]
refrac	string	Refractive Index. Can be ice water user <re> <im> file <filename>
size_distribution_file	string	Two columns file $< r[\mu m] >$ $< dN(r)/dr >$
temperature	float	Ambient temperature, used for ice/water
wvn	float [2]	Minimum and maximum wavelength [nm]
wvn_step	float	Wavelength step [nm]

Table 1.3: Inputs for mie code

In case a particle distribution is used, instead of a single particle, *size_distribution_file* should be prepared as a two columns ASCII file, containing the particle radii in μm in the first column and the corresponding densities $< dN(r)/dr >$ in the second.

'mie' code produces an ASCII output file containing for each wavelength the quantities listed in table 1.4.

Qext represents the extinction efficiency factor if r_mean is specified (single particle case) or the extinction coefficient if a particle size distribution is used. In the latter case, the original code outputs Qext in km^{-1} per unit concentration in cm^3/m^3, while the modified routine (see 1.7.2) produces extinction coefficient in $km^{-1}par^{-1}cm^3$.

MIE Code Outputs		
Parameter	Type	Description
lambda	float	Wavelength [nm]
refrac_real	float	Real part of refractive index
refrac_img	float	Imaginary part of refractive index
qext	float	Extinction efficiency factor or coefficient
omega	float	Single Scattering Albedo
gg	float	Asymmetry Parameter
spike	float	see Kylling and Mayer (2003)[pg.45]
pmom	float array	Legendre coefficients of the phase function

Table 1.4: Outputs of mie code

The scattering phase function is not available directly, but can be computed from the associated Legendre coefficients through the formula:

$$p(\mu) = \sum_{m=0}^{\infty} (2m+1) \cdot k_m \cdot P_m(\mu) \tag{1.2}$$

where μ is the scattering angle cosine, k_m the m-th Legendre coefficient and P_m the m-th order Legendre polynomial.

'mie' code is applied to the reference case for a particle size distribution, as described in 1.5, and the normalised scattering phase function is displayed in fig. 1.2.

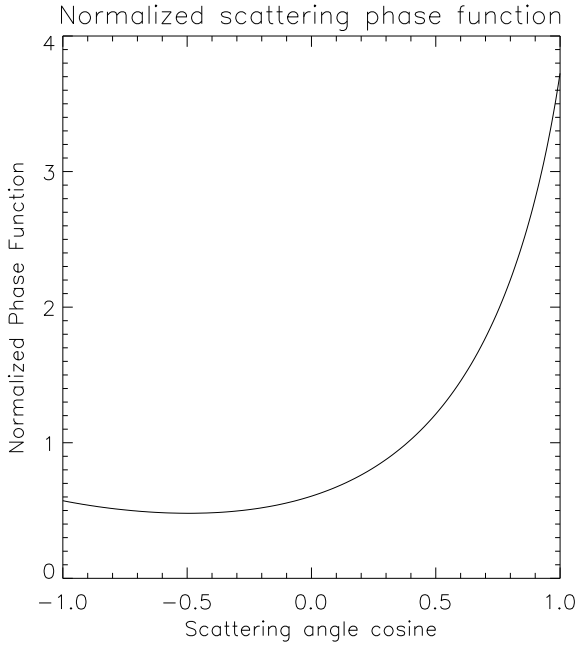

Figure 1.2: Particle distribution reference case phase function - MIE code

1.4 Oxford University routines

The Physics Department of Oxford University makes available routines to compute aerosol scattering parameters, at the site http://www-atm.physics.ox.ac.uk/code/mie/index_nocol .html. The basic routine is mie_single, which applies Mie theory to a single particle; mie_lognormal is the extension to a particle lognormal distribution, while mie_sizedist, which we have derived from the previous one, is the extension to whatever size distribution. The acronyms AOPP (Atmospheric, Oceanic and Planetary Physics - Oxford University) is used to identify the Oxford routines throughout this document.

1.4.1 Single particle case - mie_single

Routine mie_single inputs are listed in Table 1.5.

AOPP mie_single Inputs		
Parameter	Type	Description
Dx	float or float array	Particle size parameter
Cm	complex	Complex refractive index
Inp	integer	Number of scattering angles
Dqv	float array [optional]	Cosine of scattering angles

Table 1.5: Inputs for AOPP mie_single code

The routine can also accept an array of size parameter values, Dx, in which case it returns the scattering parameters for each individually. An array of cosines of scattering angles can be provided as Dqv, otherwise it is internally built from Inp parameter.

AOPP mie_single Outputs		
Parameter	Type	Description
Dqxt	float or float array	Extinction efficiency factor (i.e. Q_{ext})
Dqsc	float or float array	Scattering efficiency factor (i.e. Q_{sca})
Dg	float or float array	Asymmetry parameter
Xs1	float or float array	Amplitude of light polarised in the plane perpendicular to the directions of incident light and observation
Xs2	float or float array	Amplitude of light polarised in the plane parallel to the directions of incident light and observation
Dph	float array	Phase function

Table 1.6: Outputs for AOPP mie_single code

Outputs are listed in Table 1.6, where the original naming from AAOP routine is kept.

1.4.2 Lognormal size distribution - mie_lognormal

An extension of the single particle case computation is represented by mie_lognormal, which internally computes an array of size parameters and associated particle densities, calls mie_single on each case and weights the results according to densities. mie_lognormal inputs are described in Table 1.7.

AOPP mie_lognormal Inputs		
Parameter	Type	Description
Nd	float	Total number of particles per cm^3
Rm	float	Median radius of particle distribution [μm]
Sg	float	Spread of the distribution [μm]
Wavenumber	float	Radiation wavenumber [μm^{-1}]
Cm	complex	Complex particle refractive index
Dqv	float array [optional]	Cosine of scattering angles
Rmin	float [optional]	Minimum radius in computation
Rmax	float [optional]	Maximum radius in computation
Nqua	integer [optional]	Number of quadrature points

Table 1.7: Inputs for AOPP mie_lognormal code

Nd is the total number density in *par* cm^{-3}; it can be set to 10^{-3} in order to convert the output quantities σ^{cs}_{ext} and σ^{cs}_{sca} in μm^2 to σ_{ext} and σ_{sca} in km^{-1} per unit concentration of 1 *par* cm^{-3} (see section 1.7.2).

The routine defines the min-max range of radii through Rmin/Rmax, or, if they are not provided, it computes them internally in order to cover 99.9% of the particle number distribution. An array of Nqua radii between Rmin-Rmax and the associated weights are computed using Lobatto quadrature; particle number densities for each radius are computed using the formula:

$$n(r) = \frac{N_d}{\sqrt{2\pi}} \cdot \frac{1}{ln(S_g)} \cdot \frac{1}{r} \cdot exp(-\frac{(ln(r) - ln(r_m))^2}{2ln^2 S_g}) \tag{1.3}$$

where $n(r)$ represent the number density, i.e. dN(r)/dr, for each radius.

The extinction and scattering efficiencies are computed by mie_single for every radius, and then extinction/scattering cross-sections derived as in Equation 1.4:

$$\sigma^{cs}_{ext} = \sum_{i=1}^{N} D^i_{qxt} \cdot W^i_{qua} n(r)^i \cdot r_i^2 \cdot \pi \tag{1.4}$$

where D^i_{qxt} is the extinction efficiency for i-th radius, W^i_{qua} Lobatto quadrature weights normalised to an overall value equal to radius range width, $n(r)^i$ is the particle number density, such that:

$$\sum_{i=1}^{N} n(r)^i \cdot W^i_{qua} = N_d \tag{1.5}$$

mie_lognormal outputs quantities are described in fig. 1.8.

AOPP mie_lognormal Outputs		
Parameter	Type	Description
σ_{ext}^{cs}	float	Extinction cross-section
σ_{sca}^{cs}	float	Scattering cross-section
w	float	Single Scattering Albedo
ph	float array	Phase function

Table 1.8: Outputs for AOPP mie_lognormal code

1.4.3 Generic size distribution - mie_sizedist

This routine is an extension of mie_lognormal, which adds two main features:

- Use of whatever size particle distribution.
- Definition of the distribution either in terms of number or volume densities.

AOPP mie_sizedist Inputs		
Parameter	Type	Description
file	string	Size Distribution filename
Nd	float	Total number of particles
Wavenumber	float	Radiation wavenumber
Cm	complex	Complex particle refractive index
Dqv	float array [optional]	Cosine of scattering angles
Rmin	float [optional]	Minimum radius of the distribution
Rmax	float [optional]	Maximum radius of the distribution
Nqua	integer [optional]	Number of quadrature points
Rarr	float array [optional]	Array of radia
dNr	float array [optional]	Array of particle densities
VolConc	boolean [optional]	Volume concentration flag

Table 1.9: Inputs for AOPP mie_sizedist code

Input arguments N_d, Wavenumber, C_m and optional inputs R_{min}, R_{max} and N_{qua} have exactly the same meaning and use as in paragraph 1.4.2. Particle size distribution can be provided in the arrays R_{arr} and dN_r, which must have the same dimension, or can be located in the ASCII two-column file defined by filename. dN_r can represent either a number density distribution (i.e. dN(r)/dr) or a volume density distribution defined as dV(r)/dln(r). In the latter case, the routine computes internally the conversion:

$$\frac{dN(r)}{dr} = \frac{dV(r)}{dln(r)} \cdot \frac{1}{V(r)} \cdot \frac{dln(r)}{dr} \tag{1.6}$$

$$= \frac{dV(r)}{dln(r)} \cdot \frac{3}{4 \cdot \pi r^3} \cdot \frac{1}{r} \tag{1.7}$$

$$= \frac{dV(r)}{dln(r)} \cdot \frac{1}{4.18879 \cdot r^4} \tag{1.8}$$

Routine outputs are exactly the same as in table 1.8.

1.5 Reference cases

Reference cases are defined in order to compare results coming from the different tools, both for single particle and particle distribution conditions.

1.5.1 Single particle

Table 1.10 reports the definition of the reference case for a single particle.

Single Particle Reference Case		
Parameter	Value	Note
R_{ind}	$1.33 - 10^{-5}i$	Refractive Index
λ	0.5 μm	Wavelength
X_x	1.	Size Factor
r_{par}	0.0795775 μm	Particle radius

Table 1.10: Single Particle Reference Case

Three methods are used to retrieve aerosol parameters:

- MIEV routine

  routine : AER_MIEV_RUN (in AER_MIEV.pro)
  batch : aer_miev_sing.bat

- LibRadtran 'mie' routine

  routine : AER_MIE_RUN (in AER_MIE.pro)
  batch : aer_mie_sing.bat

- AOPP routine

  routine : mie_single (in mie_single.pro)
  batch : aer_aopp_sing.bat

Single Particle Case Results				
Tool used	Q_{ext}	Q_{sca}	SSA	Reference
MIEV	0.0939500	0.0939200	0.999681	aer_miev.bat
Mie	0.0939500	0.0939214	0.999696	aer_mie_sing.bat
AOPP	0.0939519	0.0939239	0.999694	aer_aopp_sing.bat

Table 1.11: Single Particle Case Results

Table 1.11 shows the expected good agreement of the results computed using the three tools MIEV, Mie-LibRadtran and AOPP, while Figure 1.3 displays the scattering phase functions.

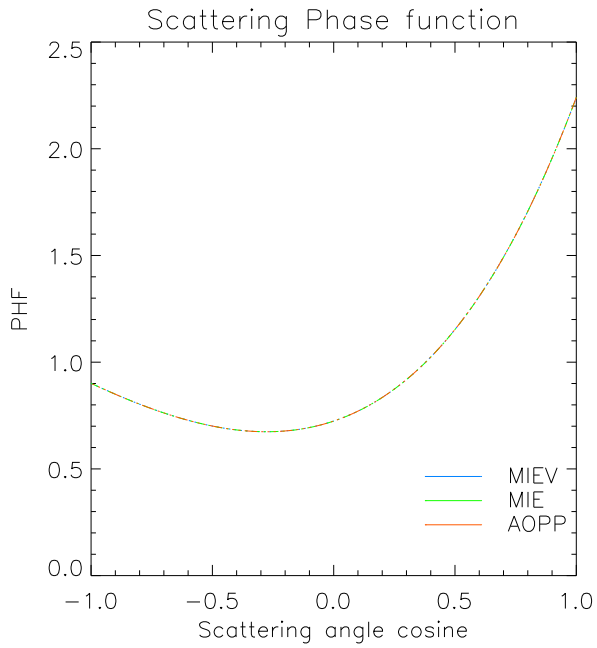

Figure 1.3: Single particle reference case - phase functions. The 3 curves are indistinguishable.

1.5.2 Particle Size Distribution

As a reference case for a particle size distribution, the SOOT component from OPAC dataset is chosen (see Hess et al. 1998). OPAC aerosol type definition is in Table 1.12.

SOOT component from OPAC		
Parameter	Value	Note
R_{ind}	$1.75 - 0.45i$	Refractive Index
R_m	0.0118 μm	Median radius
R_{min}	0.005 μm	Minimum radius
R_{max}	20.0 μm	Maximum radius
σ	2.00	Distribution width

Table 1.12: Particle Distribution Reference Case

Three methods are used to compute aerosol parameters:

- Mie-LibRadtran routine, reading from file the lognormal distribution, generated by AER_MIE_COMP_SIZE_DISTR. (see Appendix 4.3).

  routine : AER_MIE_RUN (in AER_MIE.pro)
  batch : aer_mie_dist.bat

- AOPP mie_lognormal routine

  routine : mie_lognormal (in mie_lognormal.pro)
  batch : aer_AOPP_log.bat

- AOPP mie_sizedist routine reading the lognormal distribution from file, as above.

  routine : mie_sizedist (in mie_sizedist.pro)
  batch : aer_AOPP_dist.bat

The results are displayed in table 1.13 and compared with values from literature, namely D'Almeida et al. (1991).

Soot component from OPAC - results					
Tool used	σ_{ext}	σ_{sca}	SSA	Asymm. fact.	Reference
Mie	7.151e-7	1.613e-7	0.2256	0.3531	aer_mie_dist.bat
AOPP lognormal	6.384e-7	1.441e-7	0.225749	0.3536	aer_aopp_log.bat
AOPP sizedist	7.156e-7	1.614e-7	0.2256	0.3531	aer_aopp_dist.bat
reference	6.384e-7	1.441e-7	0.2258	0.3536	d'Almeida

Table 1.13: Particle Distribution Results - range 0.005 to 20. micron. SSA is the single scattering albedo.

Note that both AAOP sizedist and Mie LibRadtran routines show a significant error on extinction and scattering coefficients, while ssa and asymmetry factor are almost correct. Both routines read the particle size distribution from an ASCII file, which contains particles densities **only** in the range 0.005 to 20 microns; the lower limit truncates about 10% of the particle distribution, which results in an erroneous over-weighting of the contributions between 0.005 and 20 microns. In other words, these two routines can be used only when the size range covers all the particle distribution, as shown in Table 1.14, where R_{min} is set to 0.001 μm.

Soot component from OPAC - results					
Tool used	σ_{ext}	σ_{sca}	SSA	Asymm. fact.	Reference
Mie	6.387e-7	1.441e-7	0.2257	0.3536	aer_mie_dist.bat
AOPP lognormal	6.386e-7	1.441e-7	0.2257	0.3536	aer_aopp_log.bat
AOPP sizedist	6.387e-7	1.441e-7	0.2257	0.3536	aer_aopp_dist.bat

Table 1.14: Particle Distribution Results - range 0.001 to 20 μm. SSA is the single scattering albedo.

1.6 Application Example - AERONET AAOT site

The routines described in this section have been used mainly to prepare aerosol properties datasets for radiative transfer computation.

Aerosol components defined in OPAC dataset (see Hess et al. 1998) are defined as lognormal distributions of particles having fixed complex refractive index, and their optical properties, including scattering phase function, are computed through mie_lognormal (see 1.5.2).

Another application, whose results are shown below, has been the computation of optical properties of aerosols measured at the AERONET Venise site, the Acqua Alta Oceanographic Tower (AAOT). The following properties have been retrieved form AERONET web-site http://aeronet.gsfc.nasa.gov/ for the period from July 1999 to October 2004, selecting level 2.0 data and Almucantar spherical particle model retrieval:

Aerosol properties retrieved			
Property	Param. number	Number of observations	Periodicity
Size Distribution	9	827	Daily average
Refractive index	10	259	Daily average
SSA	15	259	Daily average
Asymmetry factor	16	827	Daily average
Phase function	17	2934	All observations

Table 1.15: Aerosol properties retrieved for Venise AERONET site (AAOT)

We have identified observations for which all the properties above are available and disregarded the others. Size distribution and refractive index are provided as input to mie_sizedist routine, and aerosol properties in Table 1.8 computed.

The comparison of retrieved and re-computed quantities is shown in Figures 1.4 to 1.6.

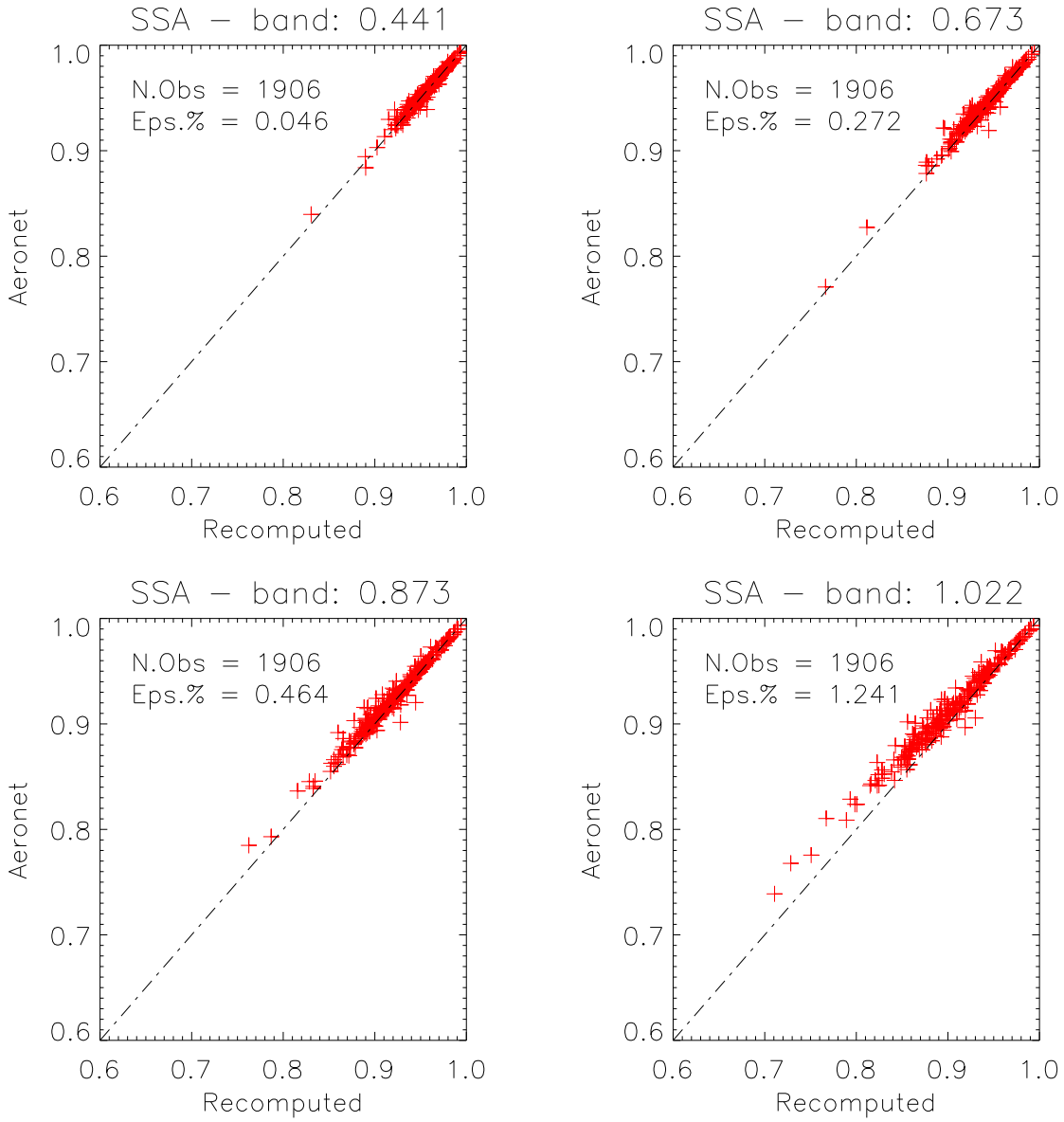

Figure 1.4: AERONET Venise site - Comparison between single scattering albedo provided by AERONET and that recomputed from the size distribution and refraction index. *Eps.*% is the mean relative absolute difference.

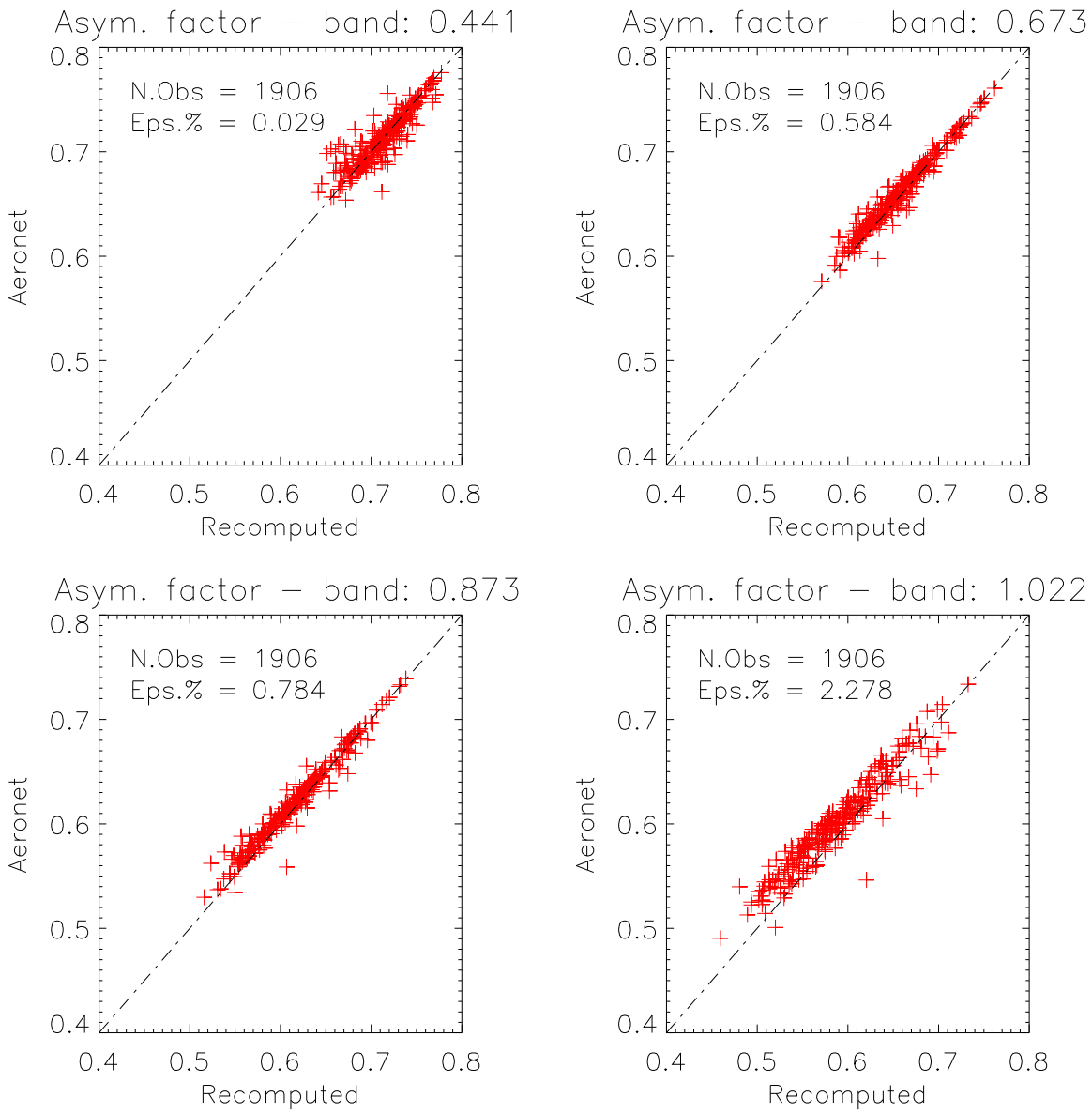

Figure 1.5: Same as Figure 1.4 for the asymmetry factor

Figure 1.6 displays scattering phase function for only one observation.

A general good agreement between retrieved and recomputed properties is found, with relative average error below 1%, for all bands but 1.022 μm.

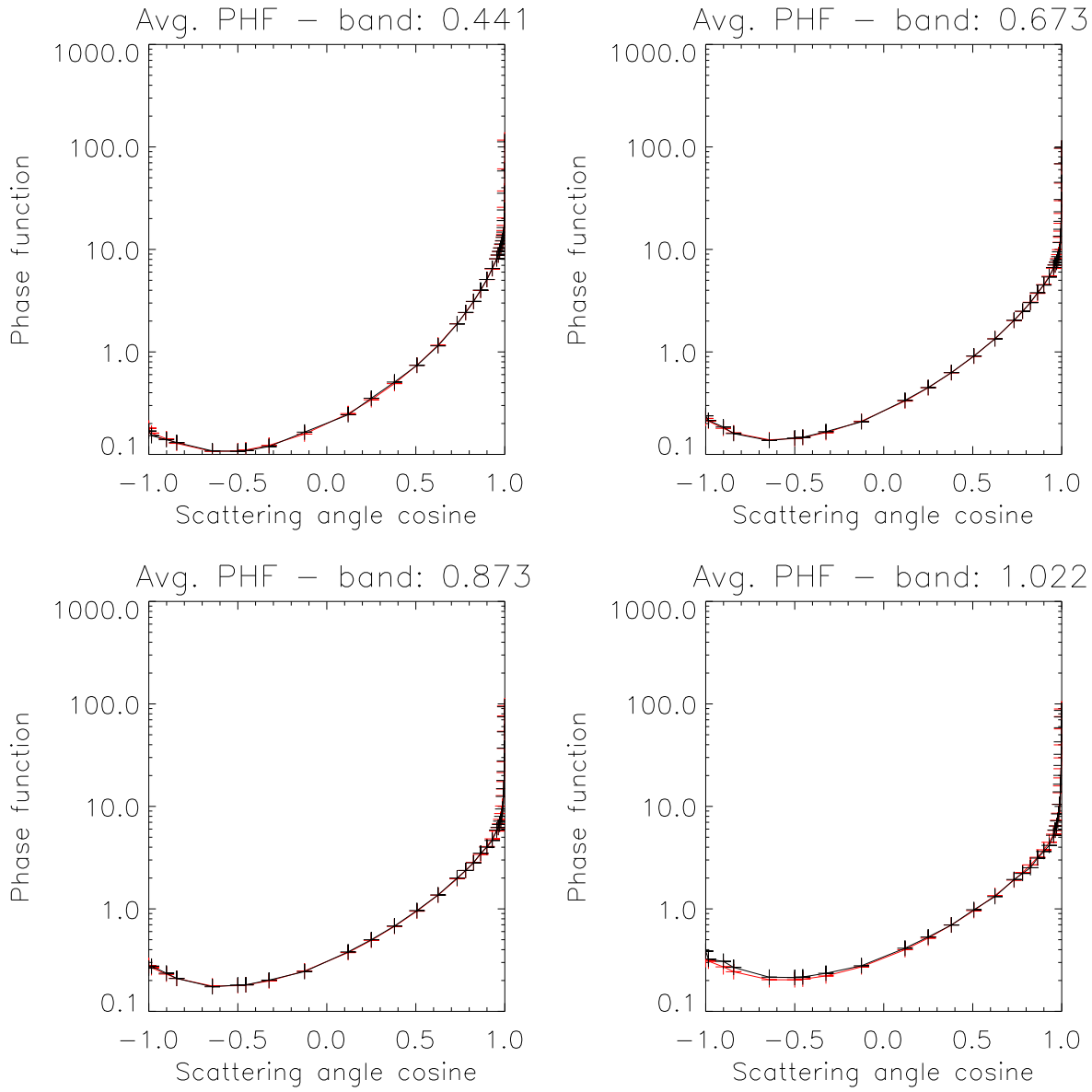

Figure 1.6: AERONET Venise site - Comparison between scattering phase function provided by AERONET and that recomputed from the size distribution and refraction index.

1.7 Notations and Units

1.7.1 Size distribution

Size distributions of aerosols have been modelled with different mathematical functions, like a Junge power law or the modified Gamma distribution (D'Almeida et al. 1991). The representation of the size distribution by several log-normal modes has also been found appropriate (e.g., O'Neill et al. 2000) and will be mostly adopted in this report. For spherical particles, if the number size distribution is log-normal, so are the surface and volume size distributions, with simple relationships between the modal radius and peak amplitude of the modes.

The general relationship for a multi-modal log-normal number size distribution is therefore:

$$\frac{dN}{dr} = \sum_{i=1}^{M} \frac{dN_i}{dr} = \sum_{i=1}^{M} \frac{N_i}{\sqrt{2\pi} r \ln \sigma_i} exp[-\frac{(\ln r - \ln r_{n,i})^2}{2(\ln \sigma_i)^2}] \tag{1.9}$$

where M is the number of modes, $r_{n,i}$ is the modal radius of the number size distribution for the mode i, σ_i is the geometrical standard deviation of the mode i. σ is often directly considered as $\ln \sigma$ or $\log \sigma$ (in which case it is necessary to specify which logarithmic base was used). Alternatively, this equation can be written as:

$$\frac{dN}{d \ln r} = \sum_{i=1}^{i=M} \frac{N_i}{\sqrt{2\pi} \ln \sigma_i} exp[-\frac{(\ln r - \ln r_{n,i})^2}{2(\ln \sigma_i)^2}] \tag{1.10}$$

The surface and volume size distributions are also written according to the same formalism:

$$\frac{dS}{d \ln r} = \sum_{i=1}^{i=M} \frac{S_i}{\sqrt{2\pi} \ln \sigma_i} \exp[-\frac{(\ln r - \ln r_{s,i})^2}{2(\ln \sigma_i)^2}] \tag{1.11}$$

$$\frac{dV}{d \ln r} = \sum_{i=1}^{i=M} \frac{V_i}{\sqrt{2\pi} \ln \sigma_i} \exp[-\frac{(\ln r - \ln r_{v,i})^2}{2(\ln \sigma_i)^2}] \tag{1.12}$$

and the relationship between number, surface and volume radii r_n, r_s and r_v (or alternatively in terms of diameter D) is:

$$\ln r_n = \ln r_s - 2 \ln^2 \sigma = \ln r_v - 3 \ln^2 \sigma \tag{1.13}$$

Equivalently, r_v is simply expressed as:

$$r_v = r_n \exp(3 \ln^2 \sigma) \tag{1.14}$$

Similarly, the volume amplitude of the mode i V_i can be expressed as a function of the number amplitude N_i, by ingesting Equation 1.14 into $dV/d \ln r = 4\pi r^3/3 . dN/d \ln r$:

$$V_i = \frac{4\pi}{3} r_{n,i}^3 N_i \exp(\frac{9 \ln^2 \sigma_i}{2}) \tag{1.15}$$

The total volume concentration C_V would then be written as:

$$C_V = \int_{r_{min}}^{r_{max}} \frac{dV(r)}{d \ln r} d \ln r \tag{1.16}$$

One can estimate the characteristics of the various modes by the following formula:

$$\ln r_v = \frac{\int_{r=r_1}^{r_2} \ln r \frac{dV(r)}{d\ln r} d\ln r}{\int_{r=r_1}^{r_2} \frac{dV(r)}{d\ln r} d\ln r} \tag{1.17}$$

$$\ln \sigma = \sqrt{\frac{\int_{r=r_1}^{r_2} (\ln r - \ln r_{v,i})^2 \frac{dV(r)}{d\ln r} d\ln r}{\int_{r=r_1}^{r_2} \frac{dV(r)}{d\ln r} d\ln r}} \tag{1.18}$$

where r_1 and r_2 are appropriately chosen.
Another quantity often reported is the effective radius defined as:

$$r_{eff} = \frac{\int_{r=0}^{\infty} r^3 \frac{dN}{dr} dr}{\int_{r=0}^{\infty} r^2 \frac{dN}{dr} dr} \tag{1.19}$$

1.7.2 Radiative characteristics

For a given particle of radius r, the extinction ("ext"), scattering ("sca") and absorption ("abs") efficiencies are noted Q_{ext}, Q_{sca} and Q_{abs}, respectively. The corresponding cross-section (in unit of surface, usually μm^2) is thus:

$$\sigma^{cs}_{ext,sca,abs}(\lambda, r, m) = Q_{ext,sca,abs}(\lambda, r, m) \cdot \pi r^2 \tag{1.20}$$

where the dependence is on wavelength λ, particle radius, and complex refractive index $m = n_r - in_i$.

The cross-section can be converted into extinction σ, usually expressed in km^{-1}. For a reference concentration of 1 particle per cm^3, it can be derived from σ^{cs} by considering a vertical column of 1 km with a section of 1 cm^2 and containing 1 particle per cm^3 (i.e., 10^5 particles in the column). The extinction coefficient can be computed from the ratio of the particle cross-section and the column width, multiplied by the total number of particles:

$$\sigma = \frac{\sigma^{cs}[cm^2]}{1cm^2} \cdot 10^5 particles \tag{1.21}$$

or:

$$\sigma = \frac{\sigma^{cs}[\mu m^2] \cdot 10^{-8}}{1cm^2} \cdot 10^5 particles = \sigma^{cs}[\mu m^2] \cdot 10^{-3} \tag{1.22}$$

Equation 1.22 is applied to AOPP routines by simply defining N_d as 10^{-3} in order to get an output in km^{-1}(particle·cm^{-3})$^{-1}$.

The *mie* tool from LibRadTran, when a size distribution is given as input, produces extinction coefficients σ_{ext} in km^{-1} per unit concentration of 1 g m^{-3}. We did some modifications to the routine mie_calc_sizedist in miecalc.c in order to compute the coefficients in km^{-1}(particle.cm^{-3})$^{-1}$, namely:

- particle radii and sections are computed in μm and μm^2 rather than m and m^2; particle volume is not needed anymore;
- the overall extinction coefficient, in km^{-1}(particle.cm^{-3})$^{-1}$, is computed as

$$\sigma_{ext} = \frac{\sum_{i=0}^{N} Q_{ext} n_i(r) \pi r_i^2 \Delta r_i}{\sum_{i=0}^{N} n_i(r) \Delta r_i} \cdot N_d \tag{1.23}$$

  where Δr_i is the i-th interval width, $n_i(r)$ is the particle number density, and N_d is set to 10^{-3} as above.

The modified routine mie_cal_sizedist is attached in Appendix 4.2.

In general, for an element of atmospheric column, the extinction, scattering and absorption coefficients σ, per unit of distance, can be expressed, for a complete size distribution, as follows:

$$\sigma_{ext,sca,abs}(\lambda) = \int_{r=r_{min}}^{r_{max}} \sigma^{cs}_{ext,sca,abs}(\lambda, r, m) \frac{dN}{d\ln r} d\ln r \tag{1.24}$$

In the rest of the report, other quantities will be used, the optical depth τ_a, the asymmetry factor g, and the single scattering albedo ω_0, defined as follows:

$$\tau_a(\lambda) = \int_{z=z_{min}}^{z_{max}} \sigma_{ext}(\lambda, z) dz \tag{1.25}$$

$$\omega_0(\lambda) = \frac{\sigma_{sca}(\lambda)}{\sigma_{ext}(\lambda)} \tag{1.26}$$

$$g(\lambda) = \frac{\int_{\theta=0}^{\pi} \cos\theta p(\lambda, \theta) d\cos\theta}{\int_{\theta=0}^{\pi} p(\lambda, \theta) d\cos\theta} \tag{1.27}$$

where p is the scattering phase function.

In turn, the spectrum of optical thickness can be approximated by the Ångström law (Ångström 1964):

$$\tau_a(\lambda) \simeq \beta\lambda^{-\alpha} \tag{1.28}$$

where β and α are the Ångström coefficient and exponent, respectively. These values are usually obtained by considering τ_a directly between 2 wavelengths or calculating a linear regression of the log-transformed data in a particular spectral range. It is emphasized that the choice of the spectral range used to compute α strongly influences its value. Also, this power law is sometimes a crude approximation and the spectrum of τ_a might be better represented by a second-degree polynomial expression (Eck et al. 1999, O'Neill et al. 2001).

Section 2

Aerosols size distributions and optical properties - Main types

A diverse suite of sensors and approaches have been applied for remote sensing of aerosols. King et al. (1999) give a complete review of remote sensing techniques used for the determination of their properties over land and ocean. Here, a few approaches applied to ocean surfaces using visible-to-near-infrared (NIR) radiances are briefly listed as illustrations. Two main groups of approaches can be arbitrarily considered: inversion methods aiming at determining the sea surface reflectance, and characterizing the aerosol component in the process, or approaches specifically aiming at determining the aerosol characteristics.

For the first category of approaches, Gordon (1997) provides a review of atmospheric correction of ocean color imagery. For a SeaWiFS (Sea-viewing Wide Field-of-view Sensor) type of sensor, Gordon and Wang (1994) use 2 channels in the NIR to choose a bracketing pair of aerosol models (from a predefined set), and calculate the single scattering aerosol radiance at the shorter wavelengths, and eventually, convert that into the multiple scattering path radiance ρ_{path} minus a hypothetical Rayleigh radiance in an aerosol free atmosphere. A null signature from the water in the NIR is one assumption. Other developments with various refinements or simplifications have been proposed (Wang and Gordon 1994a, Land and Haigh 1996, Ruddick et al. 2000, Siegel et al. 2000, Sturm and Zibordi 2002). Antoine and Morel (1999) describe a similar approach, that differs in the way the interactions between aerosols and molecules are formulated and the way the NIR channels are used: each aerosol model is associated with a relationship between the aerosol optical thickness and the ratio of path reflectance and pure Rayleigh reflectance. This is used at 775 and 865 nm, together with the assumption of null signature of the water, to constrain the choice of aerosol model. Absorbing aerosols can be detected using a third channel in the NIR (specific to MERIS, Medium Resolution Imaging Spectrometer) and 510 nm (assuming open ocean waters).

Other inversions techniques have been proposed to retrieve simultaneously water and aerosol properties, by minimizing a cost function quantifying the difference between LUT members and observed radiances. For instance, Gordon et al. (1997) aims at obtaining the aerosol model, aerosol optical thickness, *Chla* concentration and backscattering of hydrosols. Similarly, Chomko and Gordon (1998) index the aerosol characteristics by a Junge power-law exponent (determined by the NIR radiances, as well as the aerosol optical thickness at 865 nm) and simultaneously retrieve aerosol refractive index, pigment concentration and water surface backscattering. This has been further developed by Chomko and Gordon (2001) (spectral matching algorithm).

Stamnes et al. (2003) create a LUT using a radiative transfer code applied to the coupled atmosphere-ocean system. The problem is solved through an iterative process where, for the first iterations, the parameter $\epsilon(765,865)=\frac{\rho_{path}(765)-\rho_{ray}(765)}{\rho_{path}(865)-\rho_{ray}(865)}$ (with ρ_{ray} atmospheric reflectance for a pure Rayleigh atmosphere) is used to select the aerosol model, and the parameter $\gamma_{diff}(765,865)=\gamma(765)$-$\gamma(865)$, where $\gamma(\lambda)=\rho_{path}(\lambda)-\rho_{ray}(\lambda)$, is used to estimate $\tau_a(865)$. In the final iterations, the entire spectral range is used to find the simulations, members of the LUT, that match the observed top-of-atmosphere radiance. This yields the aerosol characteristics as well as *Chla*. There is no assumption with regards to the water leaving signal at 765 and 865 nm. The LUT includes only non or weakly absorbing aerosols.

Various works made use of data collected by AVHRR (Advanced Very High Resolution Radiometer) to derive the aerosol content. Among these, Rajeev et al. (2000) based their aerosol determinations around India with one AVHRR channel on the aerosol model of Satheesh et al. (1999) (i.e., developed on the basis of local measurements). Higurashi and Nakajima (1999) (or Higurashi et al. 2000) developed a two-channel aerosol algorithm for AVHRR (0.64 and 0.83 μm). In that case, the volume size distribution is assumed bi-modal with fixed characteristics for the 2 modes. The degrees of freedom are the ratio of small-to-large particle modes and the aerosol optical thickness. A LUT of pre-computed simulations yields the outputs that reproduce the observed radiances. The ocean surface signature is ignored. A similar approach by Nakajima et al. (1999) has been described for OCTS (Ocean Colour and Temperature Scanner). The scheme of Higurashi and Nakajima (1999) is completed for application to SeaWiFS with an extra constraint provided by the blue wavelengths (Higurashi and Nakajima 2002).

Tanré et al. (1997) use the spectral range 0.55-2.13 μm of MODIS (Moderate Resolution Imaging Spectroradiometer) to derive the spectral optical thickness, the fractional contribution of the accumulation mode to scattering, and the mean particle size of the dominant mode. This is done by minimizing a cost function applied to the members of a LUT. The LUT is composed of 5 small particle modes, and 6 large particle modes. The assumption is that the multiple scattering radiance resulting from the combination of 2 lognormal aerosol size distributions can be approximated by the weighted average of the radiance calculated for each mode. That restricts the tests to linear combinations of 11 sets of aerosol radiances (one for each mode). The boundary conditions are defined by ancillary data (using *Chla* and a simple bio-optical model).

Lee et al. (2004) focused on the determination of dust aerosol distribution for the ACE-Asia campaign from SeaWiFS data over land and ocean. The inversion scheme is based on an iterative process that requires a smooth non-linear spectrum of aerosol optical thickness and allows an adjustment of the surface spectral signature. A two-mode size distribution (fine and coarse particles) and a refractive index are fixed. Other similar developments are given by von Hoyningen-Huene et al. (2003) and Kokhanovsky et al. (2004).

Wang et al. (2003a) used geostationary remote sensing to study dust aerosols. Dust is specifically identified using a LUT constructed with a specified aerosol model. Similarly, Wang et al. (2003b) use ground measurements collected at various locations in the region of interest to constrain a one-channel inversion using GMS5 geostationary data during ACE-Asia (in practice, the ground measurements provide the spatial distribution of α, and the 2 modes of the size distribution are fixed based on field values).

Jamet et al. (2004) built a multi-layer perceptron neural network from a set of radiative transfer simulations that link aerosol optical thickness and Ångström exponent

with aerosol reflectance at the 3 longest SeaWiFS wavelengths. The aerosol reflectance spectrum is the SeaDAS derived reflectance corrected for pure Rayleigh scattering.

Specific characteristics of some sensors have been included in the inversion method, for instance by using the information provided by quasi-simultaneous multi-angular measurements (e.g., in the case of MISR, Multiangle Imaging Spectroradiometer, Wang and Gordon 1994b, Kahn et al. 2001) and/or polarized radiance measurements (POLDER, POlarization and Directionality of the Earth's Reflectances, Herman et al. 1997, Deuzé et al. 2000). Remote sensing in the ultraviolet spectral range has also served to produce distributions of aerosol properties (Torres et al. 1998, 2002).

As can be seen, there is a great diversity of inversion schemes, that depend on the sensor, the selection of spectral range and number of wavelengths (partly fixed by the sensor itself), that constrain the number of outputs, additional boundary conditions (for instance a black ocean in the NIR) or assumptions of particular spectral behaviors, and regional traits. Conversely, all obviously rely on a selection of aerosol candidate models. It is important to have a good knowledge of the techniques used, their advantages and weaknesses, and the assumptions that underlie them, in order to make the appropriate choices for the problem at hand. At the same time, a comprehensive view of the natural variability of the aerosol optical properties is required to ponder the representativeness of any given aerosol model.

The description of generic aerosol models is addressed in this Section, that gives a comprehensive description of some models derived from measurements or adopted for remote sensing projects. They are usually intended to cover all types of aerosols, or at least to contain enough variability to permit an inversion process. They include the models proposed by Shettle and Fenn (1979) and Hess et al. (1998), the aerosol models derived at key AERONET sites and considered representative of certain aerosol types (Dubovik et al. 2002) or resulting from statistical (clustering) analysis, the aerosol models adopted by the MODIS, MISR and TOMS projects for inversion purposes, and the synthesis of airborne measurements described by Osborne and Haywood (2005). They are completed by the literature review of the subsequent Section. In both sections, the notations are those introduced in Section 1.

(Note: For cloud screening, see Moulin et al. 1997, Moulin et al. 2001b, Martins et al. 2002, Wang et al. 2003a, Okada et al. 2003, Lee et al. 2004).

2.1 Shettle and Fenn models

Aerosol models listed by Shettle and Fenn (1979) (mono- or bi-modal):

Number size distribution:

RH %	Tropospheric	Maritime	Rural		Urban	
	r_n	r_n	$r_{n,1}$	$r_{n,2}$	$r_{n,1}$	$r_{n,2}$
0	0.02700	0.1600	0.02700	0.4300	0.02500	0.4000
50	0.02748	0.1711	0.02748	0.4377	0.02563	0.4113
70	0.02846	0.2041	0.02846	0.4571	0.02911	0.4777
80	0.03274	0.3180	0.03274	0.5477	0.03514	0.5805
90	0.03884	0.3803	0.03884	0.6462	0.04187	0.7061
95	0.04238	0.4606	0.04238	0.7078	0.04904	0.8634
98	0.04751	0.6024	0.04751	0.9728	0.05996	1.1691
99	0.05215	0.7505	0.05215	1.1755	0.06847	1.4858

Table 2.1: r in μm

Corresponding single scattering albedo:

RH %	Tropospheric	Maritime	Rural	Urban
0	0.9590	0.9820	0.9407	0.6382
50	0.9606	0.9835	0.9427	0.6484
70	0.9635	0.9870	0.9462	0.7026
80	0.9737	0.9936	0.9592	0.7805
90	0.9829	0.9955	0.9720	0.8422
95	0.9863	0.9968	0.9772	0.8852
98	0.9899	0.9980	0.9829	0.9240
99	0.9921	0.9986	0.9866	0.9421

Table 2.2: $\omega_0(550)$ for Shettle and Fenn (1979) models.

	Tropospheric	Maritime	Rural		Urban	
	r_n	r_n	$r_{n,1}$	$r_{n,2}$	$r_{n,1}$	$r_{n,2}$
N	1.	1.	0.999875	0.000125	0.999875	0.000125
r_n; ∼75% RH	0.03	0.3	0.03	0.5	0.03	0.5
σ	0.35	0.4	0.35	0.4	0.35	0.4

Table 2.3: r in μm; N in fraction; σ computed with decimal logarithm.

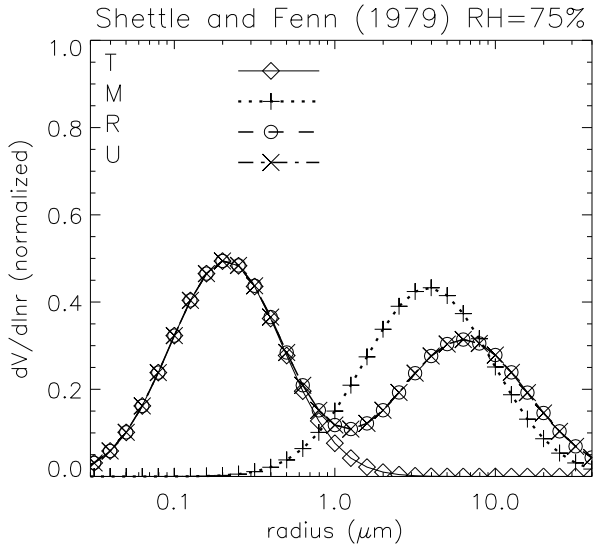

Figure 2.1: Size distribution for Tropospheric (T), Maritime Oceanic (M), Rural (R), and Urban (U) aerosol models by Shettle and Fenn.

2.2 Optical Properties of Aerosols and Clouds (OPAC)

Hess et al. (1998) made a synthesis of aerosol components and proposed a complete package of aerosol models, named OPAC (Optical Properties of Aerosols and Clouds). Aerosol types are mixtures of log-normally distributed components.

OPAC aerosol components and types:

Component	acronym	σ	r_n	r_v	r_{min}	r_{max}
Insoluble	INSO	2.51	0.471	6.00	0.005	20.0
Water soluble	WASO	2.24	0.0212	0.15	0.005	20.0
Soot	SOOT	2.00	0.0118	0.05	0.005	20.0
Sea salt (acc. mode)	SSAM	2.03	0.209	0.94	0.005	20.0
Sea salt (coa. mode)	SSCM	2.03	1.75	7.90	0.005	60.0
Mineral (nuc. mode)	MINM	1.95	0.07	0.27	0.005	20.0
Mineral (acc. mode)	MIAM	2.0	0.39	1.60	0.005	20.0
Mineral (coa. mode)	MICM	2.15	1.90	11.0	0.005	60.0
Mineral transported	MITR	2.20	0.50	3.0	0.02	5.0
Sulfate droplets	SUSO	2.03	0.0695	0.31	0.005	20.0

Table 2.4: r in μm, given for the dry state. r_{min} and r_{max} are the lower and upper limits of the aerosol size distribution, respectively.

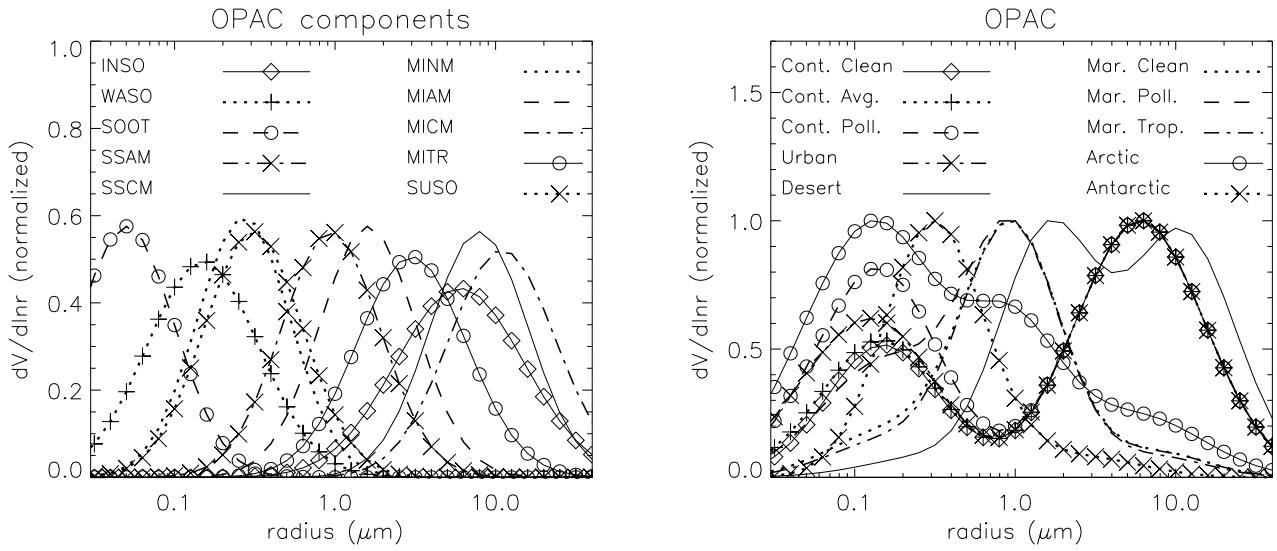

Figure 2.2: Size distribution for OPAC aerosol components and types.

Type	Acronym	Components	N	ω_0 550	g 550	α 350-500	α 500-800
Continental Clean	COCL	WASO INSO	1. 0.577E-4	0.972	0.709	1.10	1.42
Continental Average	COAV	WASO INSO SOOT	0.458 0.261E-4 0.542	0.925	0.703	1.11	1.42
Continental Polluted	COPO	WASO INSO SOOT	0.314 0.12E-4 0.686	0.892	0.698	1.13	1.45
Urban	URBA	WASO INSO SOOT	0.177 0.949E-5 0.823	0.817	0.689	1.14	1.43
Desert	DESE	WASO MINM MIAM MICM	0.87 0.117 0.133E-1 0.617E-4	0.888	0.729	0.20	0.17
Maritime Clean	MACL	WASO SSAM SSCM	0.987 0.132E-1 0.211E-5	0.997	0.772	0.12	0.08
Maritime Polluted	MAPO	WASO SSAM SSCM SOOT	0.422 0.222E-2 0.356E-6 0.576	0.975	0.756	0.41	0.35
Maritime Tropical	MATR	WASO SSAM SSCM	0.983 0.167E-1 0.217E-5	0.998	0.774	0.07	0.04
Arctic	ARCT	WASO INSO SSAM SOOT	0.197 0.152E-5 0.288E-3 0.803	0.887	0.721	0.85	0.89
Antarctic	ANTA	SUSO SSAM MITR	0.998 0.109E-2 0.123E-3	1.0	0.784	0.34	0.73
Free Troposphere *	FTRO	WASO INSO SOOT	0.6 0.17E-5 0.4	0.934	-	1.21	1.58
Stratosphere	STRA			1.0	-	0.74	1.14

Table 2.5: N mixing ratio. RH of 80%. (*): modeled components at RH 50%.

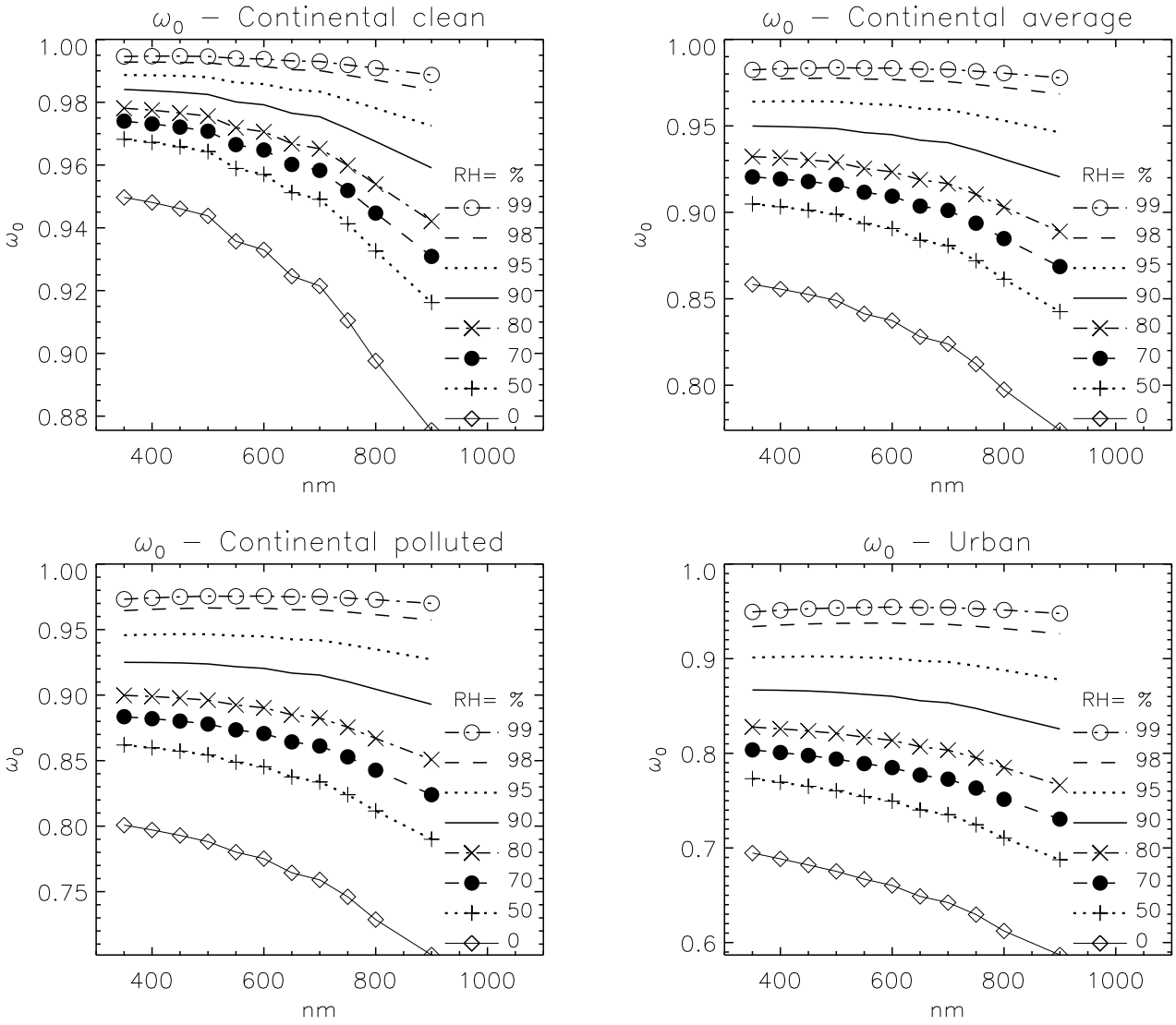

Figure 2.3: Spectral single scattering albedo for OPAC continental (COCL, COAV, COPO) and urban (URBA) types, as a function of relative humidity RH.

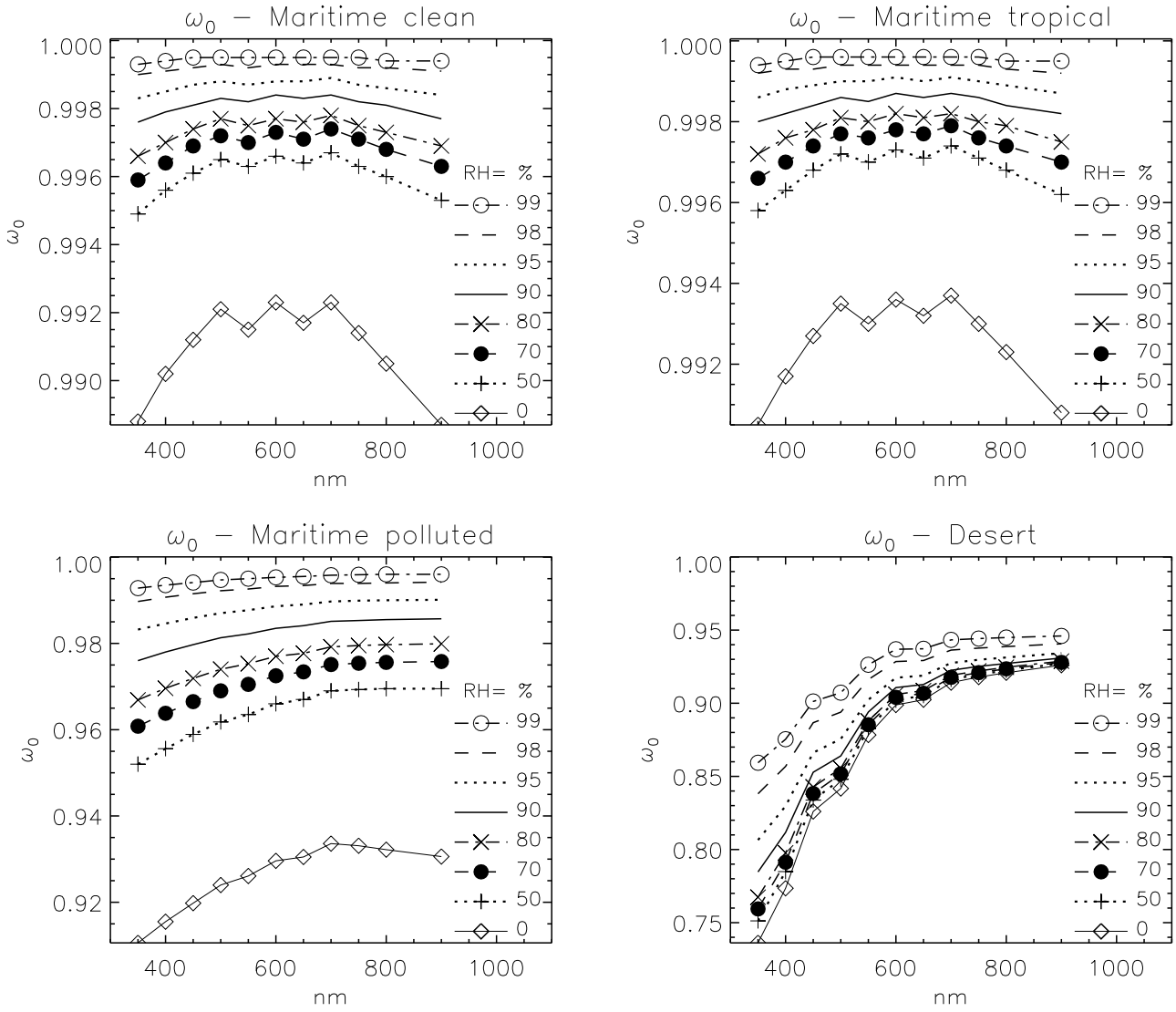

Figure 2.4: Spectral single scattering albedo for OPAC maritime (MACL, MATR, MAPO) and desert (DESE) types, as a function of relative humidity RH.

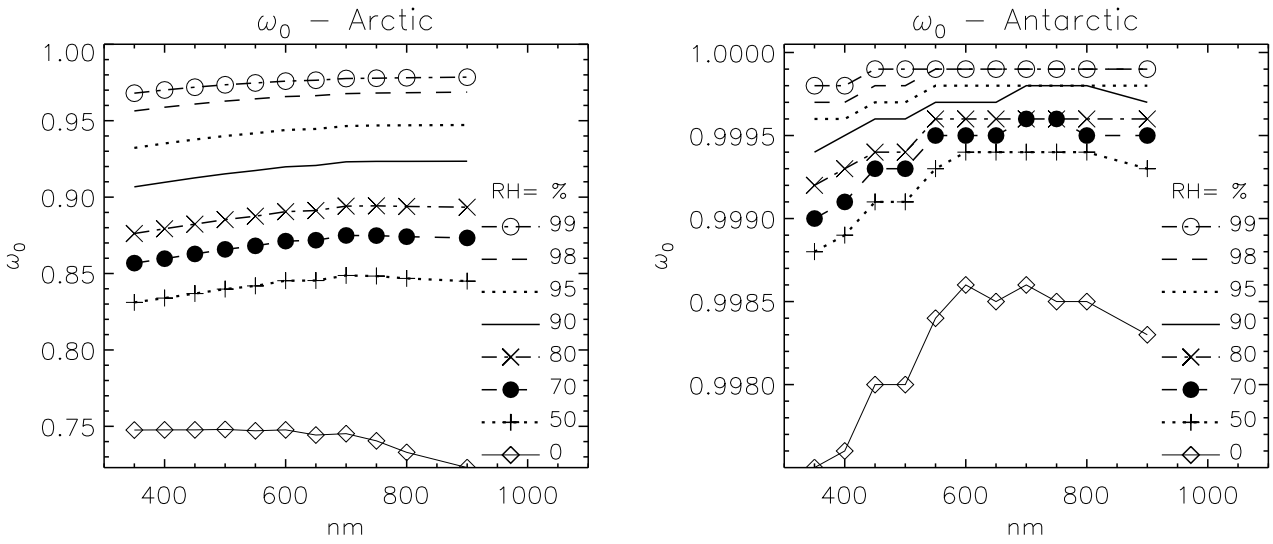

Figure 2.5: Spectral single scattering albedo for OPAC polar types (ARCT, ANTA), as a function of relative humidity RH.

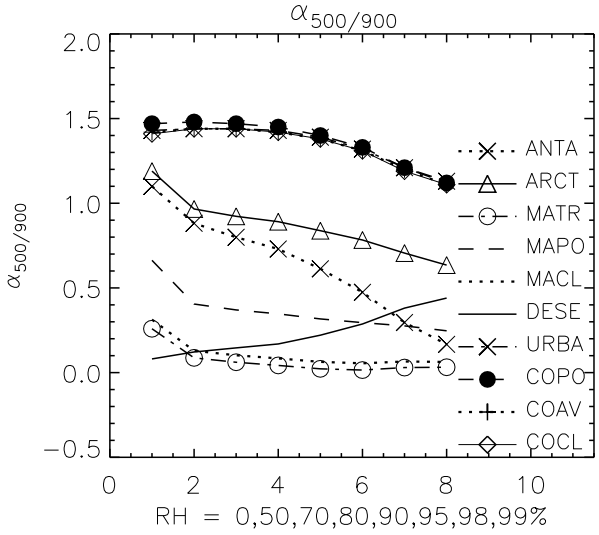

Figure 2.6: Ångström exponent α for OPAC aerosol types, as a function of relative humidity RH (the abscissa refers to categories of RH to show an even representation of the points). None of the OPAC types allows for a spectral dependence of the aerosol optical depth with α greater than $\sim$1.5.

2.3 AERONET derived generic types

- On the basis of AERONET measurements at key sites, Dubovik et al. (2002) proposed a set of aerosol models.

Region	τ_a	α	g	ω_0
Lanai	0.04 (1020nm)	0.0-1.55	0.75/0.71/0.69/0.68	0.98/0.97/0.97/0.97
HI	0.01-0.2		±0.04	±0.03
Greenbelt,	0.24 (440nm)	1.2-2.5	0.68/0.59/0.54/0.53	0.98/0.97/0.96/0.95
MD	0.1-1.0		±0.08	±0.02
Créteil,	0.26 (440nm)	1.2-2.3	0.68/0.61/0.58/0.57	0.94/0.93/0.92/0.91
France	0.1-0.9		±0.07	±0.03
Mexico	0.43 (440nm)	1.0-2.3	0.68/0.61/0.58/0.57	0.90/0.88/0.85/0.83
City	0.1-1.8		±0.07	± 0.02
Maldives	0.27 (440nm)	0.4-2.0	0.74/0.67/0.64/0.63	0.91/0.89/0.86/0.84
INDOEX	0.1-0.7		±0.05	± 0.03
Bahrain	0.22 (1020nm)	0.0-1.6	0.68/0.66/0.66/0.66	0.92/0.95/0.96/0.97
Persian G.	0.1-1.2		±0.04	±0.03
Solar Vil.	0.17 (1020nm)	0.1-0.9	0.69/0.66/0.65/0.65	0.92/0.96/0.97/0.97
Saudi A.	0.1-1.5		±0.04	±0.02
Capo Verde	0.39 (1020nm)	-0.1-0.7	0.73/0.71/0.71/0.71	0.93/0.98/0.99/0.99
	0.1-2.0		±0.04	±0.01
Amazon forest,	0.74 (440nm)	1.2-2.1	0.69/0.58/0.51/0.48	0.94/0.93/0.91/0.90
Brazil; Bolivia	0.1-3.0		±0.06	±0.02
South American	0.80 (440nm)	1.2-2.1	0.67/0.59/0.55/0.53	0.91/0.89/0.87/0.85
Cerrado	0.1-2.1		±0.03	±0.03
African savanna,	0.38 (440nm)	1.4-2.2	0.64/0.53/0.48/0.47	0.88/0.84/0.80/0.78
Zambia	0.1-1.5		±0.06	±0.015
Boreal forest,	0.40 (440nm)	1.0-2.3	0.69/0.61/0.55/0.53	0.94/0.935/0.92/0.91
U.S., Canada	0.1-2.0		±0.06	±0.02

Table 2.6: Optical characteristics of key AERONET sites. g and ω_0 are given at 440/670/870/1020 nm.

Region	n_r n_i	$r_{v,1}$ (μm) σ_1 V_1 ($\mu m^3/\mu m^2$)	$r_{v,2}$ (μm) σ_2 V_2 ($\mu m^3/\mu m^2$)
Lanai HI	1.36±0.01 0.0015±0.001	0.16±0.02 0.48±0.04 $0.40\tau_a(1020)$±0.01	2.70±0.04 0.68±0.04 $0.80\tau_a(1020)$±0.02
Greenbelt MD	1.41-$0.03\tau_a(440)$±0.01 0.003±0.003	0.21+$0.11\tau_a(440)$±0.03 0.38±0.01 $0.15\tau_a(440)$±0.03	3.03+$0.49\tau_a(440)$±0.21 0.75±0.03 0.01+$0.04\tau_a(440)$±0.01
Créteil France	1.40±0.03 0.009±0.004	0.11+$0.13\tau_a(440)$±0.03 0.43±0.05 0.01+$0.12\tau_a(440)$±0.04	2.76+$0.48\tau_a(440)$±0.30 0.79±0.05 0.01+$0.05\tau_a(440)$±0.02
Mexico City	1.47±0.03 0.014±0.006	0.12+$0.04\tau_a(440)$±0.02 0.43±0.03 $0.12\tau_a(440)$±0.03	2.72+$0.60\tau_a(440)$±0.23 0.63±0.05 $0.11\tau_a(440)$±0.03
Maldives INDOEX	1.44±0.02 0.011±0.007	0.18±0.03 0.46±0.04 $0.12\tau_a(440)$±0.03	2.62+$0.61\tau_a(440)$±0.31 0.76±0.05 $0.15\tau_a(440)$±0.04
Bahrain Persian G. Solar Vil. Saudi A. Capo Verde	1.55±0.03 0.0025/0.0014/ 0.001/0.001 ±0.001 1.56±0.03 0.0029/0.0013/ 0.001/0.001 ±0.001 1.48±0.05 0.0025/0.0007/ 0.0006/0.0006 ±0.001	0.15±0.04 0.42±0.04 0.02+$0.1\tau_a(1020)$±0.05 0.12±0.05 0.40±0.05 0.02+$0.02\tau_a(1020)$±0.03 0.12±0.03 0.49+$0.10\tau_a(1020)$±0.04 0.02+$0.02\tau_a(1020)$±0.03	2.54±0.04 0.61±0.02 -0.02+$0.92\tau_a(1020)$±0.04 2.32±0.03 0.60±0.03 -0.02+$0.98\tau_a(1020)$±0.04 1.90±0.03 0.63-$0.10\tau_a(1020)$±0.03 $0.9\tau_a(1020)$±0.09
Amazon forest Brazil; Bolivia South Amer. Cerrado Afr. savanna Zambia Boreal forest U.S., Canada	1.47±0.03 0.0093±0.003 1.52±0.01 0.015±0.004 1.51±0.01 0.021±0.004 1.50±0.04 0.0094±0.003	0.14+$0.013\tau_a(440)$±0.01 0.40±0.04 $0.12\tau_a(440)$±0.05 0.14+$0.01\tau_a(440)$±0.01 0.47±0.03 $0.1\tau_a(440)$±0.06 0.12+$0.025\tau_a(440)$±0.01 0.40±0.01 $0.12\tau_a(440)$±0.04 0.15+$0.015\tau_a(440)$±0.01 0.43±0.01 0.01+$0.1\tau_a(440)$±0.04	3.27+$0.58\tau_a(440)$±0.45 0.79±0.06 $0.05\tau_a(440)$±0.02 3.27+$0.51\tau_a(440)$±0.39 0.79±0.04 0.04+$0.03\tau_a(440)$±0.03 3.22+$0.71\tau_a(440)$±0.43 0.73±0.03 $0.09\tau_a(440)$±0.02 3.21+$0.2\tau_a(440)$±0.23 0.81±0.2 0.01+$0.03\tau_a(440)$±0.03

Table 2.7: Index of refraction n_r-in_i; and size distribution of aerosols at key AERONET sites.

NB: ω_0 and n_r-in_i computed for cases when α <0.6 and $\tau_{ext}(1020)$>0.3 for desert dust aerosols, when $\tau_a(440)$>0.4 for the other types.

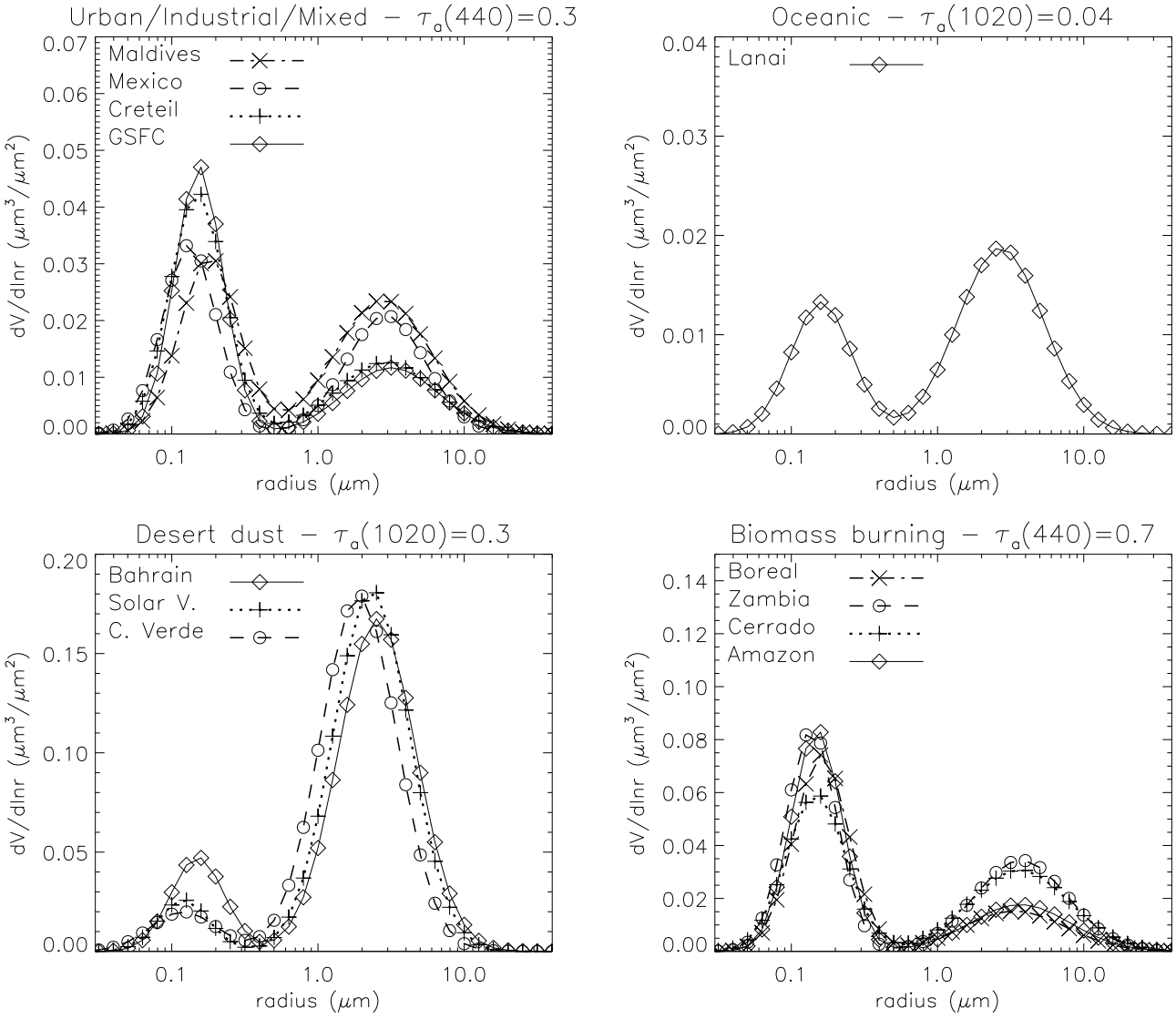

Figure 2.7: Size distribution for AERONET key sites. A value for τ_a is required for dynamic models.

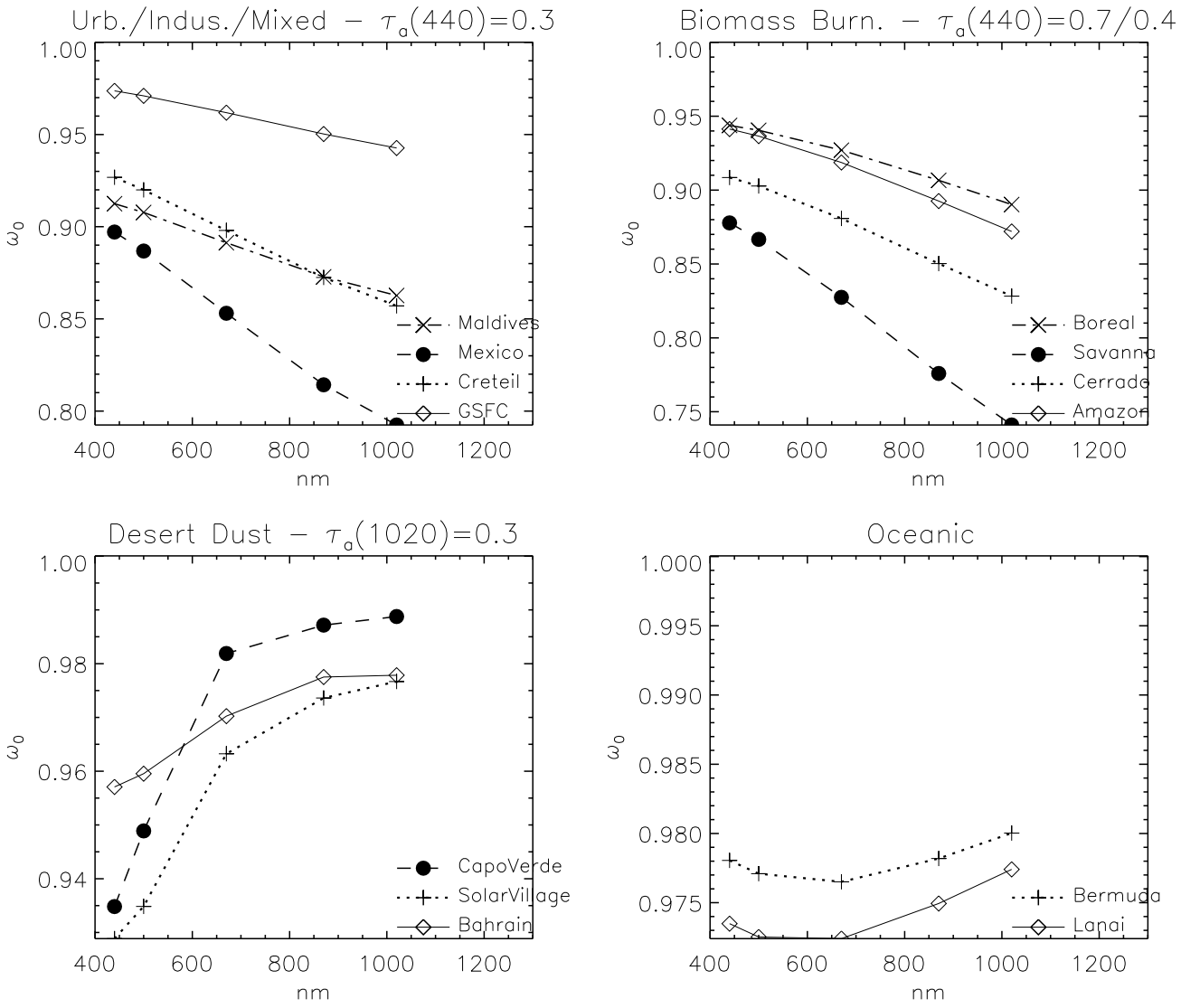

Figure 2.8: Spectral single scattering albedo for AERONET key sites. A value for τ_a is required for dynamic models. All sites are described in Dubovik et al. (2002), except the oceanic sites given in Smirnov et al. (2003a). The spectra has been computed from Mie calculations using the log-normal size distributions and indices of refraction defined above for the respective sites, and thus differ from the values tabulated.

- Omar et al. (2005): Derivation of aerosol types (6 categories) by cluster analysis using the global distribution of AERONET measurements. Categories are likely associated with desert/mineral dust (1), biomass burning (2), background/rural (3), polluted continental (4), polluted marine (5), dirty pollution (6).

Category	1	2	3	4	5	6
$\omega_0(673)$	0.93	0.80	0.88	0.92	0.93	0.72
$n_r(673)$	1.4520	1.5202	1.4494	1.4098	1.3943	1.4104
$n_i(673)$	0.0036	0.0245	0.0092	0.0063	0.0044	0.0337
$\tau_a(673)$	0.327	0.190	0.036	0.191	0.140	0.100
$\alpha(441/673)$	0.608	1.391	1.534	1.597	0.755	1.402
$g(673)$	0.668	0.603	0.580	0.612	0.711	0.594
$r_{v,1}$	0.117	0.144	0.133	0.158	0.165	0.140
σ_1	1.482	1.562	1.502	1.526	1.611	1.540
V_1	0.077	0.040	0.013	0.061	0.029	0.032
fine fraction (%)	22	33	38	53	26	49
$r_{v,2}$	2.834	3.733	3.590	3.547	3.268	3.556
σ_2	1.908	2.144	2.104	2.065	1.995	2.134
V_2	0.268	0.081	0.020	0.054	0.083	0.034

Table 2.8: n_r-in_i: refractive index; r in μm, V in $\mu m^3/\mu m^2$.

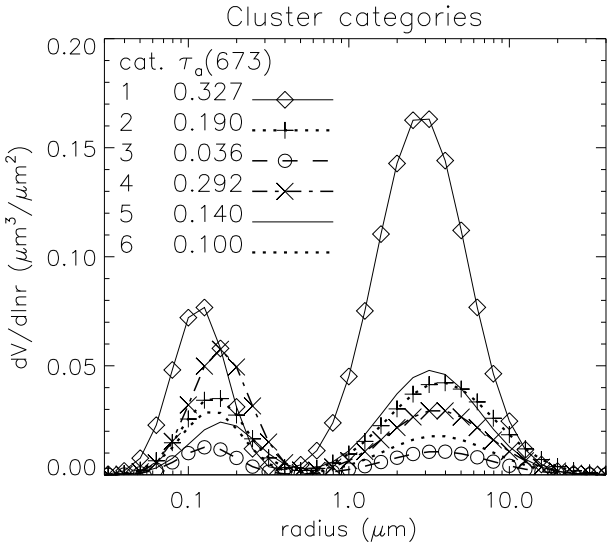

Figure 2.9: Mean size distribution for each cluster, and associated mean $\tau_a(673)$.

2.4 MODIS Aerosol models

- Tanré et al. (2001): 5 small particle (S) and 6 large particle (L) models for ocean calculations.

  Parameters of the number size distribution:

Model	r_{eff}	r_n	σ	n	$\omega_0(550)$	$g(550)$
S1	0.05	0.02	0.60	1.45-0.0035i	0.932	0.367
S2	0.10	0.04	0.60	1.45-0.0035i	0.969	0.588
S3	0.06	0.04	0.40	1.45-0.0035i	0.920	0.269
S4	0.20	0.08	0.60	1.40-0.0035i	0.976	0.720
S5	0.12	0.08	0.40	1.40-0.0035i	0.967	0.567
L1	0.98	0.40	0.60	1.40-0.0035i	0.938	0.764
L2	0.89	0.60	0.40	1.40-0.0035i	0.939	0.744
L3	1.48	0.60	0.60	1.45-0.0035i	0.905	0.763
L4	2.97	0.60	0.80	1.45-0.0035i	0.856	0.805
L5	2.46	1.0	0.60	1.50-0.0035i	0.857	0.799
L6	4.95	1.0	0.80	1.50-0.0035i	0.810	0.828

Table 2.9: n (index of refraction) taken constant spectrally. σ in natural logarithm.

- An update is given in Levy et al. (2003) and Remer et al. (2005):

Model	r_{eff}	r_n	σ	n_r	n_i 470	n_i 550	n_i 660	n_i 860
S1	0.10	0.07	0.40	1.45	0.0035	0.0035	0.0035	0.0035
S2	0.15	0.06	0.60	1.45	0.0035	0.0035	0.0035	0.0035
S3	0.20	0.08	0.60	1.40	0.0020	0.0020	0.0020	0.0020
S4	0.25	0.10	0.60	1.40	0.0020	0.0020	0.0020	0.0020
L1	0.98	0.40	0.60	1.45	0.0035	0.0035	0.0035	0.0035
L2	1.48	0.60	0.60	1.45	0.0035	0.0035	0.0035	0.0035
L3	1.98	0.80	0.60	1.45	0.0035	0.0035	0.0035	0.0035
L4	1.48	0.60	0.60	1.53	0.003	0.001	0.	0.
L5	2.50	0.50	0.80	1.53	0.003	0.001	0.	0.

Table 2.10: r in μm; n_r constant spectrally in the range 470-870 μm. σ in natural logarithm.

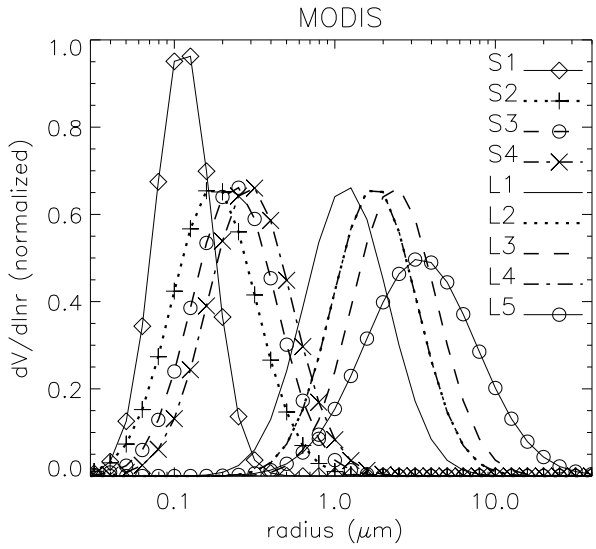

Figure 2.10: Size distribution for MODIS ocean aerosol components.

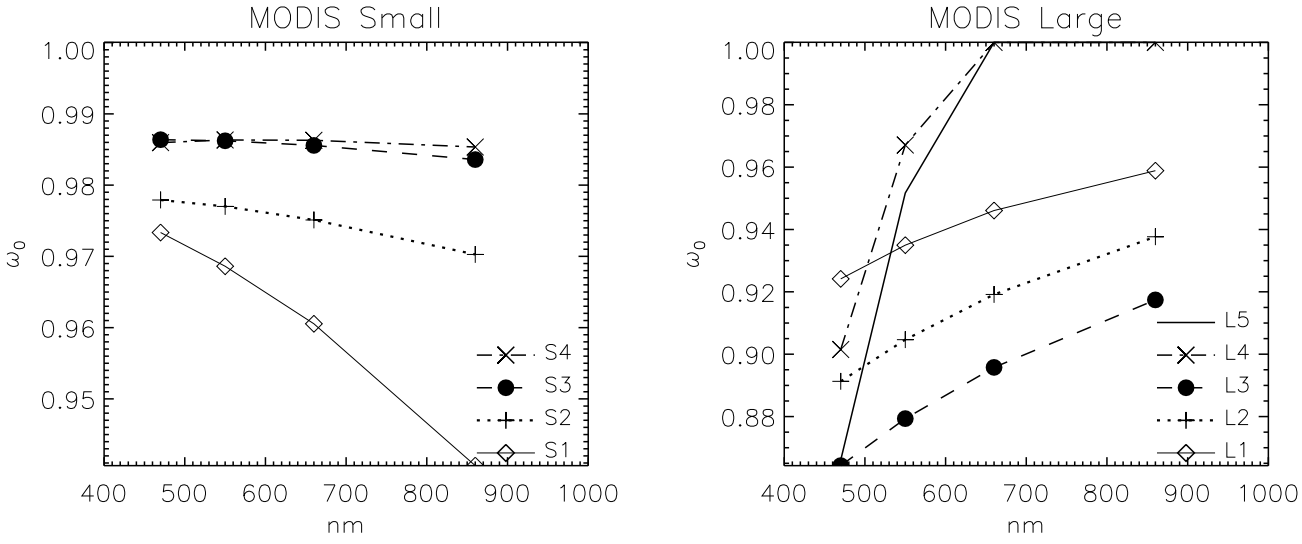

Figure 2.11: Spectral single scattering albedo for MODIS ocean aerosol components, small (S1-4) and large (L1-5). An aerosol mixture would have ω_0 weighted by contributions of a small mode and a large mode. The values have been computed by Mie calculations from the parameters defining size distributions and index of refraction.

Model	$\omega_0(470)$	$\omega_0(550)$	$\omega_0(660)$	$\omega_0(870)$	$\omega_0(1240)$	$\omega_0(1610)$	$\omega_0(2130)$
S1	0.9735	0.9683	0.9616	0.9406	0.8786	0.5390	0.4968
S2	0.9782	0.9772	0.9757	0.9704	0.9554	0.8158	0.8209
S3	0.9865	0.9864	0.9859	0.9838	0.9775	0.9211	0.9156
S4	0.9861	0.9865	0.9865	0.9855	0.9819	0.9401	0.9404
L1	0.9239	0.9358	0.9451	0.9589	0.9707	0.9753	0.9774
L2	0.8911	0.9026	0.9178	0.9377	0.9576	0.9676	0.9733
L3	0.8640	0.8770	0.8942	0.9175	0.9430	0.9577	0.9669
L4	0.9013	0.9674	1.0	1.0	1.0	1.0	1.0
L5	0.8669	0.9530	1.0	1.0	1.0	1.0	1.0

Table 2.11: Single scattering albedo for MODIS ocean aerosol models.

- Remer et al. (2005): aerosol models for land surfaces:

Mode	r_n	r_v	σ	V	$\omega_0(470)$	$\omega_0(660)$
continental						
water soluble	0.005	0.176	1.09	3.05	0.96	0.96
dust-like	0.50	17.6	1.9	7.364	0.69	0.69
soot	0.0118	0.050	0.693	0.105	0.16	0.16
urban/industrial						
accumulation 1	0.036	0.106	0.6	f1	0.96	0.96
accumulation 2	0.114	0.21	0.45	f2	0.97	0.97
coarse 1	0.99	1.3	0.3	f3	0.92	0.92
coarse 2	0.67	9.5	0.94	0.045	0.88	0.88
developing countries						
accumulation	0.061	0.13	0.50	f4	0.91	0.89
coarse	f5	f6	f7	f8	0.84	0.84
developing countries						
accumulation	0.061	0.13	0.50	f4	0.85	0.85
coarse	f5	f6	f7	f8	0.84	0.84
desert dust						
1	0.001	0.0055	0.755	6.0e-8	0.015	0.015
2	0.0218	1.230	1.160	0.01	0.95	0.95
3	6.24	21.50	0.638	0.006	0.62	0.62

Table 2.12: r in μm, V in μm^3 μm^{-2}, σ in natural logarithm. f1 = -0.015+0.51$\tau_a(660)$-1.46$\tau_a(660)^2$+1.07$\tau_a(660)^3$; f2 = 0.0038-0.086$\tau_a(660)$+0.90$\tau_a(660)^2$-0.71$\tau_a(660)^3$; f3 = -0.0012+0.031$\tau_a(660)$; f4 = -0.0089+0.31$\tau_a(660)$; f5 = 1.0-1.3$\tau_a(660)$; f6 = 6.0-11.3$\tau_a(660)$+61$\tau_a(660)^2$; f7 = 0.69+0.81$\tau_a(660)$; f8 = 0.024-0.063$\tau_a(660)$+0.37$\tau_a(660)^2$.

2.5 MISR Aerosol models

Kahn et al. (2005) described the following MISR early post-launch aerosol optical models:

Component	$r_{n,min}$	$r_{n,max}$	r_n	σ	r_{eff}	shape
1	0.001	0.4	0.03	1.65	0.06	small spherical
2	0.001	0.75	0.06	1.7	0.12	small spherical
3	0.01	1.5	0.12	1.75	0.26	medium spherical
4	0.01	4	0.24	1.87	0.57	large spherical
5	0.01	8	0.5	1.85	1.28	large spherical
6	0.05	2	0.47	2.6	1.18	medium dust low
7	0.05	2	0.47	2.6	1.18	medium dust high
8	0.5	15	1.9	2.6	7.48	coarse dust
9	0.001	0.5	0.012	2.0	0.04	black carbon

Table 2.13: r in μm. 'high' and 'low' refer to different vertical structures.

Component	$\omega_0(446)$	$\omega_0(446)$	$\omega_0(446)$	$\omega_0(446)$	$g(558)$
1	1.0	1.0	1.0	1.0	0.352
2	1.0	1.0	1.0	1.0	0.609
3	1.0	1.0	1.0	1.0	0.717
4	1.0	1.0	1.0	1.0	0.722
5	1.0	1.0	1.0	1.0	0.728
6	0.805	0.880	0.914	0.980	0.730
7	0.805	0.880	0.914	0.980	0.730
8	0.612	0.694	0.734	0.900	0.881
9	0.250	0.209	0.172	0.123	0.337

Table 2.14: Scattering properties for MISR aerosol models.

MISR early post-launch aerosol mixture properties:

mixture	type	1	2	3	4	5	6	7	8	9	$\omega_0(558)$	α
1	sph. s. clean	1.0	-	-	-	-	-	-	-	-	1.0	3.22
2	sph. s. clean	0.5	0.5	-	-	-	-	-	-	-	1.0	2.71
3	sph. s. clean	-	1.0	-	-	-	-	-	-	-	1.0	2.24
4	sph. s. clean	-	0.5	0.5	-	-	-	-	-	-	1.0	1.63
5	sph. m. clean	-	-	1.0	-	-	-	-	-	-	1.0	1.09
6	sph. m. clean	-	-	0.5	0.5	-	-	-	-	-	1.0	0.56
7	sph. m. clean	-	-	-	1.0	-	-	-	-	-	1.0	0.10
8	sph. m. clean	-	-	-	0.5	0.5	-	-	-	-	1.0	-0.05
9	sph. bim. clean	-	0.5	-	-	0.5	-	-	-	-	1.0	0.82
10	sph. bim. clean	0.5	-	-	-	0.5	-	-	-	-	1.0	1.19
11	sph. s. dirty	0.85	-	-	-	-	-	-	-	0.15	0.88	2.87
12	sph. s. dirty	0.45	0.4	-	-	-	-	-	-	0.15	0.88	2.50
13	sph. s. dirty	-	0.85	-	-	-	-	-	-	0.15	0.88	2.09
14	sph. s. dirty	-	0.45	0.4	-	-	-	-	-	0.15	0.88	1.62
15	sph. m. dirty	-	-	0.85	-	-	-	-	-	0.15	0.88	1.13
16	sph. m. dirty	-	-	0.45	0.4	-	-	-	-	0.15	0.88	0.71
17	sph. m. dirty	-	-	-	0.85	-	-	-	-	0.15	0.88	0.29
18	dusty low	-	-	0.75	-	-	0.25	-	-	-	0.97	0.72
19	dusty low	-	-	0.5	-	-	0.5	-	-	-	0.94	0.40
20	dusty low	-	-	0.25	-	-	0.75	-	-	-	0.91	0.13
21	dusty low	-	-	-	-	-	1.0	-	-	-	0.88	-0.11
22	dusty low	-	-	-	-	-	0.75	-	0.25	-	0.83	-0.08
23	dusty low	-	-	-	-	-	0.5	-	0.5	-	0.79	-0.06
24	dusty high	-	-	-	-	-	-	1.0	-	-	0.88	-0.11

Table 2.15: sph.: spherical, s.: small, m.: medium, bim.: bimodal.

2.6 TOMS Aerosols models

Aerosol models adopted for TOMS aerosol products (Torres et al. 2002):

Model	r_n	σ	r_{eff}	n_r-in_i 331	340	360	380	550
Sulfate	0.07	2.03	0.24	1.43 -0i	1.43 -0i	1.43 -0i	1.43 -0i	1.43 -0i
Carbon 1	0.08	1.45	0.10	1.55 -0.0150i	1.55 -0.0150i	1.55 -0.0150i	1.55 -0.0150i	1.55 -0.0150i
Carbon 2	0.08	1.45	0.10	1.55 -0.0350i	1.55 -0.0350i	1.55 -0.0350i	1.55 -0.0350i	1.55 -0.0350i
Carbon 3	0.08	1.45	0.10	1.55 -0.0550i	1.55 -0.0550i	1.55 -0.0550i	1.55 -0.0550i	1.55 -0.0550i
Dust 1	0.07	1.95	0.21	1.58 -0.0207i	1.58 -0.0196i	1.57 -0.0175i	1.58 -0.0150i	1.56 -0.0060i
Dust 1a	0.12	2.20	0.57	1.58 -0.0207i	1.58 -0.0196i	1.57 -0.0175i	1.58 -0.0150i	1.56 -0.0060i
Dust 2	0.25	2.20	1.13	1.58 -0.0207i	1.58 -0.0196i	1.57 -0.0175i	1.58 -0.0150i	1.56 -0.0060i
Dust 3	0.50	2.20	2.26	1.58 -0.0207i	1.58 -0.0196i	1.57 -0.0175i	1.58 -0.0150i	1.56 -0.0060i

Table 2.16: Number size distribution and spectral index of refraction (at wavelengths in nm) for TOMS aerosol models. r in μm.

2.7 Synthesis of airborne measurements

Osborne and Haywood (2005) using various airborne measurement campaigns (flights over water), during TARFOX (Tropospheric Aerosol Radiative Forcing Observational eXperiment, regional industrial pollution), northwest Atlantic), ACE-2 (Aerosol Characterization Experiment, northeast Atlantic - Canary Islands, regional industrial pollution / clean), SAFARI (South AFrican Aerosol Regional Science Initiative, southeast Atlantic, biomass burning), and SHADE (Saharan Dust Experiment, desert dust, Cape Verde).

Campaign	Mode	r_n	σ	N	ρ	RH	chem.	
TARFOX								
(i)	1	0.07(wet)	1.50	0.9969	1.304(wet)	80(wet)	H_2SO_4 OC	fresh,
		0.054(dry)			1.668(dry)	<30(dry)	BC, (water)	unproc.
	2	0.25(wet)	1.80	0.0020	1.304(wet)			
		0.192(dry)			1.668(dry)			
	3	0.70	2.20	0.0011	2.650		dust	
(ii)	1	0.10(wet)	1.31	0.9952	1.304(wet)	80(wet)		
		0.077(dry)			1.668(dry)	<30(dry)		
	2	0.25(wet)	1.41	0.0044	1.304(wet)		H_2SO_4 OC	aged,
		0.192(wet)			1.668(dry)		BC, (water)	unproc.
	3	0.70	2.10	0.0004	2.650		dust	
ACE-2								
polluted								
(i)	1	0.07	1.50	0.9984	1.487	55	$(NH_4)_2SO_4$ OC	fresh,
							BC, water	unproc.
	2	0.25	1.80	0.0014	1.487			
	3	0.75	2.20	0.0002	2.650		dust	
(ii)	1	0.09	1.40	0.9970	1.363	65	$(NH_4)_2SO_4$ OC	aged,
							BC, water	unproc.
	2	0.28	1.55	0.0020	1.363			
	3	0.75	1.90	0.0010	2.650		dust	
(iii)	1	0.13	1.25	0.9770	1.232	80	$(NH_4)_2SO_4$ OC	aged,
							BC, water	proc.
	2	0.25	1.60	0.0180	1.232			
	3	0.75	2.10	0.0050	1.215		sea salt	
clean								
(i)	1	0.11	1.30	0.813	1.205	80	$(NH_4)_2SO_4$ sea	aged
							salt, water	mar.
	2	0.53	2.53	0.187	1.215		sea salt, water	
(ii)	1	0.10	1.30	0.850	1.205	80	$(NH_4)_2SO_4$ sea	aged
							sea salt, water	mar.
	2	0.53	2.60	0.150	1.215		sea salt	
(iii)	1	0.09	1.35	0.868	1.205	80	$(NH_4)_2SO_4$ sea	aged
							salt, water	mar.
	2	0.53	3.10	0.132	1.215		sea salt	

Table 2.17: chem.: aerosol chemistry. (un)proc.: (un)processed (cycled through boundary layer clouds or not); mar.: maritime; OC: organic carbon; BC: black carbon. 'fresh' indicates aerosol having left the coast since a few hours; 'aged' indicates aerosol having left the coast since 24h or more; 'source region': indicates aerosols at most 1-2h old. r_n in μm, N in %, ρ in $g.m^{-3}$, RH in%.

Campaign	Mode	r_n	σ	N	ρ	RH	chem.	
SAFARI								
(i)	1	0.085	1.35	0.9963	1.350	<30	biomass	source region
	2	0.22	1.60	0.0033	1.350			
	3	1.0	2.20	0.0004	2.650		dust	
(ii)	1	0.12	1.30	0.9965	1.350	<30	biomass	aged unproc.
	2	0.26	1.50	0.0030	1.350			
	3	0.75	1.70	0.0005	2.650		dust	
SHADE								
	1	0.11	1.33	0.876	1.769	<30	sulphate	aged, unproc.
	2	0.28	1.50	0.108	2.650		dust	
	3	0.85	1.59	0.016	2.650			

Table 2.18: chem.: aerosol chemistry. (un)proc.: (un)processed (cycled through boundary layer clouds or not); mar.: maritime; OC: organic carbon; BC: black carbon. 'fresh' indicates aerosol having left the coast since a few hours; 'aged' indicates aerosol having left the coast since 24h or more; 'source region': indicates aerosols at most 1-2h old. r_n in μm, N in %, ρ in $g.m^{-3}$, RH in%.

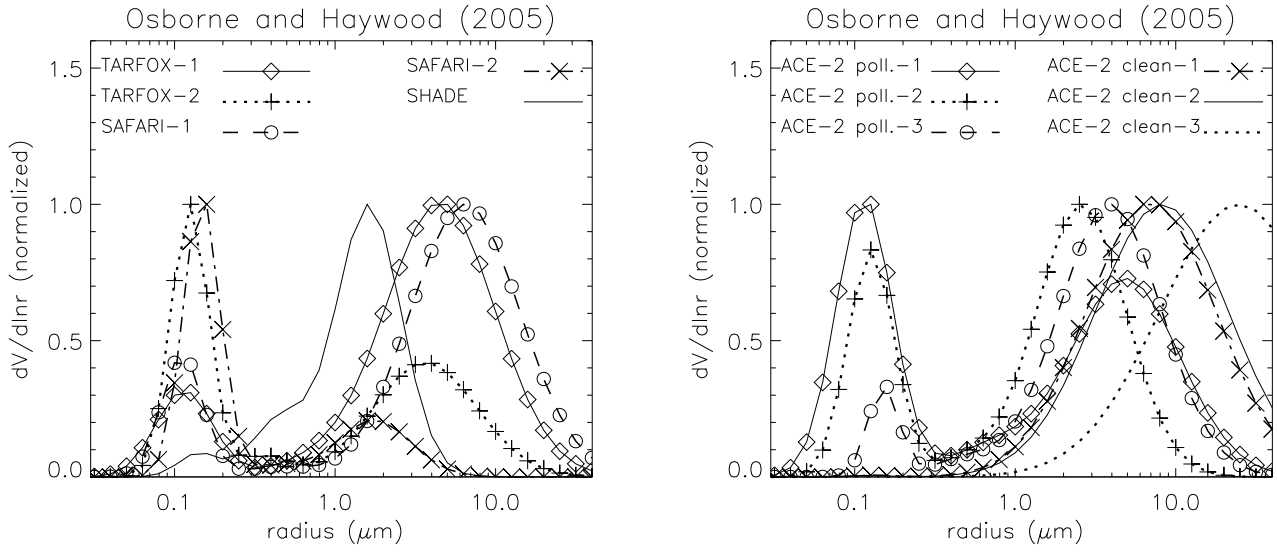

Figure 2.12: Size distribution for airborne measurements.

Campaign stage	mode	n_r-in_i	g	k_e	ω_0
TARFOX					
dry fresh unproc.	1	1.455-0.0225i	0.42	1.53	0.78
	2	1.455-0.0225i	0.76	2.75	0.85
	3	1.53-0.008i	0.83	0.19	0.73
dry aged unproc.	1	1.455-0.0225i	0.36	1.59	0.78
	2	1.455-0.0225i	0.75	4.44	0.89
	3	1.53-0.008i	0.87	0.41	0.68
wet fresh unproc.	1	1.388-0.0102i	0.52	3.41	0.89
	2	1.388-0.0102i	0.79	4.68	0.90
	3	1.53-0.008i	0.83	0.19	0.73
wet aged unproc.	1	1.53-0.0102i	0.50	3.66	0.90
	2	1.388-0.0102i	0.79	8.28	0.94
	3	1.53-0.008i	0.87	0.41	0.68
ACE-2 polluted					
fresh unproc.	1	1.512-0.0047i	0.52	3.36	0.97
	2	1.512-0.0047i	0.70	2.86	0.95
	3	1.53-0.008i	0.84	0.18	0.72
aged unproc.	1	1.512-0.0047i	0.54	5.06	0.97
	2	1.512-0.0047i	0.70	5.50	0.96
	3	1.53-0.008i	0.80	0.31	0.77
aged proc.	1	1.438-0.0045i	0.59	10.31	0.97
	2	1.438-0.0045i	0.70	8.89	0.96
	3	1.50-i.1e-8	0.76	2.12	0.99
ACE-2 clean					
aged proc.	1	1.53-1e-7.i	0.57	34.42	1.0
	2	1.34-2.3e-9.i	0.82	3.0	1.0
aged proc. +12h	1	1.53-1e-7.i	0.53	29.78	1.0
	2	1.512-0.0047i	0.83	2.62	1.0
aged proc. +24h	1	1.53-1e-7.i	0.52	28.29	1.0
	2	1.34-2.3e-9.i	0.85	1.01	1.0
SAFARI					
source region	1	1.54-0.025i	0.47	3.47	0.85
	2	1.54-0.025i	0.71	4.46	0.85
	3	1.53-0.008i	0.86	0.13	0.69
aged unproc.	1	1.54-0.018i	0.58	4.79	0.91
	2	1.54-0.018i	0.71	4.39	0.89
	3	1.53-0.008i	0.78	0.44	0.81
SHADE					
aged unproc.	1	1.53-1e-7.i	0.55	3.19	0.99
	2	1.53-0.0015i	0.67	1.64	0.98
	3	1.53-0.0015i	0.74	0.53	0.96

Table 2.19: Optical parameters at 550 nm. k_e is the mass-specific extinction coefficient.

Section 3

Aerosols size distributions and optical properties - A review

The present literature review focuses on publications that document the aerosol characteristics of interest for representing the aerosol optical properties, specifically, the aerosol size distribution, indices of refraction, single scattering albedo ω_0, asymmetry factor g, Ångström exponent α, or else (see Section 1 for a description of notations).

This document is more intended as a tool for future modelling efforts and a source of references and comparison easy to consult, and is certainly not exhaustive. The various descriptions presented can also be used to put the previous Section into perspective, with all sorts of actual measurements collected with several categories of instrumentations or methods, in different locations and conditions and for diverse aerosol types.

This Section is organized approximately on geographical grounds, with sub-sections describing measurements performed on oceanic conditions or pertaining to the global ocean, the Asian Pacific seaboard (in practice the northwest Pacific and adjacent lands), the northern Indian Ocean and adjacent lands (mainly India), the Atlantic as influenced by transport of dust from Africa, the Mediterranean basin, continental Europe, North America, and biomass burning aerosols in South America and Africa. As can be seen, this geographical distribution underlies a partition of the aerosol distributions by generic types (mixed aerosols from Asian deserts and cities in the Pacific northwest, the anthropogenic-influenced aerosols prevailing around India, particularly in part of the year, desert dust from Africa that can be transported as far as the Barbados, or the continental/urban aerosols of North America and western Europe).

Each of these parts also lists bibliographical references of interest for 3 topics not explicitly covered by this review, relationships that describe links between aerosol properties and relative humidity, interesting data documenting mass specific aerosol optical properties, and the direct radiative effect of aerosols obtained through various approaches (for general reviews also on this latter topic, see Haywood and Boucher 2000, or Satheesh and Moorthy 2005).

3.1 General oceanic

- Villevalde et al. (1994): measurements in the open Pacific (Dec. 1988-Mar. 1989) and North Atlantic oceans.

  α (least-square fit over the 461-1016 nm spectral range): 0.56 (-0.03 to 1.16) in the Pacific, 0.99 (0.29 to 1.31) in the North Atlantic.

  Geometric mean radius (derived from the optical measurements):
  fine mode: 0.08 μm, σ=1.70
  coarse mode: 1.0 μm, σ=1.20.

- Smirnov et al. (1995): α (least-square fit over the 461-1016 nm spectral range):

Air mass type	Area	α
Continental Polar	Pacific Ocean	0.82±0.14
	North Atlantic	1.27±0.14
Maritime Arctic	N. Atlantic	0.96±0.19
Maritime Polar	Pacific Ocean	0.52±0.35
Maritime Polar (modified)	N. Atlantic	1.23±0.11
Maritime Tropical	Pacific Ocean	0.42±0.23

Table 3.1: α as a function of air mass type.

- Quinn et al. (1996): RITS 93 and 94 cruises (north-south transects across the Pacific).
  Median diameter of the accumulation mode number size distribution: from 0.12 to 0.22 μm (σ from 1.37 to 1.57).

- Quinn et al. (1998): ACE-1, Nov.-Dec. 1995, south of Australia, surface measurements.
  Accumulation mode: geometric mean surface diameter D_s= 0.20 μm±20%, with total surface area concentration=6.5 $\mu m^2.cm^{-3}$±66%.
  Coarse mode: geometric mean surface diameter D_s= 1.0 μm±19%, with total surface area concentration=32 $\mu m^2.cm^{-3}$±62%.
  $\omega_0(550)\sim 0.99$.

- Quinn et al. (2000): surface shipboard measurements, ACE-1 (Nov.-Dec. 1995) and ACE-2 (Jun.-Jul. 1997):

Air mass origin	$\alpha^{(*)}$	$\omega_0(550)$
Atlantic	0.16±0.25	0.98±0.01
Polar Atlantic	0.32±0.26	0.97±0.02
Iberian Peninsula	1.0±0.39	0.95±0.03
Mediterranean	1.5±0.46	0.90±0.03
western Europe	1.1±0.26	0.96±0.02
ACE-1	-0.03±0.38	0.99±0.01

Table 3.2: Values at RH 55%; (*): =Ångström exponent computed on light scattering coefficients between 550 and 700 nm.

- Holben et al. (2001): sun photometry at Mauna Loa Observatory (Hawaii, 1996-1999): climatological monthly α (computed by linear regression between 440 and 870 nm) between 1.14 and 1.77 (annual mean: 1.50);
  Lanai (Hawaii, 1996-1999): climatological monthly α between 0.56 and 0.96 (annual mean: 0.71);
  Bermuda (1996-1999): climatological monthly α between 0.78 and 1.10 (annual mean: 0.92).

- Voss et al. (2001): sun photometry measurements during Aerosols99, cruise from Norfolk (Va, US) to Cape Town (South Africa), Jan.-Feb. 1999.

Region	$\tau_a(500)$	α
NH marine	0.09±0.02	0.27±0.28
African dust	0.29±0.05	0.36±0.13
Africa dust + BB	0.41±0.16	0.52
Biomass burning	0.36±0.13	0.88±0.30
SH marine tropics	0.10±0.03	0.45±0.20
SH marine temperate	0.10±0.01	0.35±0.07

Table 3.3: α computed with all available wavelengths. NH: North. Hemisphere, SH: South. Hemisphere, BB: biomass burning.

- Quinn et al. (2001): Surface ship measurements during Aerosols99, cruise from Norfolk (Va, US) to Cape Town (South Africa), Jan.-Feb. 1999.

Region	n_r		n_i		α	ω_0
	sub-μm	super-μm	sub-μm	super-μm		
N. America	1.51	1.42	2.3E-5	5.9E-5	0.64±0.41	
NH marine	1.45	1.44	6.3E-5	1.9E-5	-0.16±0.1	
African dust	1.54	1.47	3.9E-3	4.0E-4	-0.15±0.06	
Africa dust + BB	1.66	1.49	7.0E-2	1.1E-3	0.14±0.19	0.87±0.05
Biomass burning	1.69	1.46	5.8E-2	1.9E-4	0.71±0.21	0.79±0.04
SH marine tropics	1.57	1.44	5.4E-5	2.7E-5	0.26±0.19	
SH marine temperate	1.58	1.44	1.8E-4	1.0E-5		

Table 3.4: Values at RH 55%. sub-μm: D_{aero}<1.1μm, 1.1μm<D_{aero}<10μm. Ångström exponent computed from surface scattering coefficients at 450 and 700 nm. ω_0 from surface measurements at 550 nm. Values at 55% RH. NH: North. Hemisphere, SH: South. Hemisphere, BB: biomass burning.

Surface area size distribution (at 55% RH):

Region		Accumulation	Coarse 1	Coarse 2
N. America	S	84±23	39±20	48±14
	D_s	0.25±0.01	0.8±0.07	2.8±0.19
	σ	1.4±0.03	1.8±0.48	1.6±0.11
NH marine	S	8±2	28±12	47±17
	D_s	0.22±0.03	1.2±0.35	2.7±0.28
	σ	1.4±0.11	2.1±0.52	1.7±0.15
African dust	S	11±2	50±16	82±17
	D_s	0.18±0.01	0.9±0.16	2.1±0.11
	σ	1.4±0.03	1.9±0.22	1.6±0.06
Africa dust + BB	S	52±9	78±17	
	D_s	0.27±0.01	1.7±0.04	
	σ	1.7±0.08	1.7±0.02	
Biomass burning	S	52±13	17±6	
	D_s	0.27±0.01	1.8±0.09	
	σ	1.5±0.03	1.7±0.06	
SH marine tropics	S	19±6	27±10	
	D_s	0.3±0.02	2.1±0.08	
	σ	1.5±0.07	1.9±0.07	
SH marine temperate	S	24±4	53±7	
	D_s	0.25±0.01	2.4±0.11	
	σ	1.3±0.03	2.1±0.13	

Table 3.5: Values at RH 55%. S in $\mu m^2.cm^{-3}$, D_s in μm. NH: North. Hemisphere, SH: South. Hemisphere, BB: biomass burning.

- Smirnov et al. (2003b): Midway Island, Pacific; AERONET measurements Jan. 2001-Feb. 2002.
  Modal value of α: ~ 0.40 (almost all values below 1). Volume size distribution: 2 modes (0.10-0.11, 2.5-3.0 μm).

- Smirnov et al. (2003a): complete description of maritime aerosols using sun photometry measurements at Bermuda, Lanai (Hawaii) and Kaashidhoo (Maldives).
  Refractive index estimated at 1.37-0.001i, $\omega_0 \sim 0.98$ (spectrally independent).
  Volume size distribution:

Site	Lanai	Bermuda	Kaashidhoo
V_1	0.010	0.017	0.012
$r_{v,1}$	0.123	0.124	0.164
σ_1	0.42	0.41	0.48
$r_{eff,1}$	0.113	0.114	0.146
V_2	0.039	0.047	0.044
$r_{v,2}$	2.78	2.44	2.62
σ_2	0.73	0.77	0.79
$r_{eff,1}$	2.13	1.81	1.92

Table 3.6: V in $\mu m^3/\mu m^2$, r_v in μm.

- Okada et al. (2004): Tropical western Pacific, Jun. 2000: α=0.01-0.16, n_r=1.34-1.38 (no significant imaginary part).

- Park et al. (2004): surface measurements at the South Pole during ISCAT (Investigation of Sulfur Chemistry in the Antarctic Troposphere), Dec. 1998 and 2000.
  Size distribution with number, surface and volume mean diameter:

Date	N	S	V	D_n	D_s	D_v
Dec. 1998	190±44	3.6±0.8		66±8	100±11	
25 Nov.-18 Dec. 2000	215±150	3.5±1.9	0.09±0.07	61±13	150±26	237±55
19-27 Dec. 2000	116±18	7.8±1.1	0.49±0.08	98±10	380±20	540±200

Table 3.7: N in cm^{-3}, S in $\mu m^2.cm^{-3}$, V in $\mu m^3.cm^{-3}$, D in nm.

Mass specific optical properties: Quinn et al. (1996), Quinn et al. (1998), Maring et al. (2000), Quinn et al. (2001).

Radiative forcing: Kiehl and Briegleb (1993), Sokolik and Toon (1996), Haywood et al. (1999), Boucher and Tanré (2000), Christopher and Zhang (2002), Weaver et al. (2002), Chou et al. (2002), Bellouin et al. (2003), Kinne et al. (2003), Yu et al. (2003, 2004), Miller et al. (2004), Zhang et al. (2005), Reddy et al. (2005), Treffeisen et al. (2005) (for the Arctic).

3.2 Asian Pacific seaboard

- Holben et al. (2001): sun photometry at Dalanzadgad (Mongolia, 1997-2000): climatological monthly α (computed by linear regression between 440 and 870 nm) between 0.58 and 1.82 (annual mean: 1.14).

- Chun et al. (2001): measurements in Korea, May 1998, of dust events. α between 0.3 and 0.6.

- Sano et al. (2003):
  sun photometry at Amami-Oshima Island (south of Japan) in Dec. 2000: α between 0.5 and 1.5,
  sun photometry at the islands of Noto, Shirahama and Amami-Oshima in April 2001: α of 0.76, 0.80, 0.66, respectively, as averaged over the days of dust events, 1.3, 1.2, 0.95, respectively, as averaged over the dust free days.

- Wang et al. (2003b): ACE-Asia, Apr. 2001.
  Volume size distribution fitted to a bi-lognormal distribution, with 2 modes at 0.18 μm (σ=2.16) and 1.74 μm (σ=1.78).

- Quinn et al. (2004): ACE-Asia, ship-based measurements, spring 2001. Two size ranges are considered, sub- and super-micron.

Region / Air mass	submicron				supermicron			
	S	D_s	V	D_v	S	D_s	V	D_v
Polluted - Korea/Japan	170±60	0.32	9±3.2	0.40	26±15	1.4	11±6.5	2.5
Polluted - Japan	340±67	0.28	17±3.3	0.45	33±12	1.4	13±5.5	2.8
Volcano + Polluted	490±120	0.32	29±10	0.45	16±2	2.0	6±0.62	2.5
Dust - Frontal	490±150	0.45	33±11	0.50	130±45	2.0	47±16	2.5
Dust - Korea	240±49	0.32	11±2.7	0.50	91±54	2.0	38±22	2.8
Dust + Shanghai	310±51	0.22	15±2.7	0.45	105±45		41±17	2.5

Table 3.8: Particle surface area and volume concentration; S in $\mu m^2.cm^{-3}$, V in $\mu m^3.cm^{-3}$, D_s and D_v in μm. Values converted to 55% RH.

Region / Air mass	submicron	supermicron
Polluted - Korea/Japan	1.48(±0.01)-0.02(±0.01)i	1.48(±0.01)
Polluted - Japan	1.49(±0.01)-0.02(±0.02)i	1.51(±0.01)-0.02(±0.01)i
Volcano + Polluted	1.48(±0.005)-0.01(±0.01)i	1.50(±0.03)-0.01(±0.01)i
Dust - Frontal	1.50(±0.02)-0.02(±0.01)i	1.57(±0.01)-0.01(±0.01)i
Dust - Korea	1.55(±0.01)-0.02(±0.02)i	1.60(±0.02)-0.02(±0.01)i
Dust + Shanghai	1.49-0.03i	1.56-0.02i

Table 3.9: Regional averages of the refractive index of the bulk aerosol. Values converted to 55% RH.

$\omega_0(550)$ obtained during the measurement campaign:
marine region: 0.99±0.01 at ambient 75% RH (0.97±0.02 at 55% RH);
Polluted - Japan: 0.97±0.01 at ambient 89% RH (0.91±0.01 at 55% RH);
Dust - Frontal: 0.98±0.01 at ambient 86% RH (0.96±0.02 at 55% RH).

sun-photometer derived α (linear regression): between 0.3 and 1.0.

- Lee et al. (2004): ACE-Asia, Apr. 2001, AERONET derived average volume size distribution from the sites of Beijing, Anmyun and Gosan:

  fine mode: r_v=0.12 μm, σ=0.49, V=24%
  coarse mode: r_v=2.56 μm, σ=0.64, V=76%
  (σ in natural logarithm).

- Kim et al. (2004): SKYNET sun-photometer measurements over 1997-2001 (period is site dependent).

  The retrieved single scattering albedo is written with a power-law spectral dependence:
  $\omega_0(\lambda) = \omega_0(550).\frac{\lambda}{550}^{-\alpha_\omega}$

	$\omega_0(550)$					α_ω				
Station	DJF	MAM	JJA	SON	An.	DJF	MAM	JJA	SON	An.
Mandalgovi	0.942	0.918	0.938	0.949	0.937	0.0434	0.0498	0.0493	0.0540	0.0491
Dunhuang	0.900	0.913	0.896	0.906	0.904	-0.0337	-0.0550	-0.0379	-0.0544	-0.0453
Yinchuan	0.914	0.905	0.914	0.920	0.913	0.0099	-0.0134	0.0338	0.0275	0.0145
Sri-Samrong	0.927	0.920	0.867	0.938	0.913	0.0655	0.0892	0.0040	0.0215	0.0451

Table 3.10: Average single scattering albedo and spectral dependence by season and site: Mandalgovi (Mongolia), Dunhuang (Gansu), Yinchuan (Ningxia), Sri-Samrong (Thailand).

Volume size distribution:
fine mode at Mandalgovi ∼0.1 to 0.2 μm; at Dunhuang, only a coarse mode, ∼3-5 μm; at Yinchuan, fine and coarse modes at ∼0.2 and 5 μm; at Sri-Samrong, fine mode at ∼0.2 μm.

- Wang et al. (2004): Dunhuang, measurements by sun-photometers, 1999-2000. Overall monthly means α between 0.077 and 0.573 (overall mean 0.24), monthly means computed with the days of dust events between -0.096 and 0.239.

- Okada et al. (2004): south of Japan, Jul. 2000. α=0.92.

- Eck et al. (2005): Anmyon Island (Korea), volume size distribution derived from sun photometry for 2 years:
  for cases when α>0.75:
  fine (accumulation) mode radius increasing with τ_a from <0.2 μm to 0.25 μm
  coarse mode around 2.5 μm;
  ω_0 of 0.925-0.947 at 440 nm, 0.892-0.925 at 870 nm;
  for cases when α<0.75 (desert dust influence):

coarse mode radius of 2.1-2.9 μm (σ of 1.75-1.80).

Relationships with humidity: Carrico et al. (2003).

Mass specific optical properties: Quinn et al. (2004), Kim et al. (2005).

Radiative forcing: Conant et al. (2003), Seinfeld et al. (2004), Kim et al. (2005).

3.3 Northern Indian Ocean and adjacent lands

- Moorthy et al. (1997): cruise southwest of India, Jan.-Feb. 1996. For cases far offshore, the bi-modal number size distribution (with σ in natural logarithm) is on average centered on: $r_{n,1}$=0.042±0.01 μm (σ=0.48±0.1), $r_{n,2}$=0.74±0.15 μm (σ=0.22±0.06).

- Satheesh et al. (1999): measurements at Kaashidhoo, Feb.-Mar. 1998.
  Aerosol model for the tropical Indian Ocean:
  Mean α=1.233±0.209.

  The properties of the separate species are based on Hess et al. (1998); the refractive index for "ash" is from Patterson (1981).

  Overall mean number size distribution obtained by inversion (σ in decimal logarithm):
  $r_{n,1}$=0.135±0.032 μm, σ_1=0.394±0.042;
  $r_{n,2}$=0.955±0.142 μm, σ_2=0.312±0.051.
  ω_0(534)=0.88-0.90.

  List of the components taken, their number size distribution parameters and contribution to τ_a(500):

Type	r_n	σ	τ_a(500)
Sea salt, acc. mode	0.416	0.307	0.034 (*)
Sea salt, coarse mode	3.49	0.307	(*)
Dust, transported	0.50	0.342	0.030
nss sulfate, ammonium	0.0306	0.350	0.055
soot	0.0118	0.301	0.022
"ash"	0.08	0.20	0.016

Table 3.11: r_n in μm; σ in decimal logarithm. nss: non sea salt. Values are for 75% RH. (*): the contribution of sea salt to τ_a is all inclusive.

This model is completed by Rajeev et al. (2000):

Type	r_n	σ	N
Sea salt, acc. mode	0.397	2.03	1.19664E-4
Sea salt, coarse mode	3.33	2.03	1.10637E-6
Dust, transported	0.50	2.20	1.83485E-5
nss sulfate, ammonium	0.0295	2.24	0.20210
soot	0.0118	2.00	0.79776

Table 3.12: Number size distribution: r_n in μm, N: normalized abundance. nss: non sea salt. Values are for 75% RH.

- Holben et al. (2001): sun photometry at:
  Kaashidhoo (Maldives, 1998-1999): climatological monthly α (computed by linear regression between 440 and 870 nm) between 0.30 and 1.24 (annual mean: 0.82);
  Bahrain (1998-1999): climatological monthly α between 0.52 and 1.34 (annual mean: 0.95).

- Ramanathan et al. (2001a): INDOEX (Jan.-Mar. 1999). Synthesis of ω_0 at 530 nm: mostly in the range 0.85-0.91 close to India.

- Moorthy et al. (2001): cruises in the Indian Ocean.
  Feb.-Mar. 1998: α=0.94±0.10 north of the ITCZ, -0.23±0.20 south of the ITCZ;
  Jan.-Mar. 1999: α=0.93±0.10 north of the ITCZ, -0.48±0.18 south of the ITCZ.

- Eck et al. (2001b): Sun photometer measurements at Kaashidhoo.
  Monthly averages of α for Jan. to Jun.: 0.45 to 1.30.
  Volume size distribution for Jan.-Feb. 1999: modal radius of the accumulation mode increasing with τ_a from 0.15 μm to 0.20 μm.

  Inverted optical properties (Jan.-Feb. 1999):

	440	670	870	1020
ω_0	0.91±0.024	0.88±0.035	0.84±0.050	0.83±0.058
n_r	1.42±0.060	1.44±0.045	1.44±0.037	1.46±0.036
n_i	0.012±0.005	0.014±0.007	0.017±0.009	0.019±0.011
g	0.74±0.025	0.67±0.026	0.63±0.027	0.61±0.028

Table 3.13: Optical properties at Kaashidhoo, Jan.-Feb. 1999.

- Satheesh (2002): based on observations (Mar. 2001), the following models are proposed for Bay of Bengal, Arabian Sea and open Indian Ocean (based on single components from Hess et al. 1998):

Component	Volume mixing ratio BOB	AS	IO	r_n	σ	ρ	ω_0
Water soluble (sulphate, nitrate, organics)	0.674	0.325	0.137	0.029	2.24	1.8	0.99
Soot	0.056	0.0215	0.006	0.018	2.0	1.0	0.23
Sea salt (acc. mode)	0.099	0.238	0.842	0.378	2.03	2.2	1.0
Sea salt (coarse mode)	0.013	0.0316	0.015	3.17	2.03	2.2	1.0
Mineral dust	0.159	0.383	-	0.39	2.0	2.6	1.0

Table 3.14: Components for Bay of Bengal (BOB), Arabian Sea (AS), open Indian Ocean (IO). r_n in μm, ρ in $g.cm^{-3}$.

- Quinn et al. (2002): surface measurements, Jan.-Mar. 1999 (INDOEX). Values are grouped according to the origin of the air mass.

Region	Accumulation mode			Coarse mode		
	S	D_s	σ	S	D_s	σ
SH Indian Ocean	12±4.1	0.25±0.02	1.4±0.12	16±9.1	2.1±0.21	1.9±0.10
NH Indian Ocean	44±12	0.27±0.03	1.6±0.05	29±3.9	2.2±0.09	1.7±0.06
East Indian subcontinent	180±8.1	0.36±0.01	1.3±0.02	11±1.9	1.9±0.05	1.7±0.02
Indian subcontinent	130±35	0.32±0.02	1.4±0.05	11±3.0	1.8±0.09	1.6±0.02
Arabia	52±7.6	0.26±0.02	1.7±0.11	24±8.0	2.3±0.09	1.7±0.04
Arabia - Indian subcontinent	120±31	0.29±0.02	1.5±0.05	25±5.2	2.0±0.15	1.6±0.04
Arabian Sea - coastal India	79±24	0.30±0.01	1.4±0.06	6.7±3.6	1.7±0.22	1.6±0.04

Table 3.15: S in $\mu m.cm^{-3}$, D_s in μm (surface area fit parameters). Values reported for 55% RH.

Region	Refractive index		$\omega_0(550)$	
	sub-micron	super-micron	sub-micron	super-micron
SH Indian Ocean	1.50-0.0025i	1.44	1.0±0.02	1.0±0.04
NH Indian Ocean	1.54-0.0167i	1.44	0.95±0.02	0.89±0.01
East Indian subcontinent	1.54-0.0521i	1.44	0.86±0.01	0.85±0.01
Indian subcontinent	1.54-0.0495i	1.46	0.86±0.02	0.84±0.01
Arabia	1.52-0.0109i	1.46	0.96±0.01	0.93±0.02
Arabia - Indian subcontinent	1.53-0.020i	1.45	0.92±0.02	0.89±0.02
Arabian Sea - coastal India	1.53-0.026i	1.45	0.88±0.02	0.86±0.01

Table 3.16: Refractive index of sub- and super-micron size fractions. Values reported for 55% RH. NH/SH: Northern/Southern Hemispheres.

- Bates et al. (2002): synthesis of surface measurements, Feb.-Mar. 1999 (INDOEX), also described by Quinn et al. (2002). Values are grouped according to the origin of the air mass.

	Accumulation mode			Coarse mode		
Region	V	D_v	σ	V	D_v	σ
SH Indian Ocean	0.55±0.19	0.29±0.023	1.4±0.12	6.7±3.8	3.1±0.32	1.9±0.10
NH Indian Ocean	2.2±0.60	0.34±0.039	1.6±0.05	12±1.7	3.0±0.13	1.8±0.057
E. Indian subcont.	180±8.1	0.36±0.01	1.3±0.02	11±1.9	1.9±0.05	1.7±0.02
Indian subcont.	9.7±2.0	0.38±0.027	1.4±0.05	3.9±0.86	2.4±0.12	1.7±0.023
Arabia	2.6±0.39	0.35±0.028	1.7±0.11	10±3.4	2.9±0.11	1.7±0.044
Arabia - Indian subcont.	6.2±1,6	0.35±0.021	1.5±0.050	9.2±1.9	2.5±0.20	1.7±0.043
Arabian Sea - coastal India	4.2±1.3	0.34±0.0095	1.4±0.059	2.1±1.1	2.1±0.27	1.6±0.039
Bay of Bengal	7.6±0.54	0.34±0.0036	1.3±0.0059	1.1±0.067	1.9±0.016	1.6±0.031

Table 3.17: V in $\mu m^3.cm^{-3}$, D_v in μm. Values reported for 55% RH. NH/SH: Northern/Southern Hemispheres.

- Moorthy et al. (2003): measurements by sun photometry in the Bay of Bengal: average α of 0.93±0.001 in Jan. 2002, 1.33±0.096 in Feb. 2002, 1.21±0.135 in Mar. 2002.

- Singh et al. (2004): sun photometry in Kanpur, northern India, Jan. 2001-Dec. 2003. Monthly averages of α between 0.5 (summer) and 1.5 (winter).
  Monthly averages of the aerosol volume size distribution:

	Fine mode			Coarse mode		
Month	V	r_v	σ	V	r_v	σ
Jan.	0.024	0.148	0.020	0.033	3.85	0.027
Feb.	0.016	0.148	0.019	0.029	2.939	0.023
Mar.	0.016	0.113	0.015	0.042	2.566	0.049
Apr.	0.019	0.065	0.043	0.059	2.24	0.112
May	0.026	0.17	0.062	0.109	2.566	0.214
Jun.	0.028	0.098	0.039	0.074	2.24	0.112
Jul.	0.031	0.098	0.029	0.109	2.939	0.12
Aug.	0.038	0.098	0.049	0.19	3.85	0.221
Sep.	0.025	0.129	0.026	0.039	2.24	0.055
Oct.	0.026	0.148	0.027	0.038	2.566	0.038
Nov.	0.028	0.148	0.024	0.035	2.939	0.03
Dec.	0.025	0.169	0.023	0.027	2.939	0.023

Table 3.18: V in $\mu m^3.\mu m^{-2}$, r_v in μm.

- Sumanth et al. (2004): Bay of Bengal in Oct. 2003, sun photometry measurements. $\omega_0(500)$ ∼0.94.

Mass specific optical properties: Satheesh et al. (1999), Gras et al. (1999), Quinn et al. (2002).

Radiative forcing: Meywerk and Ramanathan (1999), Satheesh et al. (1999), Satheesh and Ramanathan (2000), Ramanathan et al. (2001a), Babu et al. (2002), Satheesh (2002), Satheesh et al. (2002), Podgorny et al. (2003) (Indonesian forest fires), Babu et al. (2004), Sumanth et al. (2004), Moorthy et al. (2005), Ramachandran (2005).

3.4 Atlantic Ocean as influenced by transport of African dust

- D'Almeida (1987) : tri-normal lognormal aerosol number size distribution measured in northern Africa and from Mie scattering modelling, using Patterson et al. (1977) (n=1.55-0.005i).

	Background	Wind carrying dust	Sandstorm
$r_{n,1}$	0.08	0.052	0.05
σ_1	2.10	2.15	2.15
N_1	301±22	1710±102	2502±126
$r_{n,2}$	0.7	1.5	1.5
σ_2	1.90	2.07	2.50
N_2	21.99±6	20.7±5	29.2±7
$r_{n,3}$	5	12	16
σ_3	1.6	1.7	1.8
N_3	1E-3	5E-3	1.2
ω_0, 300-450	0.7511	0.7060	0.7374
g, 300-450	0.7907	0.8409	0.7932
ω_0, 450-700	0.7914	0.7509	0.7777
g, 450-700	0.7726	0.8383	0.7784
ω_0, 700-1000	0.8252	0.7180	0.8121
g, 700-1000	0.7569	0.8458	0.7638

Table 3.19: r_n in μm, N_i in cm^{-3}; optical properties given in 3 spectral ranges.

- Smirnov et al. (1998): Saharan dust outbreaks observed during ACE-2, Jul. 1997, Tenerife, Canary Islands (various altitudes):
  α=0.06-0.77.

- Chiapello et al. (1999): measurements at Sal Island (Cape Verde), winter 1992; tri-modal lognormal number size distribution derived from in situ measurements of 3 aerosol types, and their contribution to mass and $\tau_a(670)$:
  sea salt: r_n=1.17 μm, σ=1.46, 24% of mass, 6% of $\tau_a(670)$,
  mineral dust: r_n=0.44 μm, σ=1.62, 2.9% of mass, 75% of $\tau_a(670)$,

excess sulfate: r_n=0.10 μm, σ=1.25, 24% in mass, 3% of $\tau_a(670)$,
carbonaceous aerosol: 2.2% of mass, 12% of $\tau_a(670)$.

- Moulin et al. (2001a) recommend various dust aerosol models for NW Africa: trimodal lognormal number size distribution.

  from Shettle (1984):

	r_n	σ	N_i
1	0.001	2.13	54.210
2	0.022	3.20	45.79
3	6.240	1.89	3.9E-5

Table 3.20: r_n in μm, N_i in %

2 other models with the proportion of N_3 multiplied by 10 and 20.
real refractive index: 1.53.
imaginary refractive index (at SeaWiFS wavelengths)=
$[0.0120, 0.0091, 0.0079, 0.0073, 0.0054, 0.0043, 0.0032, 0.0012]$ from Patterson (1981),
$[0.0080, 0.0045, 0.0040, 0.0030, 0.0020, 0.0010, 0.005, 0.005]$ from tuning to SeaWiFS observations.

ω_0 = 0.82-0.90 at 412 nm, 0.84-0.94 at 443 nm, 0.855-0.96 at 490-510 nm, 0.88-0.975 at 555 nm, 0.90-0.985 at 670 nm, 0.91-0.995 at 765-865 nm.

- Díaz et al. (2001): measurements at Tenerife (sunphotometer and AVHRR) and Mie modelling (refractive index from Patterson et al. 1977, n=1.56-0.006i):
$\omega_0(500)$=0.87, g=0.83

- Tanré et al. (2001): sunphotometer measurements at Sal Island (Cape Verde), Sde Boker (Israel), Banizoumbou (Niger), at various periods 1994-1998.
Median α (slope from 440 to 865 nm): 0.23, 0.56, 0.07.

  Using LANDSAT over the ocean: $n_r \sim 1.53$ in the visible, n_i=0.003$\pm$0.0003 at 470 nm (for the other wavelengths, n_i not significant from 0).

Volume size distribution (accumulation and coarse modes) and optical properties:

Site	Banizoumbou	Sal Island	Sde Boker
$r_{v,1}$	0.23+0.14τ_a(1020)	0.20+0.24τ_a(1020)	0.13+0.24τ_a(1020)
$r_{eff,2}$	2.19±0.12	2.15±0.10	3.01±0.24
r_{eff}	0.62+0.91τ_a(1020)	0.42+1.39τ_a(1020)	0.17+1.70τ_a(1020)
ω_0(441)	0.95±0.03	0.94±0.05	
ω_0(670)	0.96±0.03	0.95±0.04	
ω_0(870)	0.97±0.02	0.96±0.04	
ω_0(1020)	0.97±0.02	0.96±0.04	

Table 3.21: r in μm, $r_{v,1}$ is the volume weighted radius of the accumulation mode (r<0.6 μm), $r_{eff,2}$ is the effective radius of the coarse mode (r>0.6 μm), r_{eff} is the effective radius of the total size distribution.

- Haywood et al. (2001): aircraft in situ measurements in Apr.-May 1999 offshore NW Africa and Mie modelling: at 550 nm, ω_0=0.86, g=0.73.
- Pandithurai et al. (2001): sun photometer at the sub-Sahel station of Ilorin (Nigeria):

Season	Harmattan Nov.-Mar.	non-Harmattan Apr.-Oct.
ω_0(440)	0.880	0.929
ω_0(670)	0.887	0.932
ω_0(870)	0.887	0.935
ω_0(1020)	0.889	0.938
n_r-n_ii(440)	1.436-0.0085i	1.405-0.0036i
n_r-n_ii(670)	1.468-0.0074i	1.434-0.0039i
n_r-n_ii(870)	1.475-0.0075i	1.457-0.0042i
n_r-n_ii(1020)	1.470-0.0077i	1.465-0.0044i

Table 3.22: Optical properties of aerosols at Ilorin (Nigeria).

- Holben et al. (2001): sun photometry at
  Cape Verde (1994-1999): climatological monthly α (computed by linear regression between 440 and 870 nm) between 0.16 and 0.58 (annual mean: 0.33);
  Banizoumbou (Niger, 1995-1997): climatological monthly α between 0.06 and 0.51 (annual mean: 0.19);
  Bondoukoui (Burkina Faso, 1996-1997): climatological monthly α between 0.15 and 0.78 (annual mean: 0.39);
  Bidi-Bahn (Burkina Faso, 1996-1997): climatological monthly α between 0.09 and 0.72 (annual mean: 0.31).

- Haywood et al. (2003c): SHADE (Saharan Dust Experiment), Sep. 2000, in situ measurements from C-130 with flights from Sal Island, Cape Verde.

  Average single scattering albedo: ω_0=[0.96, 0.97, 0.98] at 450, 550, 700 nm.
  Log-normal number size distribution with 5 modes, with 2 cases of relative numbers distinguished, A and B, and optical properties:

Modes	r_n	σ	N, A	N, B	$\omega_0(550)$	$g(550)$
1	0.04	1.6	70.3	75.0	0.98	0.41
2	0.11	1.3	19.5	20.8	0.99	0.55
3	0.30	1.6	7.7	3.0	0.98	0.67
4	1.07	1.3	2.0	0.7	0.94	0.75
5	1.8	1.5	0.5	0.5	0.90	0.80

Table 3.23: Number size distribution for SHADE, r_n in μm, N in %. A and B are associated with 2 different relative modal numbers.

- Livingston et al. (2003): PRIDE (Puerto Rico Dust Experiment), Jul. 2000. α (6 channels between 380 and 1021 nm), derived from airborne sun photometry, between 0.19-0.21.
- Reid et al. (2003): PRIDE, Jul. 2000.
  mass median diameter obtained from aerodynamic methods: 4.5±1.3 μm (σ=2.1±0.2),
  volume median diameter obtained from optical counter methods: 9±1 μm (σ=1.5).
- Wang et al. (2003a): PRIDE, Jul. 2000, ground-measured number size distribution.
  Effective radius r_{eff}=0.72 μm, inferred refractive index: 1.53-0.0015i at 550 nm.

Modes	r_n	σ	N
1	0.02	1.71	69.972
2	0.09	1.40	28.829
3	0.38	1.42	1.072
4	1.2	1.37	0.127

Table 3.24: r_n in μm, N, number concentration, in %.

For a review of particle size characteristics of dust, see Goudie and Middleton (2001).

Relationships with humidity: Livingston et al. (2000).

Mass specific optical properties: Swap et al. (1996), Cachorro and Tanré (1997), Schulz et al. (1998), Chiapello et al. (1999), Maring et al. (2000), Haywood et al. (2003c), Kaufman et al. (2005).

Radiative forcing: Hsu et al. (2000), Moulin et al. (2001a), Díaz et al. (2001), Haywood et al. (2001), Haywood et al. (2003c), Haywood et al. (2005).

3.5 Mediterranean Basin

- Paronis et al. (1998): sun photometer measurements in 1996 and 1997 at Carloforte (Sardinia) and Finokalia (Crete):
  α and τ_a are inversely related; the most probable values for α are between 1.2 and 2.0.

- Hamonou et al. (1999): measurements at Thessalomiki (Greece), 1996-1997.
  α between 443 and 670 nm:
  most probable $\alpha \sim 1.6$ (excluding dust events), α=0.40-0.90 for dust events.

- Watson and Oppenheimer (2000): sun photometer measurements around Mount Etna, Oct. 1997. α averages 1.67.

- Sabbah et al. (2001): sun photometer measurements at Alexandria (Egypt), from Dec. 1997 to Nov. 1998. Monthly averages of α (computed between 440 and 870 nm) are between 0.5 and 1.3, but cases of low optical thickness are associated with α between 1.0 and 2.0.

- Holben et al. (2001): sun photometry at Sde Boker (Israel, 1996, 1998-1999): climatological monthly α (computed by linear regression between 440 and 870 nm) between 0.42 and 1.20 (annual mean: 0.94).

- Formenti et al. (2001b): sun photometer and surface measurements at Sde Boker, Israel, in Jun.-Jul. 1996. α computed between 415 or 440 and $\sim$870 nm. $\alpha = 1.5 \pm 0.4$; $\omega_0(550) = 0.92 \pm 0.03$.

- Formenti et al. (2001a): sun photometer and surface measurements in Jun.-Sep. 1998,
  at Sde Boker, Israel: $\alpha = 1.1 \pm 0.3$, range 0.2-1.6 (computed between 440 and 870 nm);
  at Mount Athos, Greece: $\alpha = 1.6 \pm 0.3$, range 0.7-2.3 (computed between 415 and 868 nm).

- Kouvarakis et al. (2002): surface measurements during PAUR II (Photochemical Activity and Ultraviolet Radiation), in Crete, May 1999. $\omega_0(532) = 0.85 \pm 0.05$.

- Formenti et al. (2002): aircraft measurements in Aug. 1998 in northeastern Greece (air mass influenced by an aged biomass burning plume).
  ω_0=0.91 (450 nm), 0.89 (550 nm), 0.85 (700 nm).

- Kubilay et al. (2003): sun photometer measurements at Erdemli (southern Turkey) from Jan. 2000 to Jun. 2001. Four modes of aerosol characteristics are distinguished: for high values of τ_a, α (computed between 440 and 870 nm) is between 0.0 and 0.5, and for low τ_a, it is between 1.0 and 2.0 (and two modes are in between).

- Di Iorio et al. (2003): measurements (surface and airborne) at Lampedusa, in May 1999 (PAUR II). Three days are described with air masses of different origins: northern Africa (18 May), Atlantic and Europe (25 and 27 May).

Optical properties (column integrated) and number size distribution (the first mode is imposed, $r_{n,1}$=0.07 μm, σ=1.45):

Date	α	ω_0	N_1	$r_{n,2}$	σ_2	N_2	$r_{n,3}$	σ_3	N_3
18 May 1999	0.13	0.7465	0.9988185	1.24	1.62	9.809E-4	5.30	1.14	2.006E-4
25 May 1999	1.15	0.8385	0.9989335	0.26	3.16	1.0450E-3	4.81	1.11	2.15E-5
27 May 1999	1.36	0.7895	0.9995027	0.33	3.16	4.838E-4	5.33	1.13	1.35E-5

Table 3.25: ω_0 as column integrated value at 532 nm. r_n in μm, N, number concentration, in %.

- Masmoudi et al. (2003a,b): sun photometry measurements in Apr.-Jun. 2001 for various sites. α computed between 440 and 870 nm. For Ouagadougou (Burkina-Faso) and Banizoumbou (Niger), α mostly between -0.1 and 0.4; for Thala (Tunisia), α mostly between 0.0 and 1.7; for Oristano (Sardinia), α mostly between 0.0 and 2.2; for Rome, α mostly between 0.0 and 1.8.

  At Thala, monthly means of α from Mar. to Oct. 2001 are between 0.409 and 0.882.

Site	r_{eff}	$r_{v,1}$	$r_{eff,2}$
Oristano	0.13+1.60τ_a(870)	0.13+0.3τ_a(870)	2.35±0.3
Rome	0.13+1.79τ_a(870)	0.14+0.28τ_a(870)	2.5±0.29
Thala	0.13+1.76τ_a(870)	0.13+0.29τ_a(870)	2.29±0.42
Banizoumbou	0.2+0.78τ_a(870)	0.16+0.03τ_a(870)	2.17±0.34
Ouagadougou	0.048+0.77τ_a(870)	0.1+0.05τ_a(870)	2.02±0.22

Table 3.26: r in μm, $r_{v,1}$ volume-weighted radius of the accumulation mode; $r_{eff,2}$: effective radius of the coarse mode.

Site	ω_0(440)	ω_0(670)	ω_0(870)	ω_0(1020)
Thala	0.907±0.032	0.937±0.027	0.944±0.029	0.949±0.028
Banizoumbou	0.861±0.027	0.909±0.03	0.932±0.025	0.94±0.023
Ouagadougou	0.935±0.03	0.953±0.025	0.959±0.025	0.962±0.024

Table 3.27: Single scattering albedo at 3 African sites, Thala (Tunisia), Banizoumbou (Niger), and Ouagadougou (Burkina-Faso).

- Perrone et al. (2005): sun photometer measurements in Lecce, Italy, from Mar. 2003 to Mar. 2004. α (computed between 441 and 873 nm) = 1.4±0.45.

wavelength (nm)	441	673	873	1022
ω_0	0.95±0.03	0.95±0.03	0.94±0.04	0.94±0.04
n_r	1.43±0.09	1.45±0.08	1.46±0.07	1.49±0.07
n_i	0.004±0.003	0.004±0.003	0.004±0.003	0.004±0.003

Table 3.28: Single scattering albedo and index of refraction at Lecce, Italy.

Mass specific optical properties: Dulac et al. (1992), Moulin et al. (1997 a,b), Formenti et al. (2001b), Andreae et al. (2002).

Radiative forcing: Gilman and Garrett (1994), Ichoku et al. (1999), Markowicz et al. (2002), Formenti et al. (2002), Di Iorio et al. (2003), Meloni et al. (2003), Tragou and Lascaratos (2003).

3.6 Continental Europe

- von Hoyningen-Huene and Wendisch (1994): sun photometry and sample measurements in Germany in 1991.

  imaginary index of refraction at Leipzig:
  n_i=0.0585±0.0482 in winter (0.11 in smog episodes), 0.0206±0.00219 in summer.

  average α at the site of Zingst (N. Germany), Leipzig and Maisach (S. Germany), as a function of air mass type:
  α=1.04-1.34 for aged polar air,
  α=1.01-1.16 for continental polar air,
  α=0.46-0.60 for maritime polar air,
  α=0.92-1.06 for aged subtropical air,
  α=1.03-1.12 for continental subtropical air,
  α=0.42-0.44 for maritime subtropical air.

  Parameters of the number size distribution at Maisach, derived from inversion of optical measurements:

air mass	$r_{n,1}$	σ_1	N_1	$r_{n,2}$	σ_2	N_2	$r_{n,3}$	σ_3	N_3
maritime subtropical	0.214	1.44	54.82	0.403	1.46	13.43	1.01	1.73	1.801
continental subtropical	0.116	1.54	1258.58	0.508	1.40	8.445	1.28	1.51	0.159
aged subtropical	0.144	1.40	1296.82	0.202	1.41	543.39	0.51	1.79	15.30
maritime polar	0.112	1.49	361.72	0.403	2.18	7.37			
continental polar	0.121	1.45	922.5	0.320	1.45	50.84	0.81	1.62	0.598
aged polar	0.109	1.49	2484.9	0.320	1.42	87.46	1.01	1.43	1.41

Table 3.29: Maisach, Germany. r_n in μm. Units for N is not indicated but can be seen as relative numbers.

- Kuśmierczyk-Michulec et al. (1999): optical measurements in the Baltic Sea in Jul. 1997. α computed with τ_a in the range 412-865 nm:
  1.198 for continental air masses, 0.393 for maritime air, 1.265 for continental-maritime air.

- Kuśmierczyk-Michulec and Marks (2000): optical measurements at Sopot, Poland. The most probable value for α (computed with τ_a in the range 412-865 nm) depends on the air mass affecting the site: 0.9-1.1 in summer 1997, 0.5-0.7 in spring 1998, 0.3-0.5 in summer 1998, 0.5-0.7 in autumn 1998, 1.3-1.5 in spring 1999.

- Ebert et al. (2002): the surface particle measurements during LACE-98 (Lindenberg Aerosol Characterization Experiment), Brandenburg, Germany, Jul.-Aug. 1998, gave estimates for the refractive index of aerosols n_r-in_i: n_r between 1.52 and 1.57, and n_i between 0.031 and 0.057.

- Bundke et al. (2002): surface measurements during LACE-98 (Lindenberg Aerosol Characterization Experiment), Brandenburg, Germany, Jul.-Aug. 1998.
  $\omega_0(567)$=0.826±0.02.

- Wendisch et al. (2002) and Petzold et al. (2002) give a complete description of aerosol properties (size distribution, refraction indices, single scattering albedo) as a function of altitude, for a few flights during LACE-98.

- Tunved et al. (2005): surface sample measurements in 2000 and 2001 at 4 stations in Sweden and Finland.

  Modal parameters (diameters and standard deviation) for different air masses:

modes air mass	N	D_n	σ
Nucleation			
Marine	314-957	13.6-16.3	1.6-2.8
Mixed	313-1420	13.6-15.3	1.6-2.5
Continental	114-915	11.3-16.4	1.8-3.0
Aitken			
Marine	271-1311	40.4-52.5	10.7-15.2
Mixed	305-1416	46.4-50.9	10.0-16.2
Continental	304-1553	44.1-49.3	10.9-17.1
Accumulation 1			
Marine	138-422	156.6-192.1	22.1-29.9
Mixed	232-451	162.2-190.6	23.4-29.4
Continental	291-666	158.3-179.5	19.4-32.2
Accumulation 2			
Marine	58-305	264.3-295.2	27.3-42.7
Mixed	97-189	266.5-272.9	29.7-42.8
Continental	64-188	238.7-285.7	24.9-27.0

Table 3.30: N in cm^{-3}, D_n and σ in nm. Size distribution parameters in Sweden and Finland.

- Chazette et al. (205): measurements during the ESQUIF (Etude et Simulation de la Qualité de l'air en Ile de France) program, Jul. 2000.
  Tri-modal aerosol size number distribution: $r_{n,1}$∼0.03-0.04 μm, σ_1=1.5; $r_{n,2}$∼0.08-0.12 μm, σ_2∼1.3-1.5; $r_{n,3}$∼0.40-0.45 μm, σ_3=1.25.
  Refractive index: 1.5±0.05-(0.016±0.0125)i
  ω_0(550)=0.85-0.92
  α=2.1±0.24.

- Mallet et al. (2003): measurements during ESCOMPTE (Expérience sur site pour COntraindre les Modèles de Pollution atmosphérique et de Transport d'Emissions), in Jun.-Jul. 2001, southeastern France. α between 1.10 and 1.82; ω_0(550)=0.85±0.05 (wet state). Size distribution and optical properties are given for separate components.

- Mélin and Zibordi (2005): sun photometry measurements in the northern Adriatic (AAOT site) and Ispra (Lombardy, Italy): a 7-year climatology for α (least-square regression from 440 to 870 nm) yields monthly averages between 1.35 and 1.71 at AAOT, and between 1.37 and 1.71 at Ispra.

- Cachorro et al. (2000): optical measurements in Spain (Castilla y León) in Mar.-Nov. 1995. α (computed from least-square fitting over the visible) = 1.72±0.36 (most frequent value 1.65).
- Carrico et al. (2000): surface measurements during ACE-2, Jun.-Jul. 1997, at Sagres, Portugal.
  $\omega_0(550)$=0.93±0.05 in unpolluted periods, 0.94±0.03 in polluted periods.
- Silva et al. (2002): sun photometry on the south coast of Portugal (Sagres), during ACE-2, Jun.-Jul. 1997. Two situations are distinguished: clean marine, continental polluted.

	clean marine	continental polluted
n_r-in_i	1.390±0.044-i(0.003±0.003)	1.480±0.058-i(0.01±0.003)
$r_{n,1}$ μm	0.05	0.04
σ_1	1.45	1.79
N_1 cm^{-3}	7850	29890
volume %	6	28
$r_{n,2}$ μm	0.16	0.18
σ_2	1.76	1.76
N_2 cm^{-3}	89.6	217
volume %	6	16
$r_{n,3}$ μm	0.50	1.45
σ_3	1.62	1.78
N_3 cm^{-3}	10.4	2.4
volume %	17	56
$r_{n,4}$ μm	2.18	
σ_4	1.70	
N_4 cm^{-3}	0.9	
volume %	71	
g (Mie)	0.71±0.04	0.65±0.02
α	0.218±0.099	0.81±0.077
ω_0	0.98±0.02	0.90±0.04
RH %	73±5	80±3

Table 3.31: Sagres, Portugal. ω_0 broad band single scattering albedo; α obtained by interpolation over the spectral range of the instrument.

Relationships with humidity: Carrico et al. (2000), Bundke et al. (2002).

Mass specific optical properties: Kuśmierczyk-Michulec et al. (2001).

Radiative forcing: Wendisch et al. (2002), Petzold et al. (2002), Heintzenberg et al. (2003), Cachier et al. (2005).

3.7 North America

- Smirnov et al. (1994): sun photometer measurements at Sherbrooke, Québec, Jan. 1989-Aug. 1991; annual mean α as a function of air mass origin:
  1.11±0.35 (range 0.20-2.1), 1.0±0.34 for Arctic air, 1.14±0.33 for Polar air, 1.33± 0.30 for Tropical air.

- Remer et al. (1997): in situ measurements during SCAR-A (Sulfate, Clouds and Radiation-Atlantic), in the mid-Atlantic US region, Jul. 1993:
  $\omega_0(450)\sim$0.98-0.99 .

- Remer and Kaufman (1998): dynamic aerosol model for volume size distribution.

Modes	r_v	σ	V_0	r_n
acc-1	0.11±0.1	0.60±0.11	$f_1(\tau_a(670))$	0.036
acc-2	0.21±0.025	0.45±0.07	$f_2(\tau_a(670))$	0.11
strat.	0.55±0.035	0.29±0.07	0.0053±0.0016	0.43
coarse 1 (salt)	1.30±0.10	0.30±0.10	$f_3(\tau_a(670))$	0.99
coarse 2	9.50±4.0	0.94±0.20	0.045±0.028	0.67

Table 3.32: SCAR-A, r in μm, V_0 in $\mu m^3/\mu m^2$, σ in natural logarithm. $f_1(\tau)$=-0.015+0.51τ-1.46τ^2+1.07τ^3; $f_2(\tau)$=0.0038-0.086τ+0.90τ^2-0.71τ^3; $f_3(\tau)$=-0.0012+0.031τ.

- Remer et al. (1999): α summer average at Greenbelt (Maryland) derived from sun photometry and computed between 440 and 870 nm:
  1.40±0.25 in 1993, 1.62±0.20 in 1994, 1.63±0.35 in 1995, 1.64±0.51 in 1996, 1.82±0.26 in 1997.

  Lognormal parameters of the volume size distribution (4 modes, σ in natural logarithm) obtained during TARFOX (Tropospheric Aerosol Radiative Forcing Observational Experiment), summer 1996, U.S. eastern seaboard:
  acc-1: r_v=0.13 μm (σ=0.60), acc-2: r_v=0.21 μm (σ=0.50), coarse-1: r_v=1.50 μm (σ=0.30), coarse-2: r_v=13.0 μm (σ=1.10).

- Russel et al. (1999): TARFOX airborne measurements, Jul. 1996, U.S. eastern seaboard:
  $\omega_0(550)\sim$0.95 for an assumed imaginary refractive index of 0.005, $\omega_0(550)\sim$0.86 for 0.017 (Mie calculations with measured size distribution).

- Hartley et al. (2000): in situ airborne optical measurements during TARFOX, Jul. 1996, U.S. eastern seaboard:
  ω_0(450-550)=0.95±0.03, $\omega_0(700)$=0.93±0.03, α=1.7±0.1.

- Holben et al. (2001): sun photometry at
  Thompson (Manitoba, 1994-1999, May to Oct.): climatological monthly α (computed by linear regression between 440 and 870 nm) between 1.39 and 1.86;
  Sherbrooke (Québec, 1995, 1998-2000): climatological monthly α between 1.27 and 2.03 (annual mean: 1.56);

Waskesiu (Saskatchewan, 1994-1999, May to Dec.): climatological monthly α between 1.24 and 1.55;
Greenbelt (Maryland, 1993-1999): climatological monthly α between 1.41 and 1.78 (annual mean: 1.64);
Bondville (Illinois, 1996-1999): climatological monthly α between 1.26 and 1.62 (annual mean: 1.42);
CART site (Oklahoma, 1994-1999): climatological monthly α between 1.03 and 1.71 (annual mean: 1.36);
Sevilleta (New Mexico, 1994-1999): climatological monthly α between 0.91 and 1.67 (annual mean: 1.31);
H.J. Andrews (Oregon, 1994-1999, May to Dec.): climatological monthly α between 0.74 and 1.67;
San Nicolas Island (California, 1998-2000): climatological monthly α between 0.74 and 1.49 (annual mean: 1.13);
Dry Tortugas (Florida, 1996-1999): climatological monthly α between 0.75 and 1.54 (annual mean: 1.12).

- O'Neill et al. (2002): boreal forest fire smoke, in Aug. 1998 in northern U.S. and Canada. α in the range 1.2-1.95; $\omega_0(500)$ in the range 0.85-0.99 (one value at 0.73).

- Baumgardner et al. (2000): Mexico City, $\omega_0(550) \sim$0.80-0.88.

Relationships with humidity: Kotchenruther et al. (1999).

Radiative forcing: Hignett et al. (1999), Russel et al. (1999)

3.8 Biomass burning

3.8.1 Americas

- Holben et al. (1996): sun-photometry in the Amazon basin, 1993-1994.
  α computed between 440 and 870 nm for various seasonal phases:

Sites; α	pre-burn	Transition to burn	Burning	Transition to wet	Wet
Cuiaba (1993)	0.95±0.23	1.31±0.25	1.71±0.12	1.25±0.28	1.10±0.17
Brasilia (1993)	0.55±0.15	0.87±0.27	1.59±0.19	1.15±0.26	0.97±0.31
Porto Nacional (1993)	0.79±0.32	1.29±0.26	1.26±0.50	1.30±0.24	0.50±0.21
Porto Nacional (1994)		1.57±0.67	1.78±0.53	1.27±0.41	
Alta Floresta (1993)	0.86±0.27	1.35±0.31	1.69±0.16	1.23±0.22	1.16±0.26
Alta Floresta (1994)	2.02±0.41	2.49±0.16	1.87±0.	1.48±0.25	0.93±0.23
Tucurui (1993)	0.98±0.17	1.14±0.23	1.25 ±0.30	1.34±0.30	

Table 3.33: Cuiaba, Porto Nacional, Brasilia: cerrado sites; Alta Floresta, Tucurui: forested sites.

- Remer et al. (1998) proposed a model derived from 3 years of sun-photometer measurements in the Amazon basin, with 2 (log-normal) modes (accumulation and coarse) of the volume size distribution:

Sites	Cerrado	Forest
V_1	-0.0089+0.31τ_a(670)	-0.017+0.30τ_a(670)
$r_{v,1}$	0.132±0.014	0.0740.36τ_a(670) (τ_a(670)<0.20)
		0.145τ_a(670)0.025 (τ_a(670)≥0.20)
σ_1	0.60±0.04	0.60±0.09
V_2	0.035+0.81τ_a(670)	0.15±0.11
$r_{v,2}$	11.5 (6.-40.)	9.0 (2.-30.)
σ_2	1.26±0.23	1.20±0.30

Table 3.34: r_v in μm, V in μm.

Optical properties of Cerrado model, at 440, 670, 870, 1020 nm:
ω_0=0.90
g=0.65, 0.57, 0.50, 0.45,
refractive index taken as 1.43-0.0035i.

- Artaxo et al. (1998): in situ airborne measurements during SCAR-B (Sulfate, Clouds, and Radiation-Brazil, Aug.-Sep. 1995);
  fine mode size distribution centered at 0.16 μm (aerodynamic radius).

- Reid et al. (1998): in situ surface measurements during SCAR-B (Aug.-Sep. 1995); $\omega_0(550)$ from 0.79±0.02 (young smoke) to 0.86±0.05 (depending on sites and age of smoke).

- Reid and Hobbs (1998): particle size parameters for young smoke and various environments (flaming or smoldering forest, cerrado, grass):
  particle number distribution: median diameter between 0.10 and 0.13 μm and geometric standard deviation σ between 1.68 and 1.91;
  particle volume distribution: median diameter between 0.23 and 0.30 μm and geometric standard deviation σ between 1.62 and 1.87.

- Eck et al. (1998): from irradiance measurements during SCAR-B (Aug.-Sep. 1995); $\omega_0(550)$ between 0.82 and 0.94.

- Yamasoe et al. (1998): real refractive index derived from sun photometry during SCAR-B (Aug.-Sep. 1995):
  1.53±0.04, 1.55±0.04, 1.59±0.02, 1.58±0.01 at 438, 670, 870, 1020 nm.

- Reid et al. (1999): α(338-437 nm) derived from airborne measurements during SCAR-B (Aug.-Sep. 1995):
  1.08±0.21 at Cuiabá, 0.97±0.18 at Alta Floresta, 0.82±0.15 at Ji Parana.

- Holben et al. (2001): sun photometry at
  Cuiaba (Brazil, 1993-1995, Jun. to Jan.): climatological monthly α (computed by linear regression between 440 and 870 nm) between 0.62 and 1.72;
  Alta Floresta (Brazil, 1993-1995, 1999, Jan. to Oct.): climatological monthly α between 0.57 and 1.89;
  Brasilia (Brazil, 1993-1995, Feb., Apr. to Dec.): climatological monthly α between 0.64 and 1.44;
  Arica (Chile, 1998-1999): climatological monthly α between 1.13 and 1.43 (annual mean: 1.27).

- Kreidenweis et al. (2001): smoke aerosols transported to Mexico and US (May 1998).

  For the mode i, volume median radius r_v and standard deviation are determined with integrals between $r_{v,min}$ and $r_{v,max}$, 0.05 and ∼0.60 μm for the fine mode, ∼0.60 and 15 μm for the coarse mode.

Sites	$\tau_a(670)$	$r_{v,1}$	$\sigma_{v,1}$	$r_{v,2}$	$\sigma_{v,2}$	V_1/V_2	$\alpha_{440/870}$	$\alpha_{440/670}$	$\omega_0(670)$	n_r
Louisiana	0.84						1.61	1.37		
Pensacola	0.39						1.52	1.28		
Huatulco	0.74						1.57	1.35		
Monterrey	0.52						1.69	1.58		
Monclova	0.49	0.169	0.42	3.73	0.67	1.12	1.68	1.54	0.97	1.45
Aguascalientes	0.48	0.170	0.43	3.89	0.66	1.29	1.65	1.52	0.97	1.44
CART site	0.36	0.170	0.42	2.97	0.67	1.56	1.45	1.38	0.98	1.41
Cuiaba	0.48	0.137	0.54	4.15	0.74	2.10	1.78	1.73	0.88	1.48
Alta Floresta	0.47	0.157	0.46	3.59	0.79	2.20	1.81	1.73	0.95	1.48
Rondonia	0.50	0.158	0.46	4.07	0.77	1.79	1.98	1.82	0.89	1.50
Mongu	0.44	0.139	0.43	3.73	0.71	1.85	1.85	1.76	0.86	1.50
Senanga	0.47	0.140	0.43	4.66	0.73	2.00	1.78	1.56	0.81	1.51
Zambezi	0.43	0.139	0.45	4.27	0.82	2.64	1.83	1.70	0.82	1.51
Sesheke	0.53	0.141	0.44	4.66	0.71	1.56	1.72	1.62	0.82	1.50

Table 3.35: r_v in μm; Monclova and Monterrey in northern Mexico, Aguascalientes in central Mexico, Huatulco in southern Mexico. CART site in Oklahoma. Cuiaba, Alta Floresta, Rondonia in Brazil, Senanga, Zambezi, Sesheke in Africa (Zambia).

- Procopio et al. (2003): properties for smoke aerosol derived from sun photometry in Amazonia;
  fine mode: 0.15±0.02 μm; coarse mode: 6.55±0.91 μm;
  ω_0=0.93±0.01, 0.90±0.01, 0.87±0.02, 0.85±0.02 at 440, 670, 870, 1020 nm.

- Eck et al. (2003b) for high aerosol optical thickness smoke events, in Maryland, Moldova, Brazil and Zambia:
  fine mode median radius between 0.17 and 0.25 μm, σ between 1.35 and 1.50.

3.8.2 Africa

- Holben et al. (2001): sun photometry at Mongu (Zambia, 1995-1998, Jul. to Dec.): climatological monthly α (computed by linear regression between 440 and 870 nm) between 1.10 and 1.86;
  Ilorin (Nigeria, 1998-1999): climatological monthly α between 0.50 and 1.32 (annual mean: 0.75).

- Eck et al. (2001a): ZIBBEE (Zambian International Biomass Burning Emissions Experiment), Aug.-Sep. 1997:
  $\omega_0(550)$ around 0.82-0.85, decreasing with wavelength;
  $\alpha_{500/670}$ around 1.72-1.80;
  fine mode centered around 0.12 to 0.165 μm (increasing with τ_a); confirmed by Eck et al. (2003a).

- Eck et al. (2003a): monthly mean of $\alpha_{440/870}$ from sun photometry at Mongu, Zambia:

$\sim$1 for Nov.-Feb., between 1.5 and 1.9 for Apr.-Nov.

- Haywood et al. (003ba,b): SAFARI 2000 (South AFrican Aerosol Regional Science Initiative, Aug.-Sep. 2000), in situ C-130 airborne measurements: ω_0=0.90, 0.89, 0.87, 0.85, 0.82 at 440, 550, 670, 870, 1020 nm;
  n=1.53-0.018i, 1.55-0.018i, 1.59-0.018i, 1.58-0.018i at 440, 670, 870, 1020 nm;
  number size distribution with 3 log-normal modes:
  for aged aerosol: 0.12$\pm$0.01, 0.26$\pm$0.01, 0.80$\pm$0.01 μm, σ=1.3$\pm$0.1, 1.5$\pm$0.1, 1.9$\pm$0.4,
  for fresh aerosol: 0.10, 0.22, 1.00 μm, σ=1.3, 1.5, 1.9.

  from sun-photometers (see Eck et al. 2003a) with data from Zambia to South Africa (SAFARI 2000):
  ω_0 equal to 0.88, 0.87, 0.84, 0.82 at 440, 670, 870, 1020 nm;
  n=1.51-0.020i, 1.54-0.016i, 1.56-0.016i, 1.58-0.016i at 440, 670, 870, 1020 nm.

- Bergstrom et al. (2003), during SAFARI2000 (Aug.-Sep. 2000):
  ω_0 from 0.90 at 350 nm, decreasing to 0.6 at 860 nm.

For interesting reviews: see also Kaufman et al. (1998) for Amazonia, Liousse et al. (1997).

Relationships with humidity: Kotchenruther and Hobbs (1998), Kreidenweis et al. (2001).

Mass-specific optical properties: Liousse et al. (1997), Reid et al. (1998), Martins et al. (1998), Haywood et al. (003ba,b).

Radiative forcing: Penner et al. (1992).

Section 4

Appendix

4.1 Acronyms

ACE: Aerosol Characterization Experiment
AERONET: Aerosol Robotic Network
AAOT: Acqua Alta Oceanographic Tower
AVHRR: Advanced Very High Resolution Radiometer
ESCOMPTE: Expérience sur site pour COntraindre les Modèles de Pollution atmosphérique et de Transport d'Emissions
ESQUIF: Etude et Simulation de la Qualité de l'air en Ile de France
ISCAT: Investigation of Sulfur Chemistry in the Antarctic Troposphere
LACE: Lindenberg Aerosol Characterization Experiment
MERIS: Medium Resolution Imaging Spectrometer
MISR: Multiangle Imaging Spectroradiometer
MODIS: Moderate Resolution Imaging Spectroradiometer
OCTS: Ocean Colour and Temperature Scanner
PAUR: Photochemical Activity and Ultraviolet Radiation
POLDER: POlarization and Directionality of the Earth's Reflectances
PRIDE: Puerto Rico Dust Experiment
SAFARI: South AFrican Aerosol Regional Science Initiative
SCAR-A: Sulfate, Clouds and Radiation - Atlantic
SCAR-B: Smoke, Clouds and Radiation - Brazil
SeaWiFS: Sea-viewing Wide Field-of-view Sensor
SHADE: Saharan Dust Experiment
TARFOX: Tropospheric Aerosol Radiative Forcing Observational eXperiment
TOMS: Total Ozone Mapping Spectrometer
ZIBBEE: Zambian International Biomass Burning Emissions Experiment

4.2 libRadtran modified routine

```
/*****************************************************************************/
/* Function: mie_calc_sizedist                                        @44_30i@ */
/* Description:                                                                */
/*  Mie calculations, using the MIEV0 and BHMIE codes by Warren Wiscombe       */
/*  (ftp://climate.gsfc.nasa.gov/pub/wiscombe) and Bohren and Huffman          */
/*  (ftp://astro.princeton.edu/draine/scat/bhmie/).                            */
/*                                                                             */
/* Parameters:                                                                 */
/*  mie_inp_struct input:    mie input structure (see src_c/miecalc.h)         */
/*  mie_out_struct *output:  mie output structure (see src_c/miecalc.h)        */
/*  int program:             MIEV0 or BHMIE                                    */
/*  int medium:              WATER, ICE, or USER; if USER, the refractive index */
/*                           is read from crefin                               */
/*  mie_complex crefin:      Complex refractive index (both numbers positive)  */
/*  float wavelength:        wavelength [micron]                               */
/*  float temperature:       temperature                                       */
/*  double *x_size:          size distribution, radius [um]                    */
/*  double *y_size:          size distribution, n(r)                           */
/*  int n_size:              size distribution, number of radii                */
/*  double *beta:            extinction coefficient [km-1] per unit            */
/*                           liquid water content (returned)                   */
/*  double *omega:           Single scattering albedo (returned)               */
/*  double *g:               Asymmetry parameter (returned)                    */
/*                                                                             */
/* Return value:                                                               */
/*  0  if o.k., <0 if error                                                    */
/*                                                                             */
/* Example:                                                                    */
/* Files:                                                                      */
/* Known bugs:                                                                 */
/*  Syntax and parameters of this function are subject to change.              */
/* Author:                                                                     */
/*                                                                   @i44_30@ */
/* 10.02.05 MC : modification to have Bext in [km-1/par cm3] instead of        */
/*               [km-1/g m3] marked with 'MC_10.02.05'                         */
/*                                                                             */
/*****************************************************************************/

int mie_calc_sizedist (mie_inp_struct input, mie_out_struct *output,
       int program, int medium, mie_complex crefin,
       float wavelength, float temperature,
       double *x_size, double *y_size, int n_size,
       double *beta, double *omega, double *g,
       mie_complex *ref)
{
  int status=0, is=0, ip=0, im=0;
```

```
  double xsquared=0, xcubed=0, norm=0;

  double ext=0, sca=0, asy=0, vol=0;

  /* allocate memory for fields */
  double *extinction = calloc (n_size, sizeof (double));
  double *scattering = calloc (n_size, sizeof (double));
  double *asymmetry  = calloc (n_size, sizeof (double));
  double *volume     = calloc (n_size, sizeof (double));

  double ***pmom=NULL;

  if (input.nmom>0) {
    pmom     = calloc (4, sizeof(double **));

    for (ip=0; ip<4; ip++) {
      pmom    [ip] = calloc (input.nmom+1, sizeof(double *));

      for (im=0; im<=input.nmom; im++)
pmom[ip][im] = calloc (n_size, sizeof(double));
    }
  }


  for (is=0; is<n_size; is++) {

    status = mie_calc (input, output, program, medium, crefin,
       wavelength, x_size[is], temperature, ref);
    if (status!=0) {
      fprintf (stderr, "error %d returned by mie_calc()\n", status);
      return status;
    }

/*  ++MC_10.02.05 : modify units to micrometer */

/*  xsquared = x_size[is] * x_size[is]*1E-12;       in square meter */
/*  xcubed   = xsquared   * x_size[is]*1E-06;       in cubic meter */

    xsquared = x_size[is] * x_size[is];             /* in square micrometer */
    xcubed   = xsquared   * x_size[is];             /* in cubic micrometer */

/*  --MC_10.02.05 : modify units to micrometer */

    extinction[is] = output->qext * xsquared * y_size[is];
    scattering[is] = output->qsca * xsquared * y_size[is];
    asymmetry [is] = output->gsca * scattering[is];
    volume    [is] = xcubed * y_size[is];
```

```
    /* quote from MIEV.doc, concerning the normalization of pmom[]:   */
    /*                                                                */
    /* The normalized moments are                                     */
    /*      4 / ( XX**2 * QSCA ) * PMOM,  but it is PMOM itself, not  */
    /*      these normalized moments, which should be integrated over */
    /*      a size distribution.                                      */

    if (input.nmom>0)
      for (ip=0; ip<4; ip++)
for (im=0; im<=input.nmom; im++)
      pmom[ip][im][is] = output->pmom[ip][im] * y_size[is];
  }

  norm = integrate (x_size, y_size,     n_size);

  ext  = integrate (x_size, extinction, n_size) / norm;
  sca  = integrate (x_size, scattering, n_size) / norm;
  asy  = integrate (x_size, asymmetry,  n_size) / norm;
  vol  = integrate (x_size, volume,     n_size) / norm;

  if (input.nmom>0)
    for (ip=0; ip<4; ip++)
      for (im=0; im<=input.nmom; im++)
output->pmom[ip][im] = integrate (x_size, pmom[ip][im], n_size) / norm;

/*  ++MC_10.02.05 : modify extiction coefficient computation*/

/* *beta  = 3.0*ext/(4.0*RHOH2O*vol)*1000.0;        */

   *beta  = ext*3.14159*0.001;  /*Add !pi (missing in ext) and impose Nd=10-3

/*  --MC_10.02.05 : modify extiction coefficient computation */

  *omega = sca/ext;
  *g     = asy/sca;

  /* free memory */
  free (extinction);
  free (scattering);
  free (asymmetry);
  free (volume);

  if (input.nmom>0) {
    for (ip=0; ip<4; ip++) {
      for (im=0; im<=input.nmom; im++)
free(pmom[ip][im]);
```

```
      free(pmom[ip]);
    }

    free(pmom);
  }
  return 0;
}
```

4.3 List of IDL routines

IDL routine list and description

This page was created by the IDL library routine mk_html_help. For more information on this routine, refer to the IDL Online Help Navigator or type:

```
? mk_html_help
```

at the IDL command line prompt.

Last modified: Wed Apr 27 11:34:30 2005.

List of Routines

* AER_MIE_DEFINE_CTX
* AER_MIE_DEFINE_STRUCT
* AER_MIE_COMP_SIZE_DISTR
* AER_MIE_WRITE_INPUT
* AER_MIE_RUN
* AER_MIE_READ_OUTPUT
* AER_MIE_COMP_OPAC
* AER_MIE_DISPLAY
* AER_MIEV_DEFINE_CTX
* AER_MIEV_DEFINE_STRUCT
* AER_MIEV_WRITE_INPUT
* AER_MIEV_RUN
* AER_MIEV_READ_OUTPUT
* AER_MIEV_DISPLAY
* AER_AOPP_COMP_OPAC
* MIE_LOGNORMAL
* MIE_SINGLE
* MIE_SIZEDIST

Routine Descriptions

AER_MIE_DEFINE_CTX

[Next Routine] [List of Routines]

NAME:
AER_MIE_DEFINE_CTX

PURPOSE:

```
   Define and return the local context

 CATEGORY:
   AER MIE

 CALLING SEQUENCE:

   st = AER_MIE_DEFINE_CTX(Ctx)

 INPUTS:
   none
 KEYWORD PARAMETERS:
   none
 OUTPUTS:
   Ctx:    defined context

 MODIFICATION HISTORY:
   Written by: Marco Clerici, 11.11.04

(See AER_MIE.pro)

  ------------------------------------------------------------------------

AER_MIE_DEFINE_STRUCT

[Previous Routine] [Next Routine] [List of Routines]

 NAME:
   AER_MIE_DEFINE_STRUCT

 PURPOSE:

   Define and return the structures used by the tool

 CATEGORY:
   AER MIE

 CALLING SEQUENCE:

   st = AER_MIE_DEFINE_STRUCT(str_in)

 INPUTS:
   none
 KEYWORD PARAMETERS:
   none
 OUTPUTS:
   str_in:    structure {STR_MIE_INPUT}
```

```
 MODIFICATION HISTORY:
   Written by: Marco Clerici, 10.11.04

(See AER_MIE.pro)

  ------------------------------------------------------------------------

AER_MIE_COMP_SIZE_DISTR

[Previous Routine] [Next Routine] [List of Routines]

 NAME:
   AER_MIE_COMP_SIZE_DISTR

 PURPOSE:

   Compute and write to a file (in Ctx.InputDir) a lognormal
   size distribution using the same arguments as in OPAC

 CATEGORY:
   AER MIE

 CALLING SEQUENCE:
   AER_MIE_COMP_SIZE_DISTR, Ctx, rmod, rmin, rmax, rsig, Ntot,
                            n, r [,NINT=nint] [,DISTID=distid]

 INPUTS:
   Ctx:    context
   rmod:   mode radius
   rmin:   minimum radius
   rmax:   maximum radius
   rsig:   width of the distribution
   Ntot:   total number of particles

 KEYWORD PARAMETERS:

   nint:   number of logarithmic intervals
   distid: Distribution ID (if set, write output file)
   disp:   Display/Print intermediate results

 OUTPUTS:
   n:          number of particles for each interval
   r:          radia array (nint+1 elements)
   Vtot:     total volume in cm-3 of the Ntot particles
   Ntot_eff:   actual number of particles in range r_min-r_max

 NOTE : the size distribution file for MIE code MUST contain the
        particle DENSITY, and NOT the particle NUMBER associated
```

```
        to every radii !!!!

 MODIFICATION HISTORY:
   Written by: Marco Clerici, 15.11.04

(See AER_MIE.pro)

  ------------------------------------------------------------------------

AER_MIE_WRITE_INPUT

[Previous Routine] [Next Routine] [List of Routines]

 NAME:
   AER_MIE_WRITE_INPUT

 PURPOSE:

   Write the input file

 CATEGORY:
   AER MIE

 CALLING SEQUENCE:
   AER_MIE_WRITE_INPUT, Ctx, str_in

 INPUTS:
   Ctx:    context
   str_in: structure containing input data

 KEYWORD PARAMETERS:
   none
 OUTPUTS:
   none
 MODIFICATION HISTORY:
   Written by: Marco Clerici, 10.11.04

(See AER_MIE.pro)

  ------------------------------------------------------------------------

AER_MIE_RUN

[Previous Routine] [Next Routine] [List of Routines]

 NAME:
   AER_MIE_RUN
```

```
 PURPOSE:

   Run mie code through IDL

 CATEGORY:
   AER MIE

 CALLING SEQUENCE:
   st = AER_MIE_RUN(Ctx, RID [,STR_IN=str_in]
                    [,STR_OUT=str_out] [,DISPLAY=display])

 INPUTS:
   Ctx:    context
   RID:    Run ID

 KEYWORD PARAMETERS:
   STR_IN:     input values to be written to MIE input file
   STR_OUT:    if set, returns output results therein
   DISPLAY:    if set, call AER_MIE_DISPLAY

 OUTPUTS:
   none
 MODIFICATION HISTORY:
   Written by: Marco Clerici, 11.11.04

(See AER_MIE.pro)

  ------------------------------------------------------------------------

AER_MIE_READ_OUTPUT

[Previous Routine] [Next Routine] [List of Routines]

 NAME:
   AER_MIE_READ_OUTPUT

 PURPOSE:

   Read the output file

 CATEGORY:
   AER MIE

 CALLING SEQUENCE:
   AER_MIE_READ_OUTPUT, Ctx, RID, str_out

 INPUTS:
   Ctx:    context
```

```
   RID:    run ID

 KEYWORD PARAMETERS:
   none
 OUTPUTS:
   str_out: structure containing output data

 MODIFICATION HISTORY:
   Written by: Marco Clerici, 11.11.04

(See AER_MIE.pro)

  ------------------------------------------------------------------------

AER_MIE_COMP_OPAC

[Previous Routine] [Next Routine] [List of Routines]

 NAME:
   AER_MIE_COMP_OPAC

 PURPOSE:

   Compute through mie code the OPAC aerosol component

 CATEGORY:
   AER MIE

 CALLING SEQUENCE:
   AER_MIE_COMP_OPAC, Ctx, type, str_out

 INPUTS:
   Ctx:    context
   RID:    run ID
   type:   OPAC aerosol component (e.g. SOOT)

 KEYWORD PARAMETERS:
   none
 OUTPUTS:
   str_out: structure containing output data

 MODIFICATION HISTORY:
   Written by: Marco Clerici, 29.11.04

(See AER_MIE.pro)

  ------------------------------------------------------------------------
```

```
AER_MIE_DISPLAY

[Previous Routine] [Next Routine] [List of Routines]

 NAME:
   AER_MIE_DISPLAY

 PURPOSE:

   Display/Report result of a MIE run

 CATEGORY:
   AER MIE

 CALLING SEQUENCE:
   AER_MIE_DISPLAY, Ctx, str_in, str_out [,DETAIL=detail]

 INPUTS:
   Ctx:        context
   str_in:     structure containing input values - it is needed as the
               output file does not contain all the info
   str_out:    structure containing results read from MIE0 output file

 KEYWORD PARAMETERS:
   detail:     report detail (1 -> short, 2 -> extend. 3-> all)

 OUTPUTS:
   none
 MODIFICATION HISTORY:
   Written by: Marco Clerici, 10.11.04

(See AER_MIE.pro)

  ------------------------------------------------------------------------

AER_MIEV_DEFINE_CTX

[Previous Routine] [Next Routine] [List of Routines]

 NAME:
   AER_MIEV_DEFINE_CTX

 PURPOSE:

   Define and return the local context

 CATEGORY:
   AER MIEV
```

```
 CALLING SEQUENCE:

   st = AER_MIEV_DEFINE_CTX(Ctx)

 INPUTS:
   none
 KEYWORD PARAMETERS:
   none
 OUTPUTS:
   Ctx:    defined context

 MODIFICATION HISTORY:
   Written by: Marco Clerici, 10.11.04

(See AER_MIEV.pro)

  ------------------------------------------------------------------------

AER_MIEV_DEFINE_STRUCT

[Previous Routine] [Next Routine] [List of Routines]

 NAME:
   AER_MIEV_DEFINE_STRUCT

 PURPOSE:

   Define and return the structures used by the tool

 CATEGORY:
   AER MIEV

 CALLING SEQUENCE:

   st = AER_MIEV_DEFINE_STRUCT(str_in)

 INPUTS:
   none
 KEYWORD PARAMETERS:
   none
 OUTPUTS:
   str_out:    structure {STR_MIEV_INPUT}

 MODIFICATION HISTORY:
   Written by: Marco Clerici, 10.11.04

(See AER_MIEV.pro)
```

AER_MIEV_WRITE_INPUT

[Previous Routine] [Next Routine] [List of Routines]

NAME:
AER_MIEV_WRITE_INPUT

PURPOSE:

Write the input file

CATEGORY:
AER MIEV

CALLING SEQUENCE:
AER_MIEV_WRITE_INPUT, Ctx, str_in

INPUTS:
Ctx: context
str_in: structure containing input data

KEYWORD PARAMETERS:
none
OUTPUTS:
none
MODIFICATION HISTORY:
Written by: Marco Clerici, 10.11.04

(See AER_MIEV.pro)

AER_MIEV_RUN

[Previous Routine] [Next Routine] [List of Routines]

NAME:
AER_MIEV_RUN

PURPOSE:

Run MIEV0 code through MVDrive

CATEGORY:
AER MIEV

```
 CALLING SEQUENCE:
   st = AER_MIEV_RUN(Ctx, RID [,STR_IN=str_in]
                     [,STR_OUT=str_out] [,DISPLAY=display])

 INPUTS:
   Ctx:    context
   RID:    Run ID

 KEYWORD PARAMETERS:
   STR_IN:     input values to be written to MIEV0 input file
   STR_OUT:    if set, returns output results therein
   DISPLAY:    if set, call AER_MIEV_DISPLAY

 OUTPUTS:
   none
 MODIFICATION HISTORY:
   Written by: Marco Clerici, 10.11.04

(See AER_MIEV.pro)

  ------------------------------------------------------------------------

AER_MIEV_READ_OUTPUT

[Previous Routine] [Next Routine] [List of Routines]

 NAME:
   AER_MIEV_READ_OUTPUT

 PURPOSE:

   Read the output file

 CATEGORY:
   AER MIEV

 CALLING SEQUENCE:
   AER_MIEV_READ_OUTPUT, Ctx, RID, str_out

 INPUTS:
   Ctx:    context
   RID:    run ID

 KEYWORD PARAMETERS:
   none
 OUTPUTS:
   str_out: structure containing output data
```

```
 MODIFICATION HISTORY:
   Written by: Marco Clerici, 10.11.04

(See AER_MIEV.pro)

  ------------------------------------------------------------------------

AER_MIEV_DISPLAY

[Previous Routine] [Next Routine] [List of Routines]

 NAME:
   AER_MIEV_DISPLAY

 PURPOSE:

   Display/Report result of a MIEV run

 CATEGORY:
   AER MIEV

 CALLING SEQUENCE:
   AER_MIEV_DISPLAY, Ctx, str_out [,DETAIL=detail]

 INPUTS:
   Ctx:        context
   str_out:    structure containing results read from MIEV0 output file

 KEYWORD PARAMETERS:
   DETAIL:     report detail (1 -> short, 2 -> extend. 3-> all)
   EPS:        set eps output device

 OUTPUTS:
   none
 MODIFICATION HISTORY:
   Written by: Marco Clerici, 10.11.04

(See AER_MIEV.pro)

  ------------------------------------------------------------------------

AER_AOPP_COMP_OPAC

[Previous Routine] [Next Routine] [List of Routines]

 NAME:
   AER_AOPP_COMP_OPAC
```

```
 PURPOSE:

   Compute through AOPP code the OPAC aerosol component

 CATEGORY:
   AER AOPP

 CALLING SEQUENCE:
   AER_MIE_COMP_OPAC, type, str_out, DISP=disp

 INPUTS:
   comp:   OPAC aerosol component (e.g. SOOT)

 KEYWORD PARAMETERS:
   DISP:   display output of the computation

 OUTPUTS:
   str_out: structure containing output data

 MODIFICATION HISTORY:
   Written by: Marco Clerici, 30.11.04

(See AER_AOPP.pro)

  ------------------------------------------------------------------------

MIE_LOGNORMAL

[Previous Routine] [Next Routine] [List of Routines]

 NAME:
       MIE_LOGNORMAL
 PURPOSE:
       Calculates the scattering parameters of a log normal
       distribution of spherical particles.
 CATEGORY:
       EODG Mie routines
 CALLING SEQUENCE:
       mie_lognormal, Nd, Rm, Sg, Wavenumber, Cm [, Dqv = dqv] $
       [,Bext] [,Bsca] [,w] [,g] [,ph]
 INPUTS:
       Nd:         Number density of the particle distribution
                   Use 1E-3 to convert Bext from [um2] to ext.
                   coeff. in km-1 for 1 part/cm3 density.

       Rm:         Median radius of the particle distribution
       Sg:         The spread of the distribution, such that the
```

```
                standard deviation of ln(r) is ln(S)
      Wavenumber: Wavenumber of light (units must match Rm)
      Cm:         Complex refractive index
 OPTIONAL KEYWORD PARAMETERS:
      Dqv:        An array of the cosines of scattering angles at
                  which to compute the phase function.
      Rmin:       minimum radius of the distribution
      Rmax:       maximum radius of the distribution
      Nqua:       number of quadrature points (default is 450)

 OUTPUT PARAMETERS:
      Bext:       The extinction cross section [um^2 - M.C. 02.12.04]
      Bsca:       The scattering cross section [um^2 - M.C. 02.12.04]
      w:          The single scatter albedo
      g:          The asymmetry parameter
      ph:         The phase function - an array of the same
                  dimension as Dqv. Only calculated if Dqv is
                  specified.
 RESTRICTIONS:
      Note, this procedure calls the MIE_SINGLE and QUADRATURE procedures.
 MODIFICATION HISTORY
      G. Thomas Sept. 2003 (based on mie.pro written by Don Grainger)

      G. Thomas Nov. 2003 minor bug fixes

      G. Thomas Feb. 2004 Explicit double precision added throughout

      M. Clerici Dec.2004 Add Rmin/Rmax keywords

      M. Clerici Feb.2005 Add comments on normalisation conditions

(See ../AOPP//mie_lognormal.pro)

  ------------------------------------------------------------------------

MIE_SINGLE

[Previous Routine] [Next Routine] [List of Routines]

 NAME:
      MIE_SINGLE
 PURPOSE:
      Calculates the scattering parameters of a series of particles
      using the Mie scattering theory.
 CATEGORY:
      EODG Mie routines
 CALLING SEQUENCE:
      mie_single, Dx, Cm, Inp [, Dqv = dqv] $
```

```
      [, Dqxt] [, Dqsc] [, Dqbk] [, Dg] [, Xs1] [, Xs2] [, Dph]
 INPUTS:
      Dx:         A 1D array of particle size parameters
      Cm:         The complex refractive index of the particles
      Inp:        Number of scattering angles at which to calculate
                  intensity functions etc
 OPTIONAL KEYWORD PARAMETERS:
      dqv:        An array of the cosines of scattering angles at
                  which to compute the phase function.
 OUTPUT PARAMETERS:
      Dqxt:       The extinction efficiency
      Dqsc:       The scattering efficiency
      Dg:         The asymmetry parameter
      Xs1:        The first amplitude function - amplitude of light
                  polarized in the plane perpendicular to the
                  directions of incident light propagation and
                  observation.
      Xs2:        The second amplitude function - amplitude of light
                  polarized in the plane parallel to the directions
                  of incident light propagation and observation.
                  NB. Xs1 and Xs2 are complex arrays of the same
                  dimension as Dqv and are only calculated if Dqv is
                  specified.
      Dph:        The phase function - an array of the same
                  dimension as Dqv. Also only calculated if Dqv is
                  specified.
 MODIFICATION HISTORY
      G. Thomas 1998 mie_uoc.pro (translation of mieint.f to IDL)

      D. Grainger 2001(?) mie_uoc_d.pro (Added support for arrays of
      particle sizes and included calculation of phase function)

      G. Thomas Sept. 2003 (Put into EODG routines format)

      G. Thomas Feb. 2004 (Introduced explicit double precision
      numerical values into all computational expressions)

      M. Clerici Apr. 2005 : internally builds Dqv array from Inp
                             ( Inp was forced to 1 before)

   If an array of cos(theta) is provided, calculate phase function

(See ../AOPP//mie_single.pro)

  ------------------------------------------------------------------------

MIE_SIZEDIST
```

```
NAME:
      MIE_SIZEDIST

PURPOSE:
      Calculates the scattering parameters of a generic
      distribution of spherical particles, read from file.
CATEGORY:
      EODG Mie routines
CALLING SEQUENCE:
      mie_sizedist, file, Nd, Wavenumber, Cm [, Dqv = dqv] $
      [,Bext] [,Bsca] [,w] [,g] [,ph]
INPUTS:
      File:       file containing size distribution
      Nd:         Number density of the particle distribution
                  Use 1E-3 to convert Bext from [um2] to ext.
                  coeff. in km-1 for 1 part/cm3 density.

      Wavenumber: Wavenumber of light (units must match Rm)
      Cm:         Complex refractive index

OPTIONAL KEYWORD PARAMETERS:
      Dqv:        An array of the cosines of scattering angles at
                  which to compute the phase function.
      Rmin:       minimum radius of the distribution
      Rmax:       maximum radius of the distribution
      Nqua:       number of quadrature points (default is 450)
      DISP:       display size distribution
      VOLCONC:    concentration (dNr) is expressed in volume (dV/dlnr)
                  rather than dN/dlnr

OUTPUT PARAMETERS:
      Bext:       The extinction cross section [um^2 - M.C. 02.12.04]
      Bsca:       The scattering cross section [um^2 - M.C. 02.12.04]
      w:          The single scatter albedo
      g:          The asymmetry parameter
      ph:         The phase function - an array of the same
                  dimension as Dqv. Only calculated if Dqv is
                  specified.
RESTRICTIONS:
      Note, this procedure calls the MIE_SINGLE and QUADRATURE procedures.

MODIFICATION HISTORY

      M. Clerici Feb.2005 : derived from mie_lognormal.bat

NOTE on Normalisation : file contains a distribution in terms of r , dN/dr,
```

```
                        (or dV/dlnr(*) in case, e.g., of Aeronet data)

                        which has no normalisation constrains ( if you try
                        dN/dr or 2.* dN/dr you get the same result).

                        Internal variable respect the following conditions:

                      - TOTAL(wghtr)      = Ru-Rl     (by contruction)

                      - TOTAL(W1*wghtr)   = Nd*fact   fact = 1.
                                                      if RMIN-RMAX contains
                                                      Rl-Ru, otherwise < 1.

 (*) : in case of size distribution provided as dV/dlnr (as for Aeronet) keyword
       /VOLCONC must be set and the conversion is computed as:

       dN(r)/dr (internally used unit ) = dV(r)/dlnr * 1/V(r) * dlnr/dr
                                        = dV(r)/dlnr * 3/(4*pi*r^4)
                                        = dV(r)/dlnr * 1/(4.18879*r^4)

       and 4/3*pi = 4.18879

(See ../AOPP//mie_sizedist.pro)

  ------------------------------------------------------------------------
```

Acknowledgements

The AERONET project is duly acknowledged for the continuous effort put into the quality assurance and processing of sun-photometric data. This report is as well a tribute to all investigators going in the field to collect precious measurements. Special thanks go to Giuseppe Zibordi for the maintenance of the Acqua Alta Oceanographic Tower AERONET site.

References

Andreae, T., M. Andreae, C. Ichoku, W. Maenhaut, J. Cafmeyer, A. Karnieli, and L. Orlovsky (2002). Light scattering by dust and anthropogenic aerosol at a remote site in the Negev desert, Israel. *J. Geophys. Res., 107*, 10.1029/2001JD900252.

Ångström, A. (1964). The parameters of atmospheric turbidity. *Tellus, 26*, 64–75.

Antoine, D. and A. Morel (1999). A multiple scattering algorithm for atmospheric correction of remotely sensed ocean colour (MERIS instrument): principle and implementation for atmospheres carrying various aerosols including absorbing ones. *Int. J. Remote Sens., 20*, 1875–1916.

Artaxo, P., E. Fernandes, J. Martins, M. Yamasoe, P. Hobbs, W. Maenhaut, K. Longo, and A. Castanho (1998). Large scale aerosol source apportionment in Amazonia. *J. Geophys. Res., 103*, 31837–31847.

Artaxo, P., W. Maenhaut, H. Storms, and R. Van Grieken (1990). Aerosol characteristics and sources for the Amazon Basin during the wet season. *J. Geophys. Res., 95*, 16971–16985.

Babu, S., K. Moorthy, and S. Satheesh (2004). Aerosol black carbon over Arabian Sea during intermonsoon and summer monsoon seasons. *Geophys. Res. Lett., 31*, L06104, 10.1029/2003GL018716.

Babu, S., S. Satheesh, and K. Moorthy (2002). Aerosol radiative forcing due to enhanced black carbon at an urban site in India. *Geophys. Res. Lett., 29*, 1880, 10.1029/2002GL015826.

Bates, T., D. Coffman, D. Covert, and P. Quinn (2002). Regional marine boundary layer aerosol size distributions in the Indian, Atlantic, and Pacific Oceans: A comparison of INDOEX measurements with ACE-1, ACE-2, and Aerosols99. *J. Geophys. Res., 107*, 8026, 10.1029/2001JD001174.

Baumgardner, D., G. Raga, G. Kok, J. Ogren, I. Rosas, A. Baez, and T. Novakov (2000). On the evolution of aerosol properties at a mountain site above Mexico City. *J. Geophys. Res., 105*, 22243–22253.

Bellouin, N., O. Boucher, D. Tanré, and O. Dubovik (2003). Aerosol absorption over the clear-sky oceans deduced from POLDER-1 and AERONET observations. *Geophys. Res. Lett., 30*, 1748, 10.1029/2003GL017121.

Bergstrom, R., P. Pilewskie, B. Schmid, and P. Russell (2003). Estimates of the spectral aerosol single scattering albedo and aerosol radiative effects during SAFARI 2000. *J. Geophys. Res., 108*, 8474, 10.1029/2002JD002435.

Betzer, P., K. Carder, R. Duce, J. Merrill, N. Tindale, M. Uematsu, D. Costello, R. Young, R. Felly, J. Breland, R. Bernstein, and A. Greco (1988). Long-range

transport of giant mineral aerosol particles. *Nature, 336*, 568–571.

Boucher, O. and D. Tanré (2000). Estimation of the aerosol perturbation to the Earth's radiative budget over oceans using POLDER satellite aerosol retrievals. *Geophys. Res. Lett., 27*, 1103–1106.

Bulgarelli, B., V. Kisselev, and L. Roberti (1999). Radiative transfer in the atmosphere-ocean system: The finite-element method. *Appl. Opt., 38*, 1530–1542.

Bundke, U., G. Hänel, H. Horvath, W. Kaller, S. Seidl, H. Wex, A. Wiedensohler, M. Wiegner, and V. Freudenthaler (2002). Aerosol optical properties during the Lindenberg Aerosol Characterization Experiment (LACE 98). *J. Geophys. Res., 107*, 8123, 10.1029/2000JD000188.

Cachier, H., F. Aulagnier, R. Sarda, F. Gautier, P. Masclet, J.-L. Besombes, N. Marchand, S. Despiau, D. Croci, M. Mallet, P. Laj, A. Marinoni, P.-A. Deveau, J.-C. Roger, J.-P. Putaud, R. Van Dingenen, A. Dell'Acqua, J. Viidanoja, S. Martins-Dos Santos, C. Liousse, F. Cousin, R. Rosset, E. Gardrat, and C. Galy-Lacaux (2005). Aerosol studies during the ESCOMPTE experiment: An overview. *Atmos. Res., 74*, 547–563.

Cachorro, V., P. Durán, R. Vergaz, and A. de Frutos (2000). Measurements of the atmospheric turbidity of the North-Centre continental area in Spain: Spectral aerosol optical depth and Ångström turbidity parameters. *J. Aerosol Sci., 31*, 687–702.

Cachorro, V. and D. Tanré (1997). The correlation between particle mass loading and extinction: application to desert dust aerosol content estimation. *Remote Sens. Environ., 60*, 187–194.

Carrico, C., P. Kus, M. Rood, P. Quinn, and T. Bates (2003). Mixtures of pollution, dust, sea salt, and volcanic aerosol during ACE-Asia: Aerosol radiative properties as a function of relative humidity. *J. Geophys. Res., 108*, 8650, 10.1029/2003JD003405.

Carrico, C., M. Rood, J. Ogren, C. Neusüss, A. Wiedensohler, and J. Heintzenberg (2000). Aerosol optical properties at Sagres, Portugal during ACE-2. *Tellus, 52, B*, 694–715.

Charlson, R., J. Lovelock, M. Andreae, and S. Warren (1987). Oceanic phytoplankton, atmospheric sulphur, cloud albedo and climate. *Nature, 326*, 655–661.

Chazette, P., H. Randriamiarisoa, J. Sanak, P. Couvert, and C. Flamant (205). Optical properties of urban aerosol from airborne and ground-based in situ measurements performed during the Etude et Simulation de la Qualité de l'air en Ile de France (ESQUIF) program. *J. Geophys. Res., 110*, D02206, 10.1029/2004JD004810.

Chiapello, I., G. Bergametti, B. Chatenet, F. Dulac, C. Moulin, A. Vermeulen, C. Devaux, I. Jankowiak, and E. Santos Soares (1999). Contribution of the different aerosol species to the aerosol optical depth over the Northeastern Tropical Atlantic. *J. Geophys. Res., 104*, 4025–4033.

Chomko, R. and H. Gordon (1998). Atmospheric correction of ocean color imagery: use of the Junge power-law aerosol size distribution with variable refractive index to handle aerosol absorption. *Appl. Opt., 37*, 5560–5572.

Chomko, R. and H. Gordon (2001). Atmospheric correction of ocean color imagery: test of the spectral optimization algorithm with the Sea-viewing Wide Field-of-View Sensor. *Appl. Opt., 40*, 2973–2984.

Chou, M.-D., P.-K. Chan, and M. Wang (2002). Aerosol radiative forcing derived from SeaWiFS-retrieved aerosol optical properties. *J. Atmos. Sci., 59*, 748–757.

Christopher, S. and J. Zhang (2002). Shortwave aerosol radiative forcing from MODIS and CERES observations over the oceans. *Geophys. Res. Lett., 29*, 1859, 10.1029/2002GL014803.

Chuan, R., D. Woods, and M. McCormick (1981). Characterization of aerosols from eruptions of Mount St. Helens. *Science, 211*, 830–832.

Chun, Y., K. Boo, J. Kim, S. Park, and M. Lee (2001). Synopsis, transport, and physical characteristics of Asian dust in Korea. *J. Geophys. Res., 106*, 18461–18469.

Conant, W., J. Seinfeld, J. Wang, G. Carmichael, Y. Tang, I. Uno, P. Flatau, K. Markowicz, and P. Quinn (2003). A model for the radiative forcing during ACE-Asia derived from CIRPAS Twin Otter and R/V Ronald H. Brown data and comparison with observations. *J. Geophys. Res., 108*, 8661, 10.1029/2002JD003260.

D'Almeida, G. (1987). On the variability of desert aerosol radiative characteristics. *J. Geophys. Res., 92*, 3017–3026.

D'Almeida, G., P. Koepke, and E. Shettle (1991). *Atmospheric Aerosol*. Hampton: A.Deepak Publishing.

Deuzé, J.-L., P. Goloub, M. Herman, A. Marchand, G. Perry, S. Susana, and D. Tanré (2000). Estimate of the aerosol properties over the ocean with POLDER. *J. Geophys. Res., 105*, 15329–15346.

Di Iorio, T., A. di Sarra, W. Junkermann, M. Cacciani, G. Fiocco, and D. Fuà (2003). Tropospheric aerosols in the Mediterranean: 1. Microphysical and optical properties. *J. Geophys. Res., 108*, 4316, 10.1029/2002JD002815.

Díaz, J., F. Expósito, C. Torres, F. Herrera, J. Prospero, and M. Romero (2001). Radiative properties of aerosols in Saharan dust outbreaks using ground-based and satellite data: Applications to radiative forcing. *J. Geophys. Res., 106*, 18403–18416.

Dubovik, O., B. Holben, T. Eck, A. Smirnov, Y. Kaufman, M. King, D. Tanré, and I. Slutsker (2002). Variability of absorption and optical properties of key aerosol types observed in worldwide locations. *J. Atmos. Sci., 59*, 590–608.

Duce, R., P. Liss, J. Merrill, E. Atlas, P. Buat-Menard, B. Hicks, J. Miller, J. Prospero, R. Arimoto, T. Church, W. Ellis, J. Galloway, L. Hansen, T. Jickells, A. Knap, K. Reinhardt, B. Schneider, A. Soudine, J. Tokos, S. Tsunogai, R. Wollast, and M. Zhou (1991). The atmospheric input of trace species to the world ocean. *Global Biogeochem. Cycles, 5*, 193–259.

Dulac, F., D. Tanré, G. Bergametti, P. Buat-Menard, M. Desbois, and D. Sutton (1992). Assessment of the African airborne dust mass over the western Mediterranean Sea using Meteosat data. *J. Geophys. Res., 97*, 2489–2506.

Ebert, M., S. Weinbruch, A. Rausch, G. Gorzaski, P. Hoffmann, H. Wex, and G. Helas (2002). Complex refractive index of aerosols during LACE 98 as derived from the analysis of individual particles. *J. Geophys. Res., 107*, 8121, 10.1029/2000JD000195.

Eck, T., B. Holben, O. Dubovik, A. Smirnov, P. Goloub, H. Chen., B. Chatenet, L. Gomes, X.-Y. Zhang, S.-C. Tsay, Q. Ji, D. Giles, and I. Slutsker (2005). Columnar aerosol optical properties at AERONET sites in central eastern Asia

and aerosol transport to the tropical mid-Pacific. *J. Geophys. Res., 110*, D0602, 10.10292004JD005274.

Eck, T., B. Holben, O. Dubovik, A. Smirnov, I. Slutsker, J. Lobert, and V. Ramanathan (2001b). Column-integrated aerosol optical properties over the Maldives during the northeast monsoon for 1998-2000. *J. Geophys. Res., 106*, 28555–28566.

Eck, T., B. Holben, J. Reid, O. Dubovik, A. Smirnov, N. O'Neill, I. Slutsker, and S. Kinne (1999). The wavelength dependence of the optical depth of biomass burning, urban and desert dust areosols. *J. Geophys. Res., 104*, 31333–31350.

Eck, T., B. Holben, J. Reid, N. O'Neill, J. Schafer, O. Dubovik, A. Smirnov, M. Yamasoe, and P. Artaxo (2003b). High aerosol optical depth biomass burning events: A comparison of optical properties for different source regions. *Geophys. Res. Lett., 30*, 2035, 10.1029/2003GL017861.

Eck, T., B. Holben, I. Slutsker, and A. Setzer (1998). Measurements of irradiance attenuation and estimation of aerosol single scattering albedo for biomass burning aerosols in Amazonia. *J. Geophys. Res., 103*, 31865–31878.

Eck, T., B. Holben, D. Ward, O. Dubovik, J. Reid, A. Smirnov, M. Mukelabai, N. Hsu, N. O'Neill, and I. I. Slutsker (2001a). Charaterization of the optical properties of biomass burning aerosols in Zambia during the 1997 ZIBBEE field campaign. *J. Geophys. Res., 106*, 3425–3448.

Eck, T., B. Holben, D. Ward, M. Mukelabai, O. Dubovik, A. Smirnov, J. Schafer, N. Hsu, S. Piketh, A. Queface, J. Le Roux, R. Swap, and I. Slutsker (2003a). Variability of biomass burning aerosol optical characteristics in southern Africa during the SAFARI 2000 dry season campaign and a comparison of single scattering albedo estimates from radiometric measurements. *J. Geophys. Res., 108*, 8477, 10.1029/2002JD002321.

Formenti, P., M. Andreae, T. Andreae, E. Galani, A. Vasaras, C. Zerefos, V. Amiridis, L. Orlovsky, A. Karnieli, M. Wendisch, H. Wex, B. Holben, W. Maenhaut, and J. Lelieveld (2001a). Aerosol optical properties and large scale transport of air masses: observations at a coastal and semiarid site in the eastern Mediterranean during summer 1998. *J. Geophys. Res., 106*, 9807–9826.

Formenti, P., M. Andreae, T. Andreae, C. Ichoku, G. Schebeske, J. Kettle, W. Maenhaut, J. Cafmeyer, J. Ptasinsky, A. Karnieli, and J. Lelieveld (2001b). Physical and chemical characteristics of aerosols over the Negev desert (Israel) during summer 1996. *J. Geophys. Res., 106*, 4871–4890.

Formenti, P., O. Boucher, T. Reiner, D. Sprung, M. Andreae, M. Wendisch, H. Wex, D. Kindred, M. Tzortziou, A. Vasaras, and C. Zerefos (2002). STAAARTE-MED 1998 summer airborne measurements over the Aegean Sea. 2. Aerosol scattering and absorption, and radiative calculations. *J. Geophys. Res., 107*, 4451, 10.1029/2001JD001536.

Gilman, C. and C. Garrett (1994). Heat flux parameterizations for the Mediterranean Sea: the role of atmospheric aerosols and constraints from the water budget. *J. Geophys. Res., 99*, 5119–5134.

Gordon, H. (1997). Atmospheric correction of ocean color imagery in the Earth Observing System era. *J. Geophys. Res., 102*, 17081–17106.

Gordon, H., T. Du, and T. Zhang (1997). Remote sensing of ocean color and aerosol properties: resolving the issue of aerosol absorption. *Appl. Opt., 36*, 8670–8684.

Gordon, H. and M. Wang (1994). Retrieval of water-leaving radiance and aerosol optical thickness over the oceans with SeaWiFS: a preliminary algorithm. *Appl. Opt., 33*, 443–452.

Goudie, A. and N. Middleton (2001). Saharan dust storms: nature and consequences. *Earth Sci. Rev., 56*, 179–204.

Gras, J., J. Jensen, K. Okada, M. Ikegami, Y. Zaizen, and Y. Makino (1999). Some optical properties of smoke aerosol in Indonesia and tropical Australia. *Geophys. Res. Lett., 26*, 1393–1396.

Guerzoni, S., R. Chester, F. Dulac, B. Herut, M.-D. Loÿe-Pilot, C. Measures, C. Migon, E. Molinaroli, C. Moulin, P. Rossini, C. Saydam, A. Soudine, and P. Ziveri (1999). The role of atmospheric deposition in the biogeochemistry of the Mediterranean Sea. *Prog. Oceanogr., 44*, 147–190.

Hamonou, E., P. Chazette, D. Balis, F. Dulac, X. Schneider, E. Galani, G. Ancellet, and A. Papayannis (1999). Characterization of the vertical structure of Saharan dust export to the Mediterranean basin. *J. Geophys. Res., 104*, 22257–22270.

Hao, W. and M. Liu (1994). Spatial and temporal distribution of tropical biomass burning. *Global Biogeochem. Cycles, 8*, 495–503.

Hartley, W., P. Hobbs, J. Ross, P. Russell, and J. Livingston (2000). Properties of aerosols aloft relevant to direct radiative forcing off the mid-Atlantic coast of the United states. *J. Geophys. Res., 105*, 9859–9885.

Haywood, J., R. Allan, I. Culverwell, T. Slingo, S. Milton, J. Edwards, and N. Clerbaux (2005). Can desert dust explain the outgoing longwave radiation anomaly over the Sahara during July 2003? *J. Geophys. Res., 110*, D05105, 10.1029/2004JD005232.

Haywood, J. and O. Boucher (2000). Estimates of the direct and indirect radiative forcing due to tropospheric aerosols: A review. *Rev. Geophys., 38*, 513–543.

Haywood, J., P. Francis, O. Dubovik, M. Glew, and B. Holben (2003a). Comparison of aerosol size distributions, radiative properties, and optical depths determined by aircraft observations and Sun photometers during SAFARI 2000. *J. Geophys. Res., 108*, 8471, 10.1029/2002JD002250.

Haywood, J., P. Francis, M. Glew, and J. Taylor (2001). Optical properties and direct radiative effect of Saharan dust: A case study of two Saharan dust outbreaks using aircraft data. *J. Geophys. Res., 106*, 18417–18430.

Haywood, J., P. Francis, S. Osborne, M. Glew, N. Loeb, E. Highwood, D. Tanré, G. Myhre, P. Formenti, and E. Hirst (2003c). Radiative properties and direct radiative effect of Saharan dust measured by the C-130 aircraft during SHADE. 1. Solar spectrum. *J. Geophys. Res., 108*, 8577, 10.1029/2002JD002687.

Haywood, J., S. Osborne, P. Francis, A. Keil, P. Formenti, M. Andreae, and P. Kaye (2003b). The mean physical and optical properties of regional haze dominated by biomass burning aerosol measured from the C-130 aircraft during SAFARI 2000. *J. Geophys. Res., 108*, 8473, 10.1029/2002JD002226.

Haywood, J., V. Ramaswamy, and B. Soden (1999). Tropospheric aerosol climate forcing in clear-sky satellite observations over the oceans. *Science, 283*, 1299–1303.

Heintzenberg, J., T. Tuch, B. Wehner, A. Wiedensohler, H. Wex, A. Ansmann, D. Mattis, I. Müller, M. Wendisch, S. Eckhardt, and A. Stohl (2003). Arctic haze over central Europe. *Tellus, B, 55*, 796–807.

Herman, M., J. Deuzé, C. Devaux, P. Goloub, F.-M. Bréon, and D. Tanré (1997). Remote sensing of aerosols over land surfaces including polarization measurements and application to POLDER measurements. *J. Geophys. Res., 102*, 17039–17049.

Hess, M., P. Koepke, and I. Schult (1998). Optical properties of aerosols and clouds: The software package OPAC. *Bull. Amer. Meteor. Soc., 79*, 831–844.

Hignett, P., J. Taylor, P. Francis, and M. Glew (1999). Comparison of observed and modeled direct aerosol forcing during TARFOX. *J. Geophys. Res., 104*, 2279–2287.

Higurashi, A. and T. Nakajima (1999). Development of a two-channel aerosol retrieval algorithm on global scale using NOAA AVHRR. *J. Atmos. Sci., 56*, 924–941.

Higurashi, A. and T. Nakajima (2002). Detection of aerosol types over the East China Sea near Japan from four-channel satellite data. *Geophys. Res. Lett., 29*, 1836, 10.1029/2002GL015357.

Higurashi, A., T. Nakajima, B. Holben, A. Smirnov, R. Frouin, and B. Chatenet (2000). A study of global aerosol optical climatology with two channel AVHRR remote sensing. *J. Clim., 13*, 2011–2027.

Holben, B., T. Eck, I. Slutker, D. Tanré, J. Buis, A. Setzer, E. Vermote, J. Reagan, Y. Kaufman, T. Nakajima, F. Lavenu, I. Jankowiak, and A. Smirnov (1998). AERONET - A federated instrument network and data archive for aerosol characterization. *Remote Sens. Environ., 66*, 1–16.

Holben, B., A. Setzer, T. Eck, A. Pereira, and I. Slutsker (1996). Effect of dry season biomass burning on Amazon basin aerosol concentrations and optical properties, 1992-1994. *J. Geophys. Res., 101*, 19465–19481.

Holben, B. N., D. Tanré, A. Smirnov, T. Eck, I. Slutsker, N. Abuhassan, W. W. Newcomb, J. S. Schafer, B. Chatenet, F. Lavenu, Y. J. Kaufman, J. Vande Castle, A. Setzer, B. Markham, D. Clark, R. Frouin, R. Halthore, A. Karneli, N. O'Neill, C. Pietras, R. Pinker, K. Voss, and G. Zibordi (2001). An emerging ground-based aerosol climatology: Aerosol optical depth from AERONET. *J. Geophys. Res., 106*, 12067–12097.

Hsu, N., J. Herman, and C. Weave (2000). Determination of radiative forcing of Saharan dust using combined TOMS and ERBE. *J. Geophys. Res., 105*, 20649–20661.

Ichoku, C., M. Andreae, T. Andreae, F. Meixner, G. Schebeske, P. Formenti, W. Maenhaut, J. Cafmeyer, J. Ptasinski, A. Karnieli, and L. Orlovsky (1999). Interrelationship between aerosol characteristics and light scattering during late winter in an eastern Mediterranean environment. *J. Geophys. Res., 104*, 24371–24393.

IPCC (2001). *Intergovernmental Panel on Climate Change (IPCC) - The scientific basis*. Cambridge: Cambridge University Press, Cambridge.

Jamet, C., C. Moulin, and S. Thiria (2004). Monitoring aerosol optical properties over the Mediterranean from SeaWiFS images using a neural network inversion. *Geophys. Res. Lett., 31*, L13107, 10.1029/2004GL019951.

Jickells, T., Z. An, K. Andersen, A. Baker, G. Bergametti, N. Brooks, J. Cao, P. Boyd, R. Duce, K. Hunter, H. Kawahata, N. Kubilay, J. LaRoche, P. Liss, N. Mahowald, J. Prospero, A. Ridgwell, I. Tegen, and R. Torres (2005). Global iron connections between desert dust, ocean biogeochemistry, and climate. *Science, 308*, 67–71.

Kahn, R., P. Banerjee, and D. McDonald (2001). Sensitivity of multiangle imaging to natural mixtures of aerosols over the oceans. *J. Geophys. Res., 106*, 18219–18238.

Kahn, R., B. Gaitley, J. Martonchik, D. Diner, K. Crean, and B. Holben (2005). Multiangle Imaging Spectroradiometer (MISR) global aerosol optical depth validation based on 2 years of coincident Aerosol Robotic Network (AERONET) observations. *J. Geophys. Res., 110*, D10S04, 10.1029/2004JD004706.

Kalashnikova, O. and I. Sokolik (2002). Importance of shapes and compositions of wind-blown dust particles for remote sensing at solar wavelengths. *Geophys. Res. Lett., 29*, 1398, 10.1029/2002GL014947.

Kaufman, Y., P. Hobbs, V. Kirchhoff, P. Artaxo, L. Remer, B. Holben, M. King, D. Ward, E. Prins, K. Longo, L. Mattos, C. Nobre, J. Spinhirne, Q. Ji, A. Thompson, J. Gleason, S. Christopher, and S.-C. Tsay (1998). Smoke, Clouds, and Radiation-Brazil (SCAR-B) experiment. *J. Geophys. Res., 103*, 31783–31808.

Kaufman, Y., I. Koren, L. Remer, D. Tanré, P. Ginoux, and S. Fan (2005). Dust transport and deposition observed from the Terra-Moderate Resolution Imaging Spectroradiometer (MODIS) spacecraft over the Atlantic Ocean. *J. Geophys. Res., 110*, D10S12, 10.1029/2003JD004436.

Kaufman, Y., D. Tanré, and O. Boucher (2002). A satellite view of aerosols in the climate system. *Nature, 419*, 215–223.

Kiehl, J. and B. Briegleb (1993). The relative role of sulfate aerosols and greenhouse gases in climate forcing. *Science, 260*, 311–314.

Kim, D.-H., B.-J. Sohn, T. Nakajima, and T. Takamura (2005). Aerosol radiative forcing over east Asia determined from ground-based solar radiation measurements. *J. Geophys. Res., 110*, D10S22, 10.1029/2004JD004678.

Kim, D.-H., B.-J. Sohn, T. Nakajima, T. Takamura, T. Takemura, B.-C. Choi, and S.-C. Yoon (2004). Aerosol optical properties over East Asia determined from ground-based sky radiation measurements. *J. Geophys. Res., 109*, D02209, 10.1029/2003JD003387.

Kim, S.-W., S.-C. Yoon, A. Jefferson, J. Ogren, E. Dutton, J.-G. Won, Y. Ghim, B.-I. Lee, and J.-S. Han (2005). Aerosol optical, chemical and physical properties at Gosan, Korea during Asian dust and pollution episodes in 2001. *Atmos. Env., 39*, 39–50.

King, M., Y. Kaufman, D. Tanré, and T. Nakajima (1999). Remote sensing of tropospheric aerosols from space: past, present and future. *Bull. Amer. Meteor. Soc., 80*, 2229–2259.

Kinne, S., U. Lohmann, J. Feichter, M. Schulz, C. Timmreck, S. Ghan, R. Easter, M. Chin, P. Ginoux, T. Takemura, I. Tegen, D. Koch, M. Herzog, J. Penner, G. Pitari, B. Holben, T. Eck, A. Smirnov, O. Dubovik, I. Slutsker, D. Tanré, O. Torres, M. Mishchenko, I. Geogdzhayev, D. Chu, and Y. Kaufman (2003). Monthly

averages of aerosol properties: A global comparison among models, satellite data, and AERONET ground data. *J. Geophys. Res., 108*, 4634, 10.1029/2001JD001253.

Kokhanovsky, A., W. von Hoyningen-Huene, H. Bovensmann, and J. Burrows (2004). The determination of the atmospheric optical thickness over western Europe using SeaWiFS imagery. *IEEE Trans. Geosci. Remote Sens., 42*, 824–832.

Kotchenruther, R. and P. Hobbs (1998). Humidification factors of aerosols from biomass burning in Brazil. *J. Geophys. Res., 103*, 32081–32090.

Kotchenruther, R., P. Hobbs, and D. Hegg (1999). Humidification factors of atmospheric aerosols off the mid-Atlantic coast of the United States. *J. Geophys. Res., 104*, 2239–2251.

Kouvarakis, G., Y. Doukelis, N. Mihalopoulos, S. Rapsomanikis, J. Sciare, and M. Blumthaler (2002). Chemical, physical, and optical characterization of aerosols during PAUR II experiment. *J. Geophys. Res., 107*, 8141, 10.1029/2000JD000291.

Kreidenweis, S., L. Remer, R. Bruintjes, and O. Dubovik (2001). Smoke aerosol from biomass burning in Mexico: hygroscopic smoke optical model. *J. Geophys. Res., 106*, 4831–4844.

Kubilay, N., T. Cokacar, and T. Oguz (2003). Optical properties of mineral dust outbreaks over the northeastern Mediterranean. *J. Geophys. Res., 108*, 4666, 10.1029/2003JD003798.

Kuśmierczyk-Michulec, J., O. Krüger, and R. Marks (1999). Aerosol influence on the Sea-viewing Wide Field-of-view Sensor bands: extinction measurements in a marine summer atmosphere over the Baltic Sea. *J. Geophys. Res., 104*, 14293–14307.

Kuśmierczyk-Michulec, J. and R. Marks (2000). The influence of sea-salt aerosols on the atmospheric extinction over the Baltic and the North Seas. *J. Aerosol Sci., 31*, 1299–1316.

Kuśmierczyk-Michulec, J., M. Schulz, S. Ruellan, O. Krüger, E. Plate, R. Marks, G. de Leeuw, and H. Cachier (2001). Aerosol composition and related optical properties in the marine boundary layer over the Baltic Sea. *J. Aerosol Sci., 32*, 933–955.

Kylling, A. and B. Mayer (2003, December). libRadtran - Library for radiative transfer calculations. Technical report.

Land, P. and J. Haigh (1996). Atmospheric correction over case 2 waters with an iterative fitting algorithm. *Appl. Opt., 35*, 5443–5451.

Lee, K., Y. Kim, and W. von Hoyningen-Huene (2004). Estimation of aerosol optical thickness over northeast Asia from Sea-Viewing Wide Field-of-View Sensor (SeaWiFS) data during the 2001 ACE-Asia intensive observation period. *J. Geophys. Res., 109*, D19S16, 10.1029/2003JD004126.

Levy, R., L. Remer, D. Tanré, Y. Kaufman, C. Ichoku, B. Holben, J. Livingston, P. Russell, and H. Maring (2003). Evaluation of the Moderate-Resolution Imaging Spectroradiometer (MODIS) retrievals of dust aerosol over the ocean during PRIDE. *J. Geophys. Res., 108*, 8594, 10.1029/2002JD002460.

Liousse, C., F. Dulac, H. Cachier, and D. Tanré (1997). Remote sensing of carbonaceous aerosol production by African savanna biomass burning. *J. Geophys. Res., 102*, 5895–5911.

Lippmann, M., M. Frampton, J. Schwartz, D. Dockery, R. Schlesinger, P. Koutrakis, J. Froines, A. Nel, J. Finkelstein, J. Godleski, J. Kaufman, J. Koenig, T. Larson, D. Luchtel, L.-J. S. Liu, G. Oberdörster, A. Peters, J. Sarnat, C. Sioutas, H. Suh, J. Sullivan, M. Utell, E. Wichmann, and J. Zulikoff (2003). The U.S. Environmental Protection Agency Particulate Matter Health Effects Research Center Program: A midcourse report of status, progress, and plans. *Environ. Health Perspect. 111*, 1074–1092.

Livingston, J., V. Kapustin, B. Schmid, P. Russell, P. Quinn, T. Bates, P. Durkee, P. Smith, V. Freudenthaler, M. Wiegner, D. Covert, S. Gassó, D. Hegg, D. Collins, R. Flagan, J. Seinfeld, V. Vitale, and C. Tomasi (2000). Shipboard sunphotometer measurements of aerosol optical depth spectra and columnar water vapor during ACE-2, and comparison with selected land, ship, aircraft, and satellite measurements. *Tellus, 52, B*, 593–618.

Livingston, J., P. Russell, J. Reid, J. Redemann, B. Schmid, D. Allen, O. Torres, R. Levy, L. Remer, B. Holben, A. Smirnov, O. Dubovik, E. Welton, J. Campbell, J. Wang, and S. Christopher (2003). Airborne Sun photometer measurements of aerosol optical depth and columnar water vapor during the Puerto Rico Dust Experiment and comparison with land, aircraft, and satellite measurements. *J. Geophys. Res., 108*, 8588, 10.1029/2002JD002520.

Mäkelä, J., P. Aalto, V. Jokinen, T. Pohja, A. Nissinen, S. Palmroth, T. Markkanen, K. Seitsonen, H. Lihavainen, and M. Kulmala (1997). Observations of ultrafine aerosol particle formation and growth in boreal forest. *Geophys. Res. Lett., 24*, 1219–1222.

Mallet, M., J. Roger, S. Depiau, O. Dubovik, and J.-P. Putaud (2003). Microphysical and optical properties of aerosol particles in urban zone during ESCOMPTE. *Atmos. Res., 69*, 73–97.

Maring, H., D. Savoie, M. Izaguirre, C. McCormick, R. Arimoto, J. Prospero, and C. Pilinis (2000). Aerosol physical and optical properties and their relationship to aerosol composition in the free troposphere at Izaña, Tenerife, Canary Islands, during July 1995. *J. Geophys. Res., 105*, 14677–14700.

Markowicz, K., P. Flatau, M. Ramana, P. Crutzen, and V. Ramanathan (2002). Absorbing mediterranean aerosols lead to a large reduction in the solar radiation at the surface. *Geophys. Res. Lett., 29*, 10.1029/2002GL015767.

Martins, J., P. Artaxo, C. Liousse, J. Reid, P. Hobbs, and Y. Kaufman (1998). Effects of black carbon content, particle size, and mixing on light absorption by aerosol from biomass burning in Brazil. *J. Geophys. Res., 103*, 32041–32050.

Martins, J., D. Tanré, L. Remer, Y. Kaufman, S. Mattoo, and R. Levy (2002). MODIS cloud screening for remote sensing of aerosols over oceans using spatial variability. *Geophys. Res. Lett., 29*, 8009, 10.1029/2001GL013252.

Masmoudi, M., M. Chaabane, K. Medhioub, and F. Elleuch (2003). Variability of aerosol optical thickness and atmospheric turbidity in Tunisia. *Atmos. Res., 66*, 175–188.

Masmoudi, M., M. Chaabane, D. Tanré, P. Gouloup, L. Blarel, and F. Elleuch (2003). Spatial and temporal variability of aerosol: Size distribution and optical properties. *Atmos. Res., 66*, 1–19.

Mélin, F. and G. Zibordi (2005). Aerosol variability in the Po Valley analyzed from automated optical measurements. *Geophys. Res. Lett., 32*, L03810, 10.1029/2004GL021787.

Meloni, D., A. di Sarra, J. DeLuisi, T. Di Iorio, G. Fiocco, W. Junkermann, and G. Pace (2003). Tropospheric aerosols in the Mediterranean: 2. Radiative effects through model simulations and measurements. *J. Geophys. Res., 108*, 4317, 10.1029/2002JD002807.

Meywerk, J. and V. Ramanathan (1999). Observations of the spectral clear-sky aerosol forcing over the tropical Indian Ocean. *J. Geophys. Res., 104*, 24359–24370.

Miller, R., I. Tegen, and J. Perlwitz (2004). Surface radiative forcing by soil dust aerosols and the hydrological cycle. *J. Geophys. Res., 109*, D04203, 10.1029/2003JD004085.

Mishchenko, M., W. Wiscombe, J. Hovenier, and L. Travis (2000). Overview of scattering by nonspherical particles. In M.I. Mishchenko, J.W. Hovenier, L.D. Travis (Ed.), *Light scattering by nonspherical particles*, pp. 30–60. Academic Press.

Moorthy, K., S. Babu, and S. Satheesh (2003). Aerosol spectral optical depths over the Bay of Bengal: Role of transport. *Geophys. Res. Lett., 30*, 1249, 10.1029/2002GL016520.

Moorthy, K., S. Babu, and S. Satheesh (2005). Aerosol characteristics and radiative impacts over the Arabian Sea during the intermonsoon season: Results from ARMEX field campaign. *J. Atmos. Sci., 62*, 192–206.

Moorthy, K., A. Saha, B. Prasad, K. Niranjan, D. Jhurry, and P. Pillai (2001). Aerosol optical depths over peninsular India and adjoining oceans during the INDOEX campaigns: Spatial, temporal, and spectral characteristics. *J. Geophys. Res., 106*, 28539–28554.

Moorthy, K., S. Satheesh, and B. Krishna Murthy (1997). Investigations of marine aerosols over the tropical Indian Ocean. *J. Geophys. Res., 102*, 18827–18842.

Moulin, C., F. Dulac, C. Lambert, P. Chazette, I. Jankowiak, B. Chatenet, and F. Lavenu (1997). Long-term daily monitoring of Saharan dust load over ocean using Meteosat ISCCP-B2 data, 2. Accuracy of the method and validation using Sun photometer measurements. *J. Geophys. Res., 102*, 16959–16969.

Moulin, C., H. Gordon, V. Banzon, and R. Evans (2001a). Atmospheric correction of ocean color imagery through thick layers of Saharan dust. *J. Geophys. Res., 106*, 18239–18249.

Moulin, C., H. Gordon, R. Chomko, V. Banzon, and R. Evans (2001b). Atmospheric correction of ocean color imagery through thick layers of Saharan dust. *Geophys. Res. Lett., 28*, 5–8.

Moulin, C., F. Guillard, F. Dulac, and C. Lambert (1997). Long-term daily monitoring of Saharan dust load over ocean using Meteosat ISCCP-B2 data, 1. Methodology and preliminary results for 1983-1994 in the Mediterranean. *J. Geophys. Res., 102*, 16947–16958.

Nakajima, T., A. Higurashi, K. Aoki, T. Endoh, H. Fukushima, M. Toratani, Y. Mitomi, B. Mitchell, and R. Frouin (1999). Early phase analysis of OCTS radiance data for aerosol remote sensing. *IEEE Trans. Geosci. Remote Sens., 37*, 1575–1584.

O'Dowd, C., P. Aalto, K. Hämeri, M. Kulmala, and T. Hoffmann (2002). Atmospheric particles from organic vapours. *Nature, 416*, 497–498.

O'Dowd, C., M. Facchini, F. Cavalli, D. Ceburnis, M. Mircea, S. Decesari, S. Fuzzi, Y. Yoon, and J.-P. Putaud (2004). Biogenically driven organic contribution to marine aerosol. *Nature, 431*, 676–680.

O'Dowd, C., M. Smith, I. Consterdine, and J. Lowe (1997). Marine aerosol, sea-salt, and the marine sulphur cycle: A short review. *Atmos. Env., 31*, 73–80.

Okada, Y., S. Mukai, and I. Sano (2003). Modified cloud flag for SeaWiFS data over turbid water regions. *Geophys. Res. Lett., 30*, 10.1029/2002GL015714.

Okada, Y., S. Mukai, I. Sano, K. Kozai, and H. Ishida (2004). Aerosol properties from MIRAI research cruise in the tropical Pacific Ocean. *Advances Space Res., 33*, 1195–1199.

Omar, A., J.-G. Won, D. Winker, S.-C. Yoon, O. Dubovik, and M. McCormick (2005). Development of global aerosol models using cluster analysis of Aerosol Robotic Network (AERONET) measurements. *J. Geophys. Res., 110*, D10S14, 10.1029/2004JD004874.

O'Neill, N., T. Eck, B. Holben, A. Smirnov, O. Dubovik, and A. Royer (2001). Bimodal size distribution influences on the variation of Ångström derivatives in spectral and optical depth space. *J. Geophys. Res., 106*, 9787–9806.

O'Neill, N., T. Eck, B. Holben, A. Smirnov, A. Royer, and Z. Li (2002). Optical properties of boreal forest fire smoke derived from Sun photometry. *J. Geophys. Res., 107*, 10.1029/2001JD000877.

O'Neill, N., A. Ignatov, B. Holben, and T. Eck (2000). The log-normal distribution as a reference for reporting aerosol optical depth statistics: Empirical tests using multi-year, multi-site AERONET sunphotometer data. *Geophys. Res. Lett., 27*, 3333–3336.

Osborne, S. and J. Haywood (2005). Aircraft observations of the microphysical and optical properties of major aerosol species. *Atmos. Res., 73*, 173–201.

Paerl, H. (1997). Coastal eutrophication and harmful algal blooms: Importance of atmospheric deposition and groundwater as "new" nitrogen and other nutrient sources. *Limnol. Oceanogr., 42*, 1154–1165.

Pandithurai, G., R. Pinker, O. Dubovik, B. Holben, and T. Aro (2001). Remote sensing of aerosol optical characteristics in sub-Sahel, West Africa. *J. Geophys. Res., 106*, 28347–28356.

Park, J., H. Sakurai, K. Vollmers, and P. McMurry (2004). Aerosol size distributions measured at the South Pole during ISCAT. *Atmos. Env., 38*, 5493–5500.

Paronis, D., F. Dulac, P. Chazette, E. Hamonou, and G. Liberti (1998). Aerosol optical thickness monitoring in the Mediterranean. *J. Aerosol Sci., 29*, S671–S672.

Patterson, E. (1981). Optical properties of crustal aerosols: Relation to chemical and physical characteristics. *J. Geophys. Res., 86*, 3236–3246.

Patterson, E., D. Gillette, and B. Stockton (1977). Complex index of refraction between 300 and 700 nm from Saharan aerosols. *J. Geophys. Res., 82*, 3153–3160.

Penner, J., R. Dickinson, and C. O'Neill (1992). Effects of aerosol from biomass burning on the global radiation budget. *Science, 256*, 1432–1434.

Perrone, M., M. Santese, A. Tafuro, B. Holben, and A. Smirnov (2005). Aerosol load characterization over South-East Italy for on year of AERONET sun-photometer measurements. *Atmos. Res., 75*, 111–133.

Petzold, A., M. Fiebig, H. Flentje, A. Keil, U. Leiterer, F. Schröder, A. Stifter, M. Wendisch, and P. Wendling (2002). Vertical variability of aerosol properties observed at a continental site during the Lindenberg Aerosol Characterization Experiment (LACE 98). *J. Geophys. Res., 107*, 8128, 10.1029/2001JD001043.

Podgorny, I., F. Li, and V. Ramanathan (2003). Large aerosol radiative forcing due to the 1997 Indonesian forest fire. *Geophys. Res. Lett., 30*, 1028, 10.1029/2002GL015979.

Pósfai, M., J. Li, J. Anderson, and P. Buseck (2003). Aerosol bacteria over the Southern Ocean during ACE-1. *Atmos. Res., 66*, 231–240.

Procopio, A., L. Remer, P. Artaxo, Y. Kaufman, and B. Holben (2003). Modeled spectral optical properties for smoke aerosols in Amazonia. *Geophys. Res. Lett., 30*, 2265, 10.1029/2003GL018063.

Prospero, J. (1999). Long term measurements of the transport of African mineral dust to the Southern US: implications for regional air quality. *J. Geophys. Res., 104*, 15917–15927.

Prospero, J., P. Ginoux, O. Torres, S. Nicholson, and T. Gill (2002). Environmental characterization of global sources of atmospheric soil dust identified with the Nimbus-7 Total Ozone Mapping Spectrometer (TOMS) absorbing aerosol product. *Rev. Geophys., 40*, 1–31.

Putaud, J.-P., F. Raes, R. Van Dingenen, E. Brüggemann, M.-C. Facchini, S. Decesari, S. Fuzzi, R. Gehrig, C. Hüglin, P. Laj, G. Lorbeer, W. Maenhaut, N. Mihalopoulos, K. Müller, X. Querol, S. Rodriguez, J. Schneider, G. Spindler, H. ten Brink, K. Tørseth, and A. Wiedensohler (2004). A European aerosol phenomenology. 2. Chemical characteristics of particulate matter at kerbside, urban, rural and background sites in Europe. *Atmos. Env., 38*, 2579–2595.

Quinn, P., T. Bates, D. Coffman, T. Miller, J. Johnson, D. Covert, J.-P. Putaud, C. Neusseus, and T. Novakov (2000). A comparison of aerosol chemical and optical properties from the 1st and 2nd Aerosol Characterization Experiments. *Tellus, B, 52*, 239–257.

Quinn, P., D. Coffman, T. Bates, T. Miller, J. Johnson, K. Voss, E. Welton, and C. Neusüss (2001). Dominant aerosol chemical components and their contribution to extinction during the Aerosols99 cruise across the Atlantic. *J. Geophys. Res., 106*, 20783–20809.

Quinn, P., D. Coffman, T. Bates, T. Miller, J. Johnson, E. Welton, C. Neusüss, M. Miller, and P. Sheridan (2002). Aerosol optical properties during INDOEX 1999: Means, variabilities, and controlling factors. *J. Geophys. Res., 107*, 8020, 10.1029/2000JD00037.

Quinn, P., D. Coffman, T. Bates, E. Welton, D. Covert, T. Miller, J. Johnson, S. Maria, L. Russell, R. Arimoto, C. Carrico, M. Rood, and J. Anderson (2004). Aerosol

optical properties measured on board the Ronald H. Brown during ACE-Asia as a function of aerosol chemical composition and source region. *J. Geophys. Res., 109*, D19S01, 10.1029/2003JD004010.

Quinn, P., D. Coffman, V. Kapustin, T. Bates, and D. Covert (1998). Aerosol optical properties in the marine boundary layer during the First Aerosol Characterization Experiment (ACE 1) and the underlying chemical and physical aerosol properties. *J. Geophys. Res., 103*, 16547–16563.

Quinn, P., V. Kapustin, T. Bates, and D. Covert (1996). Chemical and optical properties of marine boundary layer aerosol of the mid-Pacific in relation to sources and meteorological transport. *J. Geophys. Res., 101*, 6931–6951.

Rajeev, K., V. Ramanathan, and J. Meywerk (2000). Regional aerosol distribution and its long-range transport over the Indian Ocean. *J. Geophys. Res., 105*, 2029–2043.

Ramachandran, S. (2005). Premonsoon shortwave aerosol radiative forcings over the Arabian Sea and tropical Indian Ocean: Yearly and monthly mean variabilities. *J. Geophys. Res., 110*, D07207, 10.1029/2004JD005563.

Ramanathan, V., P. Crutzen, J. Kiehl, and D. Rosenfeld (2001b). Aerosols, climate, and the hydrological cycle. *Science, 249*, 2119–2124.

Ramanathan, V., P. Crutzen, J. Lelieveld, A. Mitra, D. Althausen, J. Anderson, M. Andreae, W. Cantrell, G. Cass, C. Chung, A. Clarke, J. Coakley, W. Collins, W. Conant, F. Dulac, J. Heintzenberg, J. Heymsfield, A, B. Holben, S. Howell, J. Hudson, A. Jayaraman, J. Kiehl, T. Krishnamurti, D. Lubin, G. McFarquhar, T. Novakov, J. Ogren, I. Podgorny, K. Prather, K. Priestley, J. Prospero, P. Quinn, K. Rajeev, P. Rasch, S. Rupert, R. Sadourny, S. Satheesh, G. Shaw, P. Sheridan, and F. Valero (2001a). Indian Ocean Experiment: an integrated analysis of the climate forcing and effects of the great Indo-Asian haze. *J. Geophys. Res., 106*, 28371–28398.

Reddy, M., O. Boucher, N. Bellouin, M. Schulz, Y. Balkanski, J.-L. Dufresne, and M. Pham (2005). Estimates of global multicomponent aerosol optical depth and direct radiative perturbation in the Laboratoire de Météorologie Dynamique general circulation model. *J. Geophys. Res., 110*, D10S16, 10.1029/2004JD004757.

Reid, J., T. Eck, S. Christopher, P. Hobbs, and B. Holben (1999). Use of the Ångström exponent to estimate the variability of optical and physical properties of aging smoke particles in Brazil. *J. Geophys. Res., 104*, 27473–27489.

Reid, J. and P. Hobbs (1998). Physical and optical properties of young smoke from individual biomass fires in Brazil. *J. Geophys. Res., 103*, 32013–32031.

Reid, J., P. Hobbs, R. Ferek, D. Blake, J. Martins, M. Dunlap, and C. Liousse (1998). Physical, chemical and optical properties of regional hazes dominated by smoke in Brazil. *J. Geophys. Res., 103*, 32059–32080.

Reid, J., H. Jonsson, H. Maring, A. Smirnov, D. Savoie, S. Cliff, E. Reid, J. Livingstone, M. Meier, O. Dubovik, and S.-C. Tsay (2003). Comparison of size and morphological measurements of coarse mode dust particles from Africa. *J. Geophys. Res., 108*, 8593, 10.1029/2002JD002485.

Remer, L., S. Gasso, D. Hegg, Y. Kaufman, and B. Holben (1997). Urban/industrial aerosol: ground-based Sun/sky radiometer and in-situ measurements. *J. Geophys. Res., 102*, 16849–16859.

Remer, L. and Y. Kaufman (1998). Dynamic aerosol model: urban/industrial aerosol. *J. Geophys. Res., 103*, 13859–13871.

Remer, L., Y. Kaufman, and B. Holben (1999). Interannual variation of ambient aerosol characteristics on the east coast of the United States. *J. Geophys. Res., 104*, 2223–2231.

Remer, L., Y. Kaufman, B. Holben, A. Thompson, and D. McNamara (1998). Biomass burning aerosol size distribution and modeled optical properties. *J. Geophys. Res., 103*, 31879–31891.

Remer, L., Y. Kaufman, D. Tanré, S. Mattoo, D. Chu, J. Martins, R.-R. Li, C. Ichoku, R. Levy, R. Kleidman, T. Eck, E. Vermote, and B. Holben (2005). The MODIS aerosol algorithm, products, and validation. *J. Atmos. Sci., 62*, 947–973.

Ruddick, K., F. Ovidio, and M. Rijkeboer (2000). Atmospheric correction of SeaWiFS imagery for turbid coastal and inland waters. *Appl. Opt., 39*, 897–912.

Russel, P., J. Livingstone, E. Dutton, R. Pueschel, J. Reagan, T. DeFoor, M. Box, D. Allen, P. Pilewskie, B. Herman, S. Kinne, and D. Hofman (1993). Pinatubo and pre-Pinatubo optical depth spectra: Mauna Loa measurements, comparisons, inferred particle size distributions, radiative effects, and relationship to lidar data. *J. Geophys. Res., 98*, 22969–22985.

Russel, P., J. Livingstone, P. Hignett, S. Kinne, J. Wong, A. Chien, R. Bergstrom, P. Durkee, and P. Hobbs (1999). Aerosol-induced radiative flux changes off the United States mid-Atlantic coast: Comparison of values calculated from sunphotometer and in situ data with those measured by airborne pyranometer. *J. Geophys. Res., 104*, 2289–2307.

Sabbah, I., C. Ichoku, Y. Kaufman, and L. Remer (2001). Full year cycle of desert dust spectral optical thickness and precipitable water vapor over Alexandria, Egypt. *J. Geophys. Res., 106*, 18305–18316.

Sano, I., S. Mukai, Y. Okada, B. Holben, S. Ohta, and T. Takamura (2003). Optical properties of aerosols during APEX and ACE-Asia experiments. *J. Geophys. Res., 108*, 8649, 10.1029/2002JD003263.

Satheesh, S. (2002). Radiative forcing by aerosols over Bay of Bengal region. *Geophys. Res. Lett., 29*, 10.1029/2002GL015334.

Satheesh, S. and K. Moorthy (2005). Radiative effects of natural aerosols: A review. *Atmos. Env., 39*, 2089–2110.

Satheesh, S. and V. Ramanathan (2000). Large differences in tropical aerosol forcing at the top of the atmosphere and Earth's surface. *Nature, 405*, 60–63.

Satheesh, S., V. Ramanathan, B. Holben, K. Krishna Moorthy, N. Loe, H. Maring, J. Prospero, and D. Savoie (2002). Chemical, physical and radiative properties of Indian Ocean aerosols. *J. Geophys. Res., 107*, 4725, doi:10.1029/2002JD002463.

Satheesh, S., V. Ramanathan, X. Li-Jones, J. Robert, I. Podgorny, J. Prospero, B. Holben, and N. Loeb (1999). A model for the natural and anthropogenic aerosols over the tropical Indian Ocean derived from Indian Ocean Experiment data. *J. Geophys. Res., 104*, 27421–27440.

Schulz, M., Y. Balkanski, W. Guelle, and F. Dulac (1998). Role of aerosol size distribution and source location in a three-dimensional simulation of a Saharan dust episode tested against satellite-derived optical thickness. *J. Geophys. Res., 103*, 10579–10592.

Seinfeld, J., G. Carmichael, R. Arimoto, W. Conant, F. Brechtel, T. Bates, C. Cahill, A. Clarke, S. Doherty, P. Flatau, B. Huebert, J. Kin, K. Markowicz, P. Quinn, L. Russell, P. Russell, A. Shimizu, Y. Shinozuka, C. Song, Y. Tang, I. Uno, A. Vogelmann, R. Weber, J.-H. Woo, and X. Zhang (2004). ACE-Asia. Regional climatic and atmospheric chemical effects of Asian dust and pollution. *Bull. Amer. Meteor. Soc., 85*, 367–380.

Shettle, E. (1984). Optical and radiative properties of a desert aerosol model. In G. Fiocco (Ed.), *Proc. Symposium on Radiation in the Atmosphere*, Hampton, Va, pp. 74–77.

Shettle, E. and R. Fenn (1979). Models for the aerosols of the lower atmosphere and the effects of humidity variations on their optical properties. In *AFGL-TR-79-0214*, Chapter 676, pp. 94. Environmental Research Paper.

Siegel, D., M. Wang, S. Maritorena, and W. Robinson (2000). Atmospheric correction of satellite ocean colour imagery: the black pixel assumption. *Appl. Opt., 39*, 3582–3591.

Silva, A., M. Bugalho, M. Costa, W. von Hoyningen-Huene, T. Schmidt, J. Heintzenberg, and S. Hennin (2002). Aerosol optical properties from columnar data during the second Aerosol Characterization Experiment on the south coast of Portugal. *J. Geophys. Res., 107*, 4642, 10.1029/2002JD002196.

Singh, R., S. Dey, S. Tripathi, and V. Tare (2004). Variability of aerosol parameters over Kanpur, northern India. *J. Geophys. Res., 109*, D23206, 10.1029/2004JD004966.

Smirnov, A., B. Holben, O. Dubovik, R. Frouin, T. Eck, and I. Slutsker (2003a). Maritime component in aerosol optical models derived from Aerosol Robotic Network data. *J. Geophys. Res., 108*, 4033, 10.1029/2002JD002701.

Smirnov, A., B. Holben, T. Eck, O. Dubovik, and I. Slutsker (2003b). Effect of wind speed on columnar aerosol optical properties at Midway Island. *J. Geophys. Res., 108*, 4802, 10.1029/2003JD003879.

Smirnov, A., B. Holben, I. Slutsker, E. Welton, and P. Formenti (1998). Optical properties of Sahara dust during ACE-2. *J. Geophys. Res., 103*, 28079–28092.

Smirnov, A., A. Royer, N. O'Neill, and S. Tarussov (1994). A study of the link between synoptic air mass type and atmospheric optical parameters. *J. Geophys. Res., 99*, 20967–20982.

Smirnov, A., Y. Villevalde, N. O'Neill, A. Royer, and S. Tarussov (1995). Aerosol optical depth over the oceans: analysis in terms of synoptic air mas types. *J. Geophys. Res., 100*, 16639–16650.

Sokolik, I. and O. Toon (1996). Direct radiative forcing by anthropogenic airborne mineral aerosol. *Nature, 381*, 681–683.

Sokolik, I. and O. Toon (1999). Incorporation of mineralogical composition into models of the radiative properties of mineral aerosol from UV to IR wavelengths. *J. Geophys. Res., 104*, 9423–9444.

Stamnes, K., W. Li, B. Yan, H. Eide, A. Barnard, W. Pegau, and J. Stamnes (2003). Accurate and sefl-consistent ocean color algorithms: Simultaneous retrieval of aerosol optical properties and chlorophyll concentrations. *Appl. Opt., 42*, 939–951.

Sturm, B. and G. Zibordi (2002). SeaWiFS atmospheric correction by an approximate model and vicarious calibration. *Int. J. Remote Sens., 23*, 489–501.

Sumanth, E., K. Mallikarjuna, J. Stephen, M. Moole, V. Vinoj, S. Satheesh, and K. Moorthy (2004). Measurements of aerosol optical depth and black carbon over Bay of Bengal during post-monsoon season. *Geophys. Res. Lett., 31*, L16115, 10.1029/2004GL020681.

Swap, R., S. Ulanski, M. Cobett, and M. Garstang (1996). Temporal and spatial characteristics of Saharan dust outbreaks. *J. Geophys. Res., 101*, 4205–4220.

Tanré, D., Y. Kaufman, M. Herman, and S. Mattoo (1997). Remote sensing of aerosol properties over oceans using the MODIS/EOS spectral radiances. *J. Geophys. Res., 102*, 16971–16988.

Tanré, D., Y. Kaufman, B. Holben, B. Chatenet, A. Karnieli, F. Lavenu, L. Blarel, O. Dubovik, L. Remer, and A. Smirnov (2001). Climatology of dust aerosol size distribution and optical properties derived from remotely sensed data in the solar spectrum. *J. Geophys. Res., 106*, 18205–18217.

Torres, O., P. Bhartia, J. Herman, Z. Ahmad, and J. Gleason (1998). Derivation of aerosol properties from satellite measurements of backscattered radiation. Theoretical basis. *J. Geophys. Res., 103*, 17099–17110.

Torres, O., P. Bhartia, J. Herman, A. Sinyuk, P. Ginoux, and B. Holben (2002). A long-term record of aerosol optical depth from TOMS observations and comparison to AERONET measurements. *J. Atmos. Sci., 59*, 398–413.

Tragou, E. and A. Lascaratos (2003). Role of aerosols on the Mediterranean solar radiation. *J. Geophys. Res., 108*, 3025, 10.1029/2001JC001258.

Tratt, D., R. Frouin, and D. Westphal (2001). April 1998 Asian dust event: a southern Californian perspective. *J. Geophys. Res., 106*, 18371–18379.

Treffeisen, R., A. Rinke, M. Fortmann, K. Dethloff, A. Herber, and T. Yamanouchi (2005). A case study of the radiative effects of Arctic aerosols in March 2000. *Atmos. Env., 39*, 899–911.

Tunved, P., E. Nilsson, H.-C. Hansson, J. Ström, M. Kulmala, P. Aalto, and Y. Viisanen (2005). Aerosol characteristics of air masses in northern Europe: Influences of location, transport, sinks, and sources. *J. Geophys. Res., 110*, D07201, 10.1029/2004JD005085.

Van de Hulst, H. (1957). *Light Scattering by Small Particles*. New York: Wiley.

Villevalde, Y., A. Smirnov, N. O'Neill, S. Smyshlyaev, and V. Yakovlev (1994). Measurement of aerosol optical depth in the Pacific Ocean and North Atlantic. *J. Geophys. Res., 99*, 20983–20988.

von Hoyningen-Huene, W., M. Freitag, and J. Burrows (2003). Retrieval of aerosol optical thickness over land surfaces from top-of-atmosphere radiance. *J. Geophys. Res., 108*, 4260, 10.1029/2001JD002018.

von Hoyningen-Huene, W. and M. Wendisch (1994). Variability of aerosol optical parameters by advective processes. *Atmos. Env., 28*, 923–933.

Voss, K., E. Welton, P. Quinn, R. Frouin, M. Miller, and R. Reynolds (2001). Aerosol optical depth measurements during the Aerosols99 experiment. *J. Geophys. Res., 106*, 20811–20819.

Wang, J., S. Christopher, F. Brechtel, J. Kim, B. Schmid, J. Redemann, P. Russell, P. Quinn, and B. Holben (2003b). Geostationary satellite retrievals of aerosol optical thickness during ACE-Asia. *J. Geophys. Res., 108*, 8657, 10.1029/2003JD003580.

Wang, J., S. Christopher, J. Reid, H. Maring, D. Savoie, B. Holben, J. Livingston, P. Russell, and S.-K. Yang (2003a). GOES 8 retrieval of dust aerosol optical thickness over the Atlantic Ocean during PRIDE. *J. Geophys. Res., 108*, 8595, 10.1029/2002JD002494.

Wang, J., X. Xia, P. Wang, and S. Christopher (2004). Diurnal variability of dust aerosol optical thickness and Ångström exponent over dust source regions in China. *Geophys. Res. Lett., 31*, L08107, 10.1029/2004GL019580.

Wang, M. and H. Gordon (1994a). A simple, moderately accurate, atmospheric correction algorithm for SeaWiFS. *Remote Sens. Environ., 50*, 231–239.

Wang, M. and H. Gordon (1994b). Estimating aerosol optical properties over the oceans with the multiangle imaging spectroradiometer: some preliminary studies. *Appl. Opt., 33*, 4042–4057.

Watson, I. and C. Oppenheimer (2000). Particle size distributions of Mount Etna's aerosol plume constrained by Sun photometry. *J. Geophys. Res., 105*, 9823–9829.

Weaver, C., P. Ginoux, N. Hsu, M.-D. Chou, and J. Joiner (2002). Radiative forcing of Saharan dust: GOCART model simulations compared with ERBE data. *J. Atmos. Sci., 59*, 736–747.

Wendisch, M., A. Stifter, B. Mayer, M. Fiebig, C. Kiemle, H. Flentje, M. Wendisch, W. Armbruster, U. Leiterer, W. von Hoyningen-Huene, and A. Petzold (2002). Aerosol-radiation interaction in the cloudless atmosphere during LACE 98. 2. Aerosol-induced solar irradiance changes determined from airborne pyranometer measurements and calculations. *J. Geophys. Res., 107*, 8131, 10.1029/2000JD000288.

Wiscombe, W. (1979, June). Mie Scattering Calculations: Advances in Technique and Fast, Vector-Speed Computer Codes. Technical Report TN-140, NCAR.

Wiscombe, W. (1980). Improved Mie scattering algorithm. *Appl. Opt., 19*, 1505–1509.

Yamasoe, M., Y. Kaufman, O. Dubovik, L. Remer, B. Holben, and P. Artaxo (1998). Retrieval of the real part of the refractive index of smoke particles from Sun/sky measurements during SCAR-B. *J. Geophys. Res., 103*, 31893–31902.

Yu, H., R. Dickinson, M. Chin, M. Kaufman, Y.J. Zhou, L. Zhou, T. Y., O. Dubovik, and B. Holben (2004). Direct radiative effect of aerosols as determined from a combination of MODIS retrievals and GOCART simulations. *J. Geophys. Res., 109*, D03206, 10.1029/2003JD003914.

Yu, H., R. Dickinson, M. Chin, Y. Kaufman, B. Holben, I. Geogdzhayev, and M. Mishchenko (2003). Annual cycle of global distributions of aerosol optical depth

from integration of MODIS retrievals and GOCART model simulations. *J. Geophys. Res., 108*, 10.1029/2002JD002717.

Zhang, J., S. Christopher, L. Remer, and Y. Kaufman (2005). Shortwave aerosol radiative forcing over cloud-free oceans from Terra. 2. Seasonal and global distributions. *J. Geophys. Res., 110*, D10S23, 10.1029/2004JD005009.